UNIVERSITY OF CALIFORNIA

Santa Barbara

Structure-Function Relationships and Biological Applications of Conjugated Oligoelectrolytes

A dissertation submitted in partial satisfaction of the

requirements for the degree Doctor of Philosophy

in Chemistry

by

Alexander William Thomas

Committee in charge:

Professor Guillermo C. Bazan, Chair

Professor Mattanjah S. de Vries

Professor Michelle A. O'Malley

Professor Kevin W. Plaxco

September 2015

The dissertation of Alexander William Thomas is approved.

_____
Professor Mattanjah S. de Vries

_____
Professor Michelle A. O'Malley

_____
Professor Kevin W. Plaxco

_____
Professor Guillermo C. Bazan, Committee Chair

August 2015

Structure-Function Relationships and Biological Applications of Conjugated Oligoelectrolytes

by

Alexander William Thomas

ACKNOWLEDGEMENTS

I would like to thank the Institute for Collaborative Biotechnologies for funding the majority of this research. Professor Derek Lovley and Dr. Kelly Nevin (University of Massachusetts, Amherst) were instrumental in teaching us chemists the practical aspects of bioelectronics research and helped us obtain some important initial results. Dr. Zachary Henson synthesized an important molecule that is discussed in Chapter 2 and contributed to many important discussions throughout my graduate studies. Professor Carol Vandenberg (UCSB) was kind enough to open up her lab and teach others and me how to culture mammalian cells and also contributed greatly to the work presented in Chapter 2. Dr. Alexander Mikhailovsky (UCSB) was extremely helpful with anything spectroscopy related throughout my studies. In addition, none of the beautiful confocal microscopy images in this dissertation would have been possible without the help of Dr. Mary Raven who runs the microscopy facility for the Neuroscience Research Institute (NRI) and the Department of Molecular, Cellular and Developmental Biology at UCSB. I spent countless hours in dark rooms in the NRI and would have wasted countless more if not for her help.

Shout out to the "Bioteam" consisting of members (past and present): Dr. Logan Garner, Dr. Jenny Du, Nate Kirchhofer, Chelsea Catania, Dr. Huijie Hou, Dr. Hengjing Yan, and Zach Rengert. This project consistently lead us further from our comfort zones and into territories we had little knowledge in. The Bioteam was a great group of coworkers, a fantastic support group, and awesome friends.

I would like to separately thank a few special colleagues, the first being Dr. Logan Garner. Logan brought me under his wing when I first started and taught me everything in

my first couple years. This project really started with him and he passed the torch to me. He was seldom relaxed or subtle, was often overbearing and temperamental, and could be a huge pain in the ass, but most importantly Logan taught me how to “get shit done” (and work with anyone). He is a creative, passionate scientist, a loyal, honest friend and a true mentor. Second, Dr. Jenny Du, colleague turned close friend, is one of the best human beings I know. Through observing her I’ve learned the value of tireless work and relentless networking. She is just plain fun to be around and I can’t wait to continue working with her. Finally, Chelsea Catania and I shared an office for much of my graduate career and supported each other tremendously. There were as many venting sessions as scientific discussions and I can’t thank her enough for being a great coworker and an even better friend.

I would like to thank my advisor Professor Gui Bazan for giving me the opportunity and freedom to pursue this research through his tireless work securing funding and managing a large research group. He also provided many invaluable scientific connections and travel opportunities that helped me grow as a scientist.

Lastly, I’d like to thank my family, especially Mom, Dad and Mamma for putting up with a (grand)son in college for over a decade. I’m glad now at almost 30 years old I can finally answer the question “So when are you going to graduate?” My science friends Dr. Matt Menyo, Dr. Matt Snedaker, Dr. Michael “Jody” Busch and Joe Sirianni were all supportive friends, roommates and drinking buddies along the way. Finally, my girlfriend Dr. Christine Pieton has been with me, whether far or near, for my entire PhD course. I couldn’t have done this without her love and support.

Vita of Alexander William Thomas

August 2015

EDUCATION

Bachelor of Science in Biochemistry, University of California, Los Angeles, June 2009

Doctor of Philosophy in Chemistry, University of California, Santa Barbara, September 2015 (expected)

RESEARCH EXPERIENCE

Graduate Student Researcher – Department of Chemistry, University of California, Santa Barbara (fall 2009 – present)
Advised by Dr. Guillermo Bazan. Synthesis and characterization of amphiphilic small molecules, electrochemistry of synthetic and biological systems, culturing of bacteria, yeast and mammalian cells, confocal microscopy of biological systems

Research Intern – Protein Technologies Department, Amgen, Thousand Oaks, CA (summer 2014)
Molecular cloning and expression of recombinant membrane proteins, testing of methods for cell-free membrane protein expression, assessment of protein expression levels and quality.

Teaching Assistant – Department of Chemistry, Universty of California, Santa Barbara (various 2009 – present)
Instruction of laboratory classes: general chemistry, analytical chemistry, inorganic chemistry

Undergraduate Student Researcher – Department of Chemistry, University of California, Los Angeles (summer 2007, 2008 – 2009)
Advised by Dr. Heather Maynard. Expression and purification of recombinant protein, synthesis and characterization of poly(NIPAAm) and a small molecule neurotransmitter for conjugation to polymers.

OTHER RELEVENT EXPERIENCE

Mentor – Center for Energy Efficient Materials internship program (summer 2011)

Chemistry Outreach, Demonstrations, and Tours – Carpinteria Middle School, Ojai Valley School, Ventura High School (various 2010 – 2015)

PUBLICATIONS

1. *Tuning the surface charge in E. coli with conjugated oligoelectrolytes*
   A.W. Thomas, G.C. Bazan, submitted to *Chem. Sci.*

2. *Pendant ionic groups of conjugated oligoelectrolytes govern their ability to intercalate into microbial membranes*
   A.W. Thomas, C. Catania, L.E. Garner, G.C. Bazan, *Chem. Comm.* 2015, 51, 9294.

3. *Phenylenevinylene conjugated oligoelectrolytes as fluorescent dyes for mammalian cell imaging*
   P. Gwozdzinska, R. Pawlowska, J. Milczarek, Logan E. Garner, **A.W. Thomas**, G.C. Bazan, and A. Chworosa, *Chem. Comm.* 2014, 50, 14859.

4. *Synthesis, characterization, and biological affinity of a NIR emitting conjugated oligoelectrolyte*
   A.W. Thomas, Z.B. Henson, J. Du, C.A. Vandenberg, G.C. Bazan, *J. Am. Chem. Soc.* 2014, 136, 3736.

5. *Modeling the membrane insertion of molecules designed for transmembrane electron transfer*
   J. Hinks, Y. Wang, W.H. Poh, B. Donose, **A.W. Thomas**, S. Wuertz, S.C. Loo, G.C. Bazan, S. Kjelleberg, Y. Mu, T. Seviour, *Langmuir* 2014, 30, 2429.

6. *Self-Assembly of Poly{1,4-phenylene-[9,9-bis(4-phenoxy- butylsulfonate)]fluorene-2,7-diyl} with Oppositely Charged Phenylenevinylene Oligoelectrolytes*
   T. Costa, A. T. Marques, J. S. S. de Melo, **A. W. Thomas**, L. E. Garner, U. Scherf, G. C. Bazan, and H. D. Burrows, *J. Phys. Chem. B* 2014, 118, 613.

7. *Conjugated oligoelectrolytes increase power generation in E. coli microbial fuel cells*
   H. Hou, X. Chen, **A.W. Thomas**, C. Catania, N.D. Kirchhofer, L.E. Garner, A. Han and G.C. Bazan, *Adv. Mater.* 2013, 25, 1593.

8. *Increased Ion Conductance Across Mammalian Membranes Modified with Conjugated Oligoelectrolytes*
   J. Du, **A.W. Thomas**, X. Chen, L. Garner, C. A. Vandenberg and G. C. Bazan, *Chem. Comm.* 2013, 49, 9624.

9. *Separating Solvent and Conformational Effects on the Photophysics of a Homologous Progression of N-Terminated Phenylenevinylene Oligomers*
   T. Costa, R. E. Di Paolo, L. E. Garner, **A. W. Thomas**, J. A. S. Almeida, L. L. G. Justino, A. L. Macąnita, G. C. Bazan, and H. D. Burrows, *J. Phys. Chem. C* 2013, 117, 18353.

10. *Aggregation properties of p-phenylene vinylene based conjugated oligoelectrolytes with surfactants*
T. Costa, L.E. Garner, M. Knaapila, **A.W. Thomas**, S.E. Rogers, G.C. Bazan and H.D. Burrows, *Langmuir,* 2013, 29, 10047.

11. *A lipid membrane intercalating conjugated oligoelectrolyte enables electrode driven succinate production in Shewanella*
A.W. Thomas, L.E. Garner, K.P. Nevin, T.L. Woodard, A.E. Franks, D.R. Lovley, J.J. Sumner, C.J. Sund and G.C. Bazan, *Energ. Environ. Sci.* 2013, 6, 1761.

12. *Improving charge collection in Escherichia coli–carbon electrode devices with conjugated oligoelectrolytes*
V.B. Wang, J. Du, X. Chen, **A.W. Thomas**, N.D. Kirchhofer, L.E. Garner, M.T. Maw, W.H. Poh, J. Hinks, S. Wuertz, S. Kjelleberg, Q. Zhang, J.S.C. Loo and G.C. Bazan, *Phys. Chem. Chem. Phys.* 2013, 15, 5867.

13. *Conjugated oligoelectrolytes increase current response and organic contaminant removal in wastewater microbial fuel cells*
L.E. Garner, **A.W. Thomas**, J.J. Sumner, S.P. Harvey and G.C. Bazan, *Energ. Environ. Sci.* 2012, 5, 9449.

ABSTRACT

Structure-Function Relationships and Biological Applications of Conjugated Oligoelectrolytes

by

Alexander William Thomas

Microorganisms like bacteria have evolved over billions of years to survive in diverse environments and have developed unique functions and metabolic pathways as a result. Manipulating and harnessing their abilities has been a hallmark of the biotechnology revolution and has the potential to solve problems in areas as diverse as health, environmental remediation and energy production. With genetic engineering we now have the ability to install in microbes beneficial functionalities and chemical production processes, but have really just scratched the surface of what is possible. Truly disruptive innovations will come from controllably interfacing these microscopic workhorses with non-living systems in an effort that will likely require both genetic engineering and materials science approaches.

It is with this premise that I present my research on a class of synthetic small molecules known as conjugated oligoelectrolytes (COEs). These water-soluble oligomers spontaneously intercalate into biological membranes and in turn modify the ionic and electronic transport properties of this ubiquitous interface in a variety of microorganisms.

COEs have previously been shown to improve the performance of microbial electronic devices for power production and contaminant removal in wastewater. The research presented here demonstrates the use of COEs for the inverse process of powering a microbe, *Shewanella*, in order to drive metabolic activity, specifically the reduction of fumarate to succinate. A mechanistic investigation of this process utilizing various voltammetry techniques, microscopy, liquid chromatography, and visible spectroscopy reveals possible membrane permeabilization and enzyme excretion, contradicting a previous hypothesis of COEs acting like transmembrane "molecular wires." In addition, structure-function relationships for COEs are developed through examination of the effects of different molecular features on various biological systems. Using microscopy and electrochemistry, some effects of ionic group type and arrangement on the biological interactions of COEs are revealed. It is determined that cationic charges are necessary for interaction with *E. coli* and that a terminal end-only arrangement of charges is beneficial for lipid membrane intercalation. Finally through visible spectroscopy and zeta potential measurements it is determined that longer COEs associate in less quantity with *E. coli* but affect the cell surface charge to a greater degree than do shorter COEs. It is these relationships that will ultimately lead to new biological applications and inform future molecular design of this exciting class of molecules.

TABLE OF CONTENTS

I. Introduction

I.1 Motivation for Modifying Microorganisms

Microorganisms have evolved over billions of years to survive in diverse environments and have developed unique functions and metabolic pathways as a result. Although unknowingly until the mid nineteenth century, humans have made use of microorganisms for thousands of years in producing fermented foods and beverages.[1] Now well into the 21st century, the true potential of harnessing the varied abilities of microorganisms has only just begun to be realized. For example, microorganisms are now used like tiny factories to produce beneficial proteins and chemicals with pharmaceutical or industrial utility.[2,3] In addition, microbes are increasingly used in wastewater treatment and environmental remediation.[4,5] Also recently there has been increased interest in interfacing bacteria with electronic systems in order to produce power or sequester carbon.[6,7] We have certainly just scratched the surface of what microorganisms can do for us and as it turns out, the smallest forms of life may hold the largest untapped potential for addressing significant challenges like disease, pollution, and energy production.

Greatly improving the performance of microbial systems or exploiting microorganisms for new applications may ultimately require pushing microbes beyond their natural evolution in order for them to survive in increasingly unnatural environments or behave in increasingly unnatural ways. Manipulating or engineering microbial cell properties offers this potential but is a significant challenge due to the required aqueous environment, nanoscale features, and overall complexity.[8] Genetic engineering has certainly been

effective at installing new features and metabolic pathways[9] but is limited to materials the cell itself is capable of producing. Furthermore, genetically engineered organisms may alter ecosystems in unforeseen ways if used in natural environments. Synthetic nanomaterials and molecular systems, however, can offer microbes new or improved functionalities that are not encountered in nature and can be better controlled since the scientist and not the microorganism is doing the synthesis and administration.

A feasible and logical target for exogenously delivered synthetic materials in microorganisms is the outermost interface *i.e*. the outer membrane or cell wall. It is this barrier that defines the microorganism in terms of its separation from the outside world and any exploitive interaction on our end will certainly be affected by the nature of this interface. In fact, researchers have used polyelectrolytes in layer-by-layer assemblies to coat the outer surface of living microbes in order to impart properties like UV-protection,[10] enhanced survival,[11], non-native substrate utilization,[12] and even magnetic functionalization.[13] In an application especially relevant to this dissertation, bacteria have also been modified with redox active polymers,[14] nanoparticles[15] and carbon nanotubes[16] in order to increase their transmembrane electrical and ionic conductance. Lipid membrane intercalating small molecules known as conjugated oligoelectrolytes (COEs) have also been used for this purpose[17,18] and are the subject of this dissertation.

I.2 Introduction to Conjugated Oligoelectrolytes

COEs are synthetic molecules generally characterized by 3 – 5 π-conjugated repeat units (RUs) equipped with pendant ionic groups to impart solubility in polar media. COEs are related to conjugated polyelectrolytes used in optoelectronics,[19-22] biosensing[23-25] and

bioimaging.[26,27] COEs thus share attractive photophysical properties similar to those of their polymeric analogs, but are monodisperse and have much smaller length scales, on par with biological architectures like proteins[28,29] and lipid membranes.[17,30-33] As such, a variety of COEs have found utility in bioimaging[34-40] and biological detection schemes[41-46] of their own.

A distinct subset of COEs, and that used throughout this dissertation, is distinguished by ionic functionalities tethered at the two terminal ends of a phenylenevinylene sequence. This bolaamphiphilic structure, like that of **DSSN+** in Figure I.1, has been shown to spontaneously intercalate into lipid bilayers with a concomitant increase in fluorescence quantum yield[17]. They have also been implicated in boosting the performance of a variety of microbial electronic devices[47,48] employing organisms ranging from yeast[17], to *E. coli*[49,50] and *Shewanella*,[51,52] and even naturally occurring bacteria in wastewater.[53] Although the exact mechanism of their action is still unclear,[18,52,54] it is thought that COEs' ability to intercalate into microbial membranes is paramount for linking intracellular metabolism to extracellular electrodes in these devices.[55]

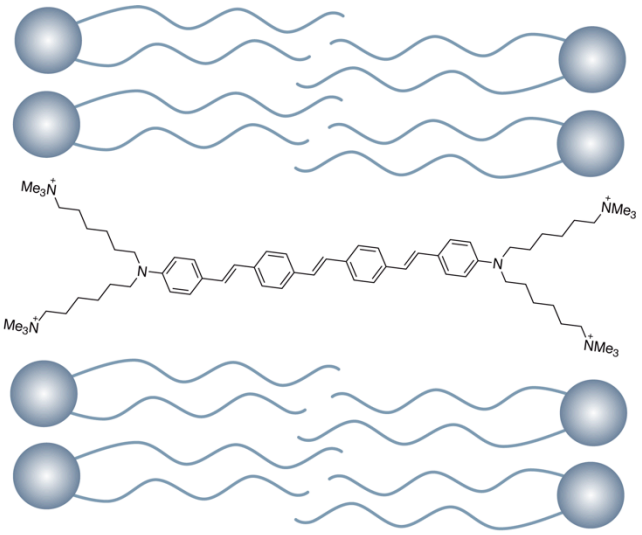

Figure I.1. Structure of 4,4'-bis(4'-(*N*,*N*-bis(6"-(*N*,*N*,*N*-trimethylammonium)hexyl)amino)-styryl)stilbene tetraiodide (**DSSN+**), and a cartoon representation of the proposed ordered orientation within a lipid bilayer.

I.3 Prior Foundational Research

Oligophenylenevinylene COEs like **DSSN+** were originally synthesized to study the effects of polar solvents on the photophysical properties of the conjugated core.[56] Through observing their solubility in water and noticing the bolaamphiphilic structure of these COEs, it was soon realized that these molecules might be well suited for incorporation into lipid bilayers. Along these lines, Logan Garner and coworkers first reported the incorporation of **DSSN+** into model lipid membranes. [17] Due to intramolecular charge transfer (IMCT) upon photoexcitation of **DSSN+** and the resulting environmental sensitivity of the chromophore, its incorporation into the hydrophobic lipid bilayer could be monitored simply by observing spectral changes, namely a red shift in absorbance, blue shift in emission and a large increase in photoluminescence quantum yield. In addition, evidence of the proposed ordered orientation of **DSSN+** within a lipid bilayer (as pictured in Figure I.1) came from uneven

fluorescence emission profiles upon polarized photoexcitation during laser scanning confocal microscopy. Furthermore, it was hypothesized that the electronically delocalized backbone could transport electrons across insulating lipid bilayers. Evidence supporting this was presented through voltammetry experiments in which an electrode was insulated with a lipid bilayer and exposed to a solution containing a redox active solute. The lipid bilayer effectively insulated the electrode but conductivity returned with the addition of **DSSN+**. This observation finally led to the successful application of **DSSN+** to microbial electronics utilizing yeast[17] and wastewater[53] with the results suggesting that **DSSN+** could impart or improve transmembrane electron transfer in a variety of microbes.

I.4 Summary and Objective

In summary, previous work has established that COEs can orient within lipid bilayers and improve the performance of microbial fuel cells, that is, the extraction of metabolically derived electrons from microbes to an external electrode. The overall objective of the research presented in this dissertation is to uncover new biological applications for COEs and better understand their interactions with cells while ultimately informing the molecular design of the next generation of molecules. In Chapter 1 it is demonstrated that **DSSN+** can enable an electrode driven, biocatalyzed reaction (the reduction of fumarate to succinate) with the bacteria *Shewanella oneidensis*. Through various voltammetry experiments it was determined that rather than act like a molecule wire as was postulated before, **DSSN+** causes the enzyme responsible for this reaction, fumarate reductase, to be released from the cell where it can interact directly with the electrode. In chapters 2 – 4, structure-function relationships are developed by examining the effects of ionic charge distribution (Chapter

2), ionic charge type (Chapter 3) and molecular length (Chapter 4) of COEs on various biological systems. In Chapter 2 the placement of cationic groups distributed evenly throughout the molecule rather than at the terminal ends was found to impair the ability of the COE to intercalate and remain in biological membranes. In Chapter 3 an anionic COE is found to intercalate into lipid bilayers but does not interact with bacteria, indicating an important electrostatic interaction in living systems. Finally in Chapter 4, COE association with bacteria is quantified and used to tune the surface charge of bacteria, with longer COEs having a greater impact on cell zeta potential than shorter ones.

I.5 References

1. Barnett, J. A. A history of research on yeasts 2: Louis Pasteur and his contemporaries, 1850–1880. *Yeast* (2000).
2. Denyer, S. P., Hodges, N. A., Gorman, S. P. & Gilmore, B. F. *Hugo and Russell's Pharmaceutical Microbiology, 8th Edition*. (John Wiley & Sons, 2011).
3. Okafor, N. *Modern industrial microbiology and biotechnology*. (Science Pub Inc, 2007).
4. Wiesmann, U., Choi, I. S. & Dombrowski, E.-M. *Fundamentals of Biological Wastewater Treatment*. (John Wiley & Sons, 2007).
5. Singh, A. & Ward, O. P. *Biodegradation and Bioremediation*. (Springer Science & Business Media, 2004).
6. Logan, B. E. *Microbial Fuel Cells*. (John Wiley & Sons, 2008).
7. Nevin, K. P., Woodard, T. L., Franks, A. E., Summers, Z. M. & Lovley, D. R.

Microbial electrosynthesis: feeding microbes electricity to convert carbon dioxide and water to multicarbon extracellular organic compounds. *mBio* **1,** (2010).

8. Fakhrullin, R. F. & Lvov, Y. M. "Face-Lifting" and "Make-Up" for Microorganisms: Layer-by-Layer Polyelectrolyte Nanocoating. *ACS Nano* **6,** 4557–4564 (2012).
9. Smolke, C. D. & Silver, P. A. Informing Biological Design by Integration of Systems and Synthetic Biology. *Cell* **144,** 855–859 (2011).
10. Eby, D. M. *et al*. Bacterial Sunscreen: Layer-by-Layer Deposition of UV-Absorbing Polymers on Whole-Cell Biosensors. *Langmuir* **28,** 10521–10527 (2012).
11. Priya, A. J., Vijayalakshmi, S. P. & Raichur, A. M. Enhanced Survival of Probiotic Lactobacillus acidophilus by Encapsulation with Nanostructured Polyelectrolyte Layers through Layer-by-Layer Approach. *J. Agric. Food Chem.* **59,** 11838–11845 (2011).
12. Mak, W. C., Sum, K. W., Trau, D. & Renneberg, R. Nanoscale surface engineered living cells with extended substrate spectrum. *IEE Proc., Nanobiotechnol.* **151,** 67 (2004).
13. a-Alonso, J. G., Fakhrullin, R. F. & Paunov, V. N. *Biosens. Bioelectron.* **25,** 1816–1819 (2010).
14. Vostiar, I., Ferapontova, E. E. & Gorton, L. Electrical 'wiring' of viable Gluconobacter oxydans cells with a flexible osmium-redox polyelectrolyte. *Electrochem. Commun.* **6,** 621–626 (2004).
15. Wu, X. *et al*. A Role for Microbial Palladium Nanoparticles in Extracellular Electron Transfer. *Angew. Chem. Int. Ed.* **50,** 427–430 (2010).

16. Geng, J., Kim, K., Zhang, J., Escalada, A. & Tunuguntla, R. Stochastic transport through carbon nanotubes in lipid bilayers and live cell membranes. *Nature* (2014).

17. Garner, L. E. *et al*. Modification of the Optoelectronic Properties of Membranes via Insertion of Amphiphilic Phenylenevinylene Oligoelectrolytes. *J. Am. Chem. Soc.* **132,** 10042–10052 (2010).

18. Du, J. *et al*. Increased ion conductance across mammalian membranes modified with conjugated oligoelectrolytes. *Chem. Commun.* **49,** 9624–9626 (2013).

19. *Conjugated Polyelectrolytes: Fundamentals and Applications*. (WILEY-VCH Verlag GmbH, 2013).

20. Duarte, A., Pu, K.-Y., Liu, B. & Bazan, G. C. Recent Advances in Conjugated Polyelectrolytes for Emerging Optoelectronic Applications. *Chem. Mater.* **23,** 501–515 (2011).

21. Jiang, H., Taranekar, P., Reynolds, J. R. & Schanze, K. S. Conjugated Polyelectrolytes: Synthesis, Photophysics, and Applications. *Angew. Chem. Int. Ed.* **48,** 4300–4316 (2009).

22. Lee, W., Seo, J. H. & Woo, H. Y. Conjugated polyelectrolytes: A new class of semiconducting material for organic electronic devices. *Polymer* **54,** 5104–5121 (2013).

23. Feng, F. *et al*. Fluorescent Conjugated Polyelectrolytes for Biomacromolecule Detection. *Adv. Mater.* **20,** 2959–2964 (2008).

24. Zhan, R. & Liu, B. Benzothiadiazole-Containing Conjugated Polyelectrolytes for Biological Sensing and Imaging. *Macromol. Chem. Phys.* **216,** 131–144 (2014).

25. Nilsson, K. P. R. & Hammarström, P. Luminescent Conjugated Polymers: Illuminating the Dark Matters of Biology and Pathology. *Adv. Mater.* **20,** 2639–2645 (2008).

26. Feng, G., Ding, D. & Liu, B. Fluorescence bioimaging with conjugated polyelectrolytes. *Nanoscale* **4,** 6150 (2012).

27. Klingstedt, T. & Nilsson, K. P. R. Conjugated polymers for enhanced bioimaging. *Biochim. Biophys. Acta* **1810,** 286–296 (2011).

28. Herland, A. *et al.* Electroactive Luminescent Self-Assembled Bio-organic Nanowires: Integration of Semiconducting Oligoelectrolytes within Amyloidogenic Proteins. *Adv. Mater.* **17,** 1466–1471 (2005).

29. Klingstedt, T. *et al.* Synthesis of a library of oligothiophenes and their utilization as fluorescent ligands for spectral assignment of protein aggregates. *Org. Biomol. Chem.* **9,** 8356–8370 (2011).

30. Hinks, J. *et al.* Modeling Cell Membrane Perturbation by Molecules Designed for Transmembrane Electron Transfer. *Langmuir* **30,** 2429–2440 (2014).

31. Sakai, N., Gerard, D. & Matile, S. Electrostatics of Cell Membrane Recognition: Structure and Activity of Neutral and Cationic Rigid Push-Pull Rods in Isoelectric, Anionic, and Polarized Lipid Bilayer Membranes. *J. Am. Chem. Soc.* **123,** 2517–2524 (2001).

32. Wang, Y. *et al.* Effect of Polymer Chain Length on Membrane Perturbation Activity of Cationic Phenylene Ethynylene Oligomers and Polymers. *Langmuir* **27,** 10770–10775 (2011).

33. Hill, E. H., Stratton, K., Whitten, D. G. & Evans, D. G. Molecular Dynamics Simulation Study of the Interaction of Cationic Biocides with Lipid Bilayers: Aggregation Effects and Bilayer Damage. *Langmuir* **28,** 14849–14854 (2012).

34. Yan, P., Xie, A., Wei, M. & Loew, L. M. Amino(oligo)thiophene-Based Environmentally Sensitive Biomembrane Chromophores. *J. Org. Chem.* **73,** 6587–6594 (2008).

35. Thomas, A. W., Henson, Z. B., Du, J., Vandenberg, C. A. & Bazan, G. C. Synthesis, characterization, and biological affinity of a near-infrared-emitting conjugated oligoelectrolyte. *J. Am. Chem. Soc.* **136,** 3736–3739 (2014).

36. Gwozdzinska, P. *et al*. Phenylenevinylene conjugated oligoelectrolytes as fluorescent dyes for mammalian cell imaging. *Chem. Commun.* **50,** 14859–14861 (2014).

37. Cieślar-Pobuda, A. *et al*. Cell type related differences in staining with pentameric thiophene derivatives. *Cytometry* **85,** 628–635 (2014).

38. Schmid, S., Schneider, E. M. & Brier, E. Self-organizing carbohydrate-oligothiophene-hybrids for eukaryotic membrane-labelling. *J. Mater. Chem. B* **2** 7861–7865 (2014).

39. Dal Molin, M. *et al*. Fluorescent Flippers for Mechanosensitive Membrane Probes. *J. Am. Chem. Soc.* **137,** 568–571 (2015).

40. Palamà, I. *et al*. Live-Cell-Permeant Thiophene Fluorophores and Cell-Mediated Formation of Fluorescent Fibrils. *J. Am. Chem. Soc.* **133,** 17777–17785 (2011).

41. Klingstedt, T. *et al*. The Structural Basis for Optimal Performance of Oligothiophene-Based Fluorescent Amyloid Ligands: Conformational Flexibility is Essential for

Spectral Assignment of a Diversity of Protein Aggregates. *Chem. Eur. J.* **19,** 10179–10192 (2013).

42. Wigenius, J., Persson, G., Widengren, J. & Inganäs, O. Interactions Between a Luminescent Conjugated Oligoelectrolyte and Insulin During Early Phases of Amyloid Formation. *Macromol. Biosci.* **11,** 1120–1127 (2011).

43. Herland, A. *et al.* Synthesis of a Regioregular Zwitterionic Conjugated Oligoelectrolyte, Usable as an Optical Probe for Detection of Amyloid Fibril Formation at Acidic pH. *J. Am. Chem. Soc.* **127,** 2317–2323 (2005).

44. Duarte, A., Chworos, A., Flagan, S. F., Hanrahan, G. & Bazan, G. C. Identification of Bacteria by Conjugated Oligoelectrolyte/Single-Stranded DNA Electrostatic Complexes. *J. Am. Chem. Soc.* **132,** 12562–12564 (2010).

45. Li, H. & Bazan, G. C. Conjugated Oligoelectrolyte/ssDNA Aggregates: Self-Assembled Multicomponent Chromophores for Protein Discrimination. *Adv. Mater.* **21,** 964–967 (2009).

46. Cai, L. *et al.* Butterfly-Shaped Conjugated Oligoelectrolyte/Graphene Oxide Integrated Assay for Light-Up Visual Detection of Heparin. *Anal. Chem.* **83,** 7849–7855 (2011).

47. Yan, H., Catania, C. & Bazan, G. C. Membrane-Intercalating Conjugated Oligoelectrolytes: Impact on Bioelectrochemical Systems. *Adv. Mater.* **27,** 2958–2973 (2015).

48. Du, J., Catania, C. & Bazan, G. C. Modification of Abiotic–Biotic Interfaces with Small Molecules and Nanomaterials for Improved Bioelectronics. *Chem. Mater.* **26,**

686–697 (2014).

49. Wang, V. B. *et al*. Improving charge collection in Escherichia coli-carbon electrode devices with conjugated oligoelectrolytes. *Phys*. *Chem*. *Chem*. *Phys*. **15,** 5867–5872 (2013).

50. Hou, H. *et al*. Conjugated oligoelectrolytes increase power generation in E. coli microbial fuel cells. *Adv*. *Mater*. **25,** 1593–1597 (2013).

51. Thomas, A. W. *et al*. A lipid membrane intercalating conjugated oligoelectrolyte enables electrode driven succinate production in Shewanella. *Energy Environ*. *Sci*. **6,** 1761–1765 (2013).

52. Kirchhofer, N. D. *et al.* The conjugated oligoelectrolyte DSSN+ enables exceptional coulombic efficiency via direct electron transfer for anode-respiring Shewanella oneidensis MR-1-a mechanistic study. *Phys. Chem. Chem. Phys.* **16,** 20436–20443 (2014).

53. Garner, L. E., Thomas, A. W., Sumner, J. J., Harvey, S. P. & Bazan, G. C. Conjugated oligoelectrolytes increase current response and organic contaminant removal in wastewater microbial fuel cells. *Energy Environ*. *Sci*. **5,** 9449–9452 (2012).

54. Sivakumar, K. *et al*. Membrane permeabilization underlies the enhancement of extracellular bioactivity in Shewanella oneidensis by a membrane-spanning conjugated oligoelectrolyte. *Appl*. *Microbiol*. *Biotechnol*. **98,** 9021–9031 (2014).

55. Thomas, A. W., Catania, C., Garner, L. E. & Bazan, G. C. Pendant ionic groups of conjugated oligoelectrolytes govern their ability to intercalate into microbial

membranes. *Chem. Commun.* **51,** 9294–9297 (2015).

56. Woo, H. Y. *et al.* Solvent Effects on the Two-Photon Absorption of Distyrylbenzene Chromophores. *J. Am. Chem. Soc.* **127,** 14721–14729 (2005).

1. Facilitating Microbial Electrosynthesis with a COE

1.1. Introduction

The use of microorganisms to catalyze electrically driven chemical reactions, known as microbial electrosynthesis,[1-3] has applications in bioremediation[4-6] and is a promising strategy to produce biofuels.[7-9] The success of such technologies ultimately relies on electrons transferring from an electrode into bacteria across insulating lipid membranes: a difficult feat owing to the limited number of applicable microorganisms that have been shown capable of such a process. The microbe–electrode interface thus becomes a key area of focus for improving the performance and expanding the scope of biocatalyzed, electrode driven reactions and some effort has been put forth in electrode engineering for this very purpose.[10]

An alternate approach is to use a conjugated oligoelectrolyte (COE) to modify the microbe. In fact, **DSSN+** already has proven useful in electron extraction from microorganisms,[11-13] what if it could be used to inject electrons as well? It has been presumed that **DSSN+** facilitates a more intimate electronic interaction between microorganisms and electrodes by enabling a transmembrane extracellular charge transfer mechanism. A similar effect has been achieved via membrane modication of *Desulfovibrio desulfuricans* with Pd nanoparticles that improve extracellular electron transfer.[14] Electrical wiring of microorganisms with electrodes via osmium redox polyelectrolytes has also been demonstrated.[15]

Microorganisms that possess innate extracellular electron transfer mechanisms have found utility in a variety of bioelectronics devices due to their intrinsic ability to interact with electrodes. A notable example is Geobacter sulfurreducens, due to its relevance to MFC applications.[16] It is worth pointing out that the majority of the work regarding microbe–electrode interactions has focused on processes in which electrons are transferred from microbe to electrode, such as the anode localized redox reactions in MFCs. [17,18] Microbial systems that function on the basis of electron transfer from electrodes to microbes have received more recent attention.[1,19,20] An example of such a system describes the consumption of CO_2 and production of acetate by Sporomusa ovata.[3,21]

Examples of cellular growth, metabolism, and enzymatic processes that can be influenced or driven by electron donation from electrodes to microorganisms have been achieved by multiple approaches. One early example describes the influence of an applied negative potential on *Clostridium acetobutylicum* fermentation products when using methyl viologen as an electron shuttle.[22] Neutral red has also been used in a similar manner to drive the growth and metabolism of *Actinobacillus succinogens*.[21] The diffusion based mediators[23] employed in these cases, however, may exhibit drawbacks when applied broadly, such as redox incompatibility,[24,25] cellular uptake that does not result in electron transfer, possible toxicity or solubility problems,[26] and diffusion limited kinetics.[27] Genetic engineering[28] and adaptive evolution[29] have also been examined for modulating electronic interactions between microorganisms and electrodes. It is also worth noting that the mechanisms of electron transfer into and out of microorganisms have been shown to be physically and energetically different in some instances.[2,30]

The bacteria used in this study, *Shewanella oneidensis* MR-1 is well known for its extracellular electron transfer to external acceptors[31] but its ability to accept electrons is an emerging area of research.[32,33] In the next section is described days-long electrode driven succinate production by *Shewanella* facilitated by addition of the membrane-intercalating conjugated oligoelectrolyte **DSSN+**.

1.2. Electrode Driven Succinate Production with DSSN+

In this section we describe a strategy to modify the microbe/electrode interface with a synthetic molecule in order to achieve electrode driven production of succinate by *Shewanella*. We first describe the effect of various **DSSN+** concentrations on the current injected into *Shewanella*. An illustration of the "H-cell" bioelectrochemical device (BED)[34] employed in this study that highlights the key electrochemical and bioelectrochemical processes is shown in Figure 1.1. *Shewanella* was cultured in freshwater media[35] with a lactate electron donor and fumarate electron acceptor to stationary phase at an optical density at 600 nm (OD_{600nm}) of ~0.5, isolated via centrifuge and re-suspended in sterile and oxygen-free freshwater medium. H-cells containing deoxygenated freshwater medium devoid of amino acids and vitamins and supplemented with 40 mM fumarate (cathode chamber only) operating under an applied bias of -300 mV vs. SHE were inoculated with the concentrated *Shewanella* suspension on day 0 to an OD_{600nm} of 0.5 and the current was monitored over time (Figure 1.1A, top). The cumulative number of electrons transferred by the cathodes was calculated, via integration of the current vs. time traces; these results are shown at the bottom of Figure 1.1A (solid lines) and are correlated with the number of

electrons appearing in the reduced product succinate (dotted lines), which was analyzed by periodic HPLC samples.

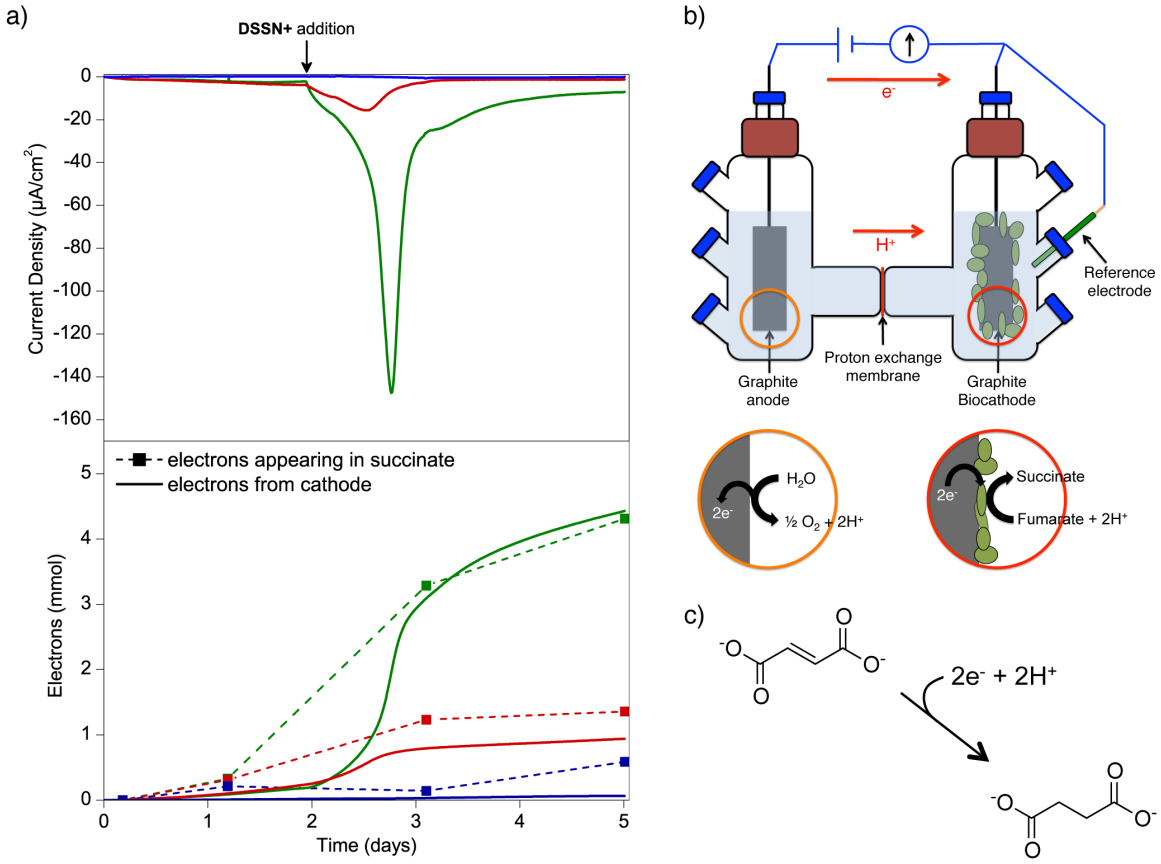

Figure 1.1. (a, top) Current vs. time traces of H-cells inoculated with concentrated *Shewanella* on day 0 and run in the presence of 0 M (blue), 1 μM (red), and 10 μM (green) **DSSN+**. **DSSN+** addition (not including blue trace) has been indicated. Steady current was established for an hour before the addition of cells and this baseline was subtracted from all curves. (bottom) The corresponding cumulative number of electrons transferred as a function of time determined by integration of the current vs. time traces (solid) and number of electrons appearing in succinate determined by HPLC analysis of aliquots from cathode chambers (dashed). (b) The 'H-cell' apparatus used in this study. A constant bias is applied to the cathode (-300 mV vs. SHE) and current is monitored via potentiostat. *Shewanella* modified with **DSSN+** accepts electrons from the cathode and subsequently converts fumarate to succinate. Charge balance is maintained by the oxidation of water at the anode. (c) The reduction of fumarate to succinate.

Negligible current response is observed for a sterile control in which **DSSN+** was added to a concentration of 5 μM (Figure 2.1) and a *Shewanella* control to which no **DSSN+** was added (Figure 2.1a, blue). These control experiments confirm the difficulty of injecting electrons into *Shewanella* and that **DSSN+** does not participate in electrochemical processes under these experimental conditions. As seen in Figure 1.1, an immediate increase in current was observed upon **DSSN+** addition to final concentrations of 1 μM and 10 μM that increased over a period of ~12 hours, ultimately reaching maxima of −16 μA cm^{-2} and −150 μA cm^{-2}, respectively. An approximately ten-fold increase in maximum current and over four-fold increase in cumulative electrons injected is observed between 1 and 10 μM **DSSN+**. The succinate produced in all cases correlates well with the number of electrons injected. In the 0 μM and 1 μM experiments there is more succinate produced than current injected which may, in part, be explained by the ability of *Shewanella* to store excess electrons during growth.[36,37] This set of experiments demonstrates the ability of **DSSN+** to facilitate electron injection over a long timescale into an organism that is otherwise incapable of utilizing an electrode as a sole electron source under these experimental conditions.

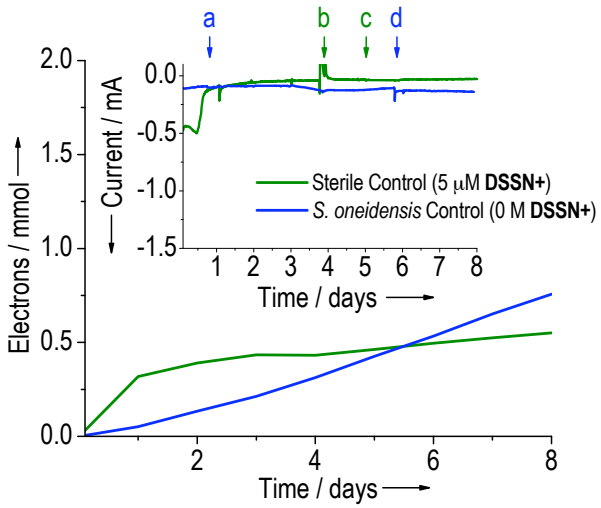

Figure 1.2. Cumulative electrons transferred and current vs. time (inset) data corresponding to a sterile control to which 5 μM **DSSN+** was added (green) and a *Shewanella* control, run in the presence of fumarate (40 mM) and absence of **DSSN+** (blue). Inset labels: a) inoculation of *Shewanella* control; b) addition of 40 mM fumarate to sterile control; c) addition of 5 μM **DSSN+** to sterile control; d) injection of additional fumarate into *Shewanella* control. Potential was -300 mV vs. SHE.

A subsequent experiment was run to confirm the effect of **DSSN+** on the current injected into *Shewanella* and to probe the influence of planktonic cells (Figure 1.3). *Shewanella* was again initially grown on lactate and fumarate, centrifuged, resuspended in fresh medium and injected into the cathode chamber of an H-cell (day 0) with 40mM fumarate operated at -300mV vs. SHE. There is little to no current observed until day 3 when **DSSN+** is added to the cathode chamber to a final concentration of 5 μM and the current steadily increases, reaching a maximum of -13 μA cm^{-2} near day 6. On day 7 the medium was exchanged to remove planktonic cells and fumarate was replenished, after which the current returns to levels near the maximum but begins to decline rapidly. Planktonic cells were centrifuged and resuspended in fresh medium and replaced back into the cathode chamber on day 8 after which the current increases steadily until day 9 when it

begins to level off around -18 μA cm^{-2}. This response is most reasonably attributed to electrons accepted by the planktonic cells, presumably upon collision with the electrode.

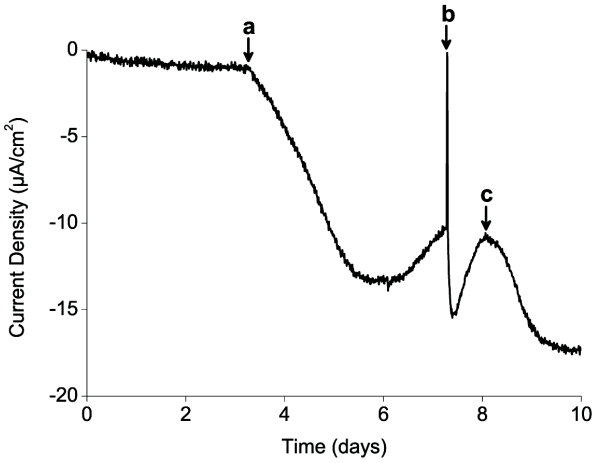

Figure 1.3. Current vs. time of an H-cell run employing *Shewanella* poised at -300 mV vs. SHE in the presence of fumarate (initially 40 mM). (a) Addition of **DSSN+** to a final concentration of 5 μM. (b) Medium exchange with removal of planktonic cells and addition of fumarate to 40 mM. (c) Replacement of planktonic cells.

Confocal laser scanning microscopy of the cathode after day 10 from the experiment corresponding to Figure 1.3 was carried out utilizing the emission response of **DSSN+** following direct excitation at 488 nm (no additional fluorescent dye was added). The results shown in Figure 1.4 indicate the presence of a sparse biofilm composed of a mostly incomplete monolayer of cells with **DSSN+** successfully incorporated throughout. Additionally, the incomplete coverage leaves open the possibility of planktonic cells interacting with exposed electrode surface. Figure 1.4b shows individual intact cells with emission profiles illustrating accumulation of **DSSN+**. It is reasonable to assume that **DSSN+** has accumulated within the lipid membranes based on previous results,[3] but it

should be noted that no direct evidence of this is presented here, nor is it ruled out that **DSSN+** is accumulating inside the cells.

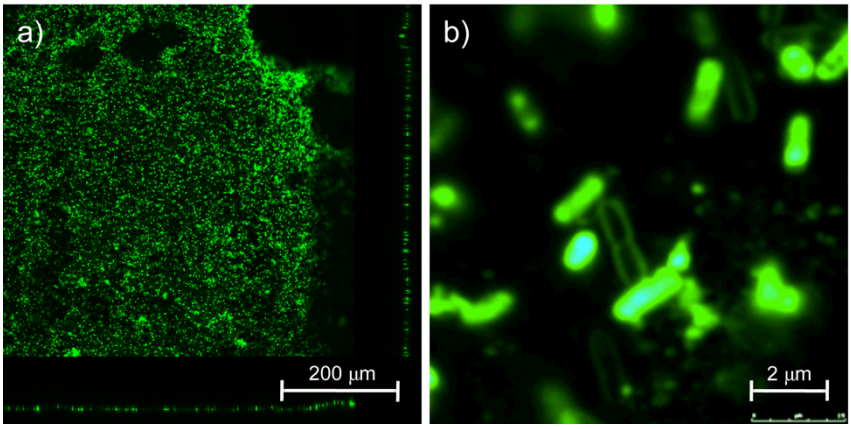

Figure 1.4. Confocal images of a graphite biocathode populated by **DSSN+** modified *Shewanella* following H-cell operation. The fluorescence response is obtained via direct excitation of **DSSN+** at 488 nm. (a) Z-stack image of the electrode surface with bottom and right margins displaying side views showing incomplete surface coverage by a monolayer of cells. Vertical and horizontal scales are equal. (b) Single slice image showing individual *Shewanella* cells on the electrode surface.

In summary, we have shown that the membrane-intercalating conjugated oligoelectrolyte **DSSN+** enables *Shewanella* to use a graphite electrode as the sole electron donor for the reduction of fumarate. Addition of **DSSN+** to operating BEDs results in an immediate and long-term current response with the number of electrons injected by the electrode showing good correlation with the electrons appearing in the reduced metabolic product succinate. The maximum current and cumulative number of electrons injected depends on the concentration of **DSSN+**, consistent with the direct role of this molecule in facilitating charge transfer. Confocal microscopy analysis of electrodes following BED operation shows that **DSSN+** reaches and remains in the *Shewanella* throughout operation. It should be mentioned that **DSSN+** at low micromolar concentrations has no effect on the

growth of *Shewanella* (Figure 1.5). These findings along with the fact that **DSSN+** is not acting as a traditional electron shuttle because it does not undergo reversible redox,[13] support a mechanism wherein the conjugated oligoelectrolye facilitates electron transport from the electrode into charge acceptor sites within the outer membrane or periplasm. Due to the large number of redox sites in and around the *Shewanella* membranes, including the well-studied Mtr respiratory pathway,[31,36,38,39] and localization of fumarate reductase in the periplasm,[40] it is reasonable to propose that electrons may be transferred to such sites. Such a process would not require **DSSN+** to span both cell membranes.

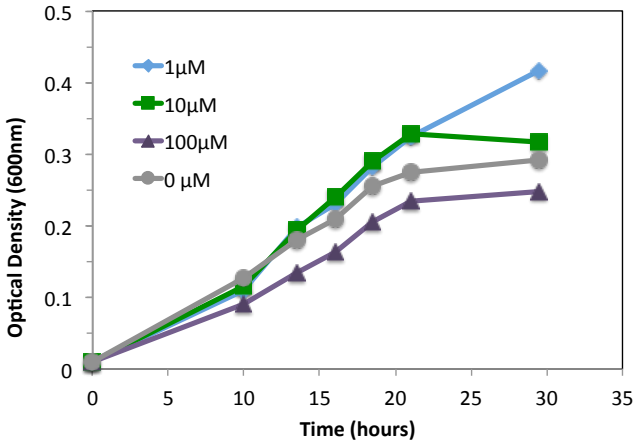

Figure 1.5. Growth curves at 30 °C of *Shewanella* in anaerobic freshwater medium supplemented with 40 mM lactate and 40mM fumarate. Culture tubes contained indicated concentrations of **DSSN+** at the time of inoculation. Optical density was monitored at 600 nm. Points are averages of 4 replicate cultures.

1.3. A Native Electron Conduit: The Mtr Pathway

In the previous section it was established that **DSSN+** enables electrode driven fumarate reduction in *Shewanella* that is otherwise incapable of utilizing a graphite electrode as an electron source. Shortly after these initial findings, Ross and coworkers descried this

exact process in *Shewanella*, unassisted by **DSSN+** or other additives.[32] How could their system, which is analogous to our controls without **DSSN+**, be consuming current and reducing fumarate to succinate? In their experiments, *Shewanella* biofilms were grown first under oxidizing conditions, essentially a microbial fuel cell complete with a carbon and electron source (lactate) and an electron acceptor (graphite electrode). Under these conditions, *Shewanella* is well known to thrive, form biofilms, and perhaps most importantly produce redox mediators like riboflavin. [41-43] In fact, Ross and coworkers implicated riboflavin in conjunction with the Mtr respiratory pathway as the conduit for inward electron flux in *Shewanella* in their experiments. That the Mtr pathway and riboflavin would be responsible for inward electron flow in *Shewanella* is interesting though not surprising given its prominent role in outward electron flow.[38,39] In our experiments, cells were grown without an electrode, rinsed and injected into the BED poised at a reducing potential. Thus, any soluble flavins produced during growth were washed away prior to our experiments.

In order to directly address the role (if any) of the Mtr pathway in **DSSN+** -assisted electrosynthesis in *Shewanella*, BEDs were once again employed. Two critical proteins in this complex are an outer membrane bound, heme-containing cytochrome MtrC and non-heme structural protein MtrB that spans the outer membrane and is responsible for the localization of MtrC and other cytochromes.[39] The question is, can **DSSN+** induce electrode driven fumarate reduction in *Shewanella* mutants deficient in these critical Mtr proteins? The answer, displayed in Figure 1.6, is yes. BEDs containing either wildtype (wt) Shewanella or deletion mutants ΔMtrC or ΔMtrB rinsed from their growth medium were poised at -300 mV vs. SHE and run with and without 10 μM **DSSN+**. Cumulative coulomb

plots derived from the chronoamperometry experiments show that the deletion mutants perform at least as well as the wt with **DSSN+**. Furthermore, the amount of succinate produced correlates well with the current consumed for all devices employing **DSSN+**. As expected all devices without **DSSN+** consumed little to no current and produced only small amounts of succinate. That the Mtr deletion mutants with **DSSN+** work just as well as wt with **DSSN+** suggests that that the Mtr proteins are not involved in the inward electron flux facilitated by **DSSN+**. In other words, **DSSN+** is involved in a completely novel pathway for electrode driven fumarate reduction in *Shewanella.*

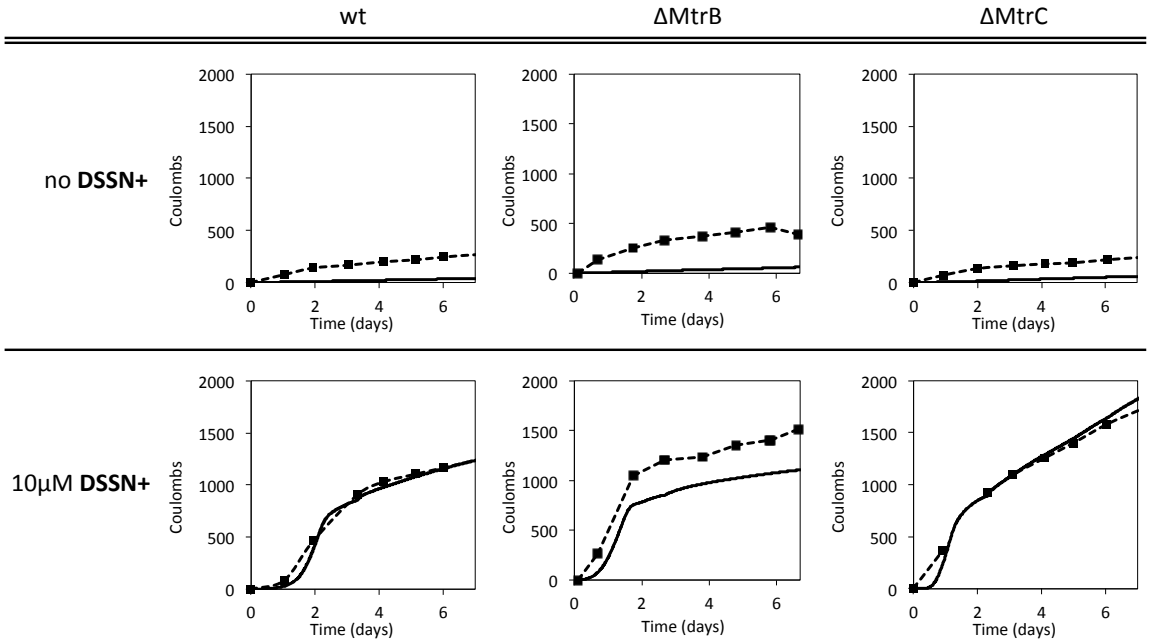

Figure 1.6. Cumulative coulombs vs. time measured during operation of wildtype (wt) *Shewanella* and deletion mutant BEDs poised at -300 mV vs. SHE. Control devices in the top row received no **DSSN+** whereas those in the bottom row received 10 μM **DSSN+** shortly after inoculation on day 0. Coulombs were calculated by integration of the current during chronoamperometry and from succinate production as monitored by HPLC (assuming a 2 electron reduction of fumarate).

In order to compare **DSSN+** to riboflavin under our experimental conditions, *Shewanella* was again cultured in with 40 mM lactate and fumarate, rinsed several times and

injected into BEDs containing only freshwater medium and 40mM fumarate. Either 10 μM riboflavin or 10 μM **DSSN+** was added shortly following inoculation and the resulting chronoamperometry traces are shown in Figure 1.7. Briefly, addition of riboflavin caused an immediate and steady current response at around -50 μA cm^{-2} that remained fairly constant, indicative of a steady state, diffusion-limited process expected for a soluble redox mediator. This demonstrates that our experimental conditions can facilitate *Shewanella* (unmodified by **DSSN+**) to use an electrode as an electron donor if exogenous riboflavin is added. In contrast, addition of **DSSN+** resulted in a very gradual initial increase in current that took 1.4 days to reach a current density of -50 μA cm^{-2} equal to that of the riboflavin device, but continued increasing to a max of -155 μA cm^{-2} by day 2. Besides the fact that **DSSN+** cannot be reduced or oxidized in the potential range of these BEDs,[13] the effect of **DSSN+** on the current consumption in the BED is not immediate like that of riboflavin and is an indication that it is not acting as a simple redox mediator.

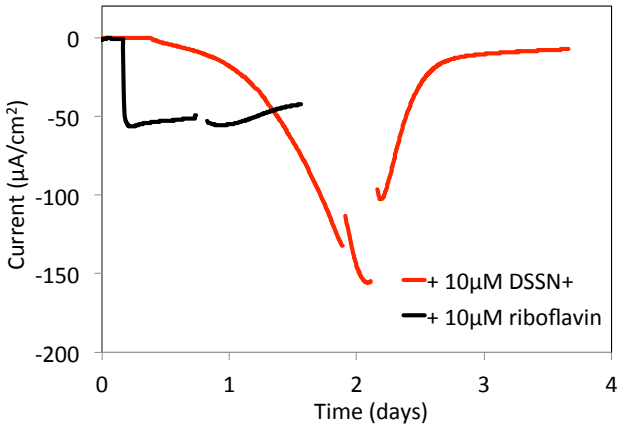

Figure 1.7. Chronoamperometry of *Shewanella* BEDs poised at -300 mV vs. SHE employing either 10 μM riboflavin or 10 μM **DSSN+** that were added immediately following inoculation. Discontinuities in the data are due to stoppages in device operation for analysis by cyclic voltammetry. The riboflavin device was discontinued after ~1.5 days.

Near maximum current consumption, each BED from Figure 1.7 was subjected to slow scan rate turnover cyclic voltammetry (noted by breaks in the chronoamperometry plots), the results of which are shown in Figure 1.8 (top). Both traces feature a large catalytic reduction wave indicative of metabolic turnover (fumarate to succinate), with the riboflavin trace displaying a reversible peak at each edge of the catalytic wave (-0.21 mV and -0.31 mV vs. SHE), characteristic of reversible electron transfer. From the first derivative plots (Figure 1.8, bottom) one can observe an 80 mV more positive midpoint potential for the catalytic wave from **DSSN+**: 150 mV versus 230 mV for riboflavin. This large positive shift indicates a unique and more energetically favorable electron transfer pathway facilitated by **DSSN+** that is not active in riboflavin/Mtr-mediated electron injection.

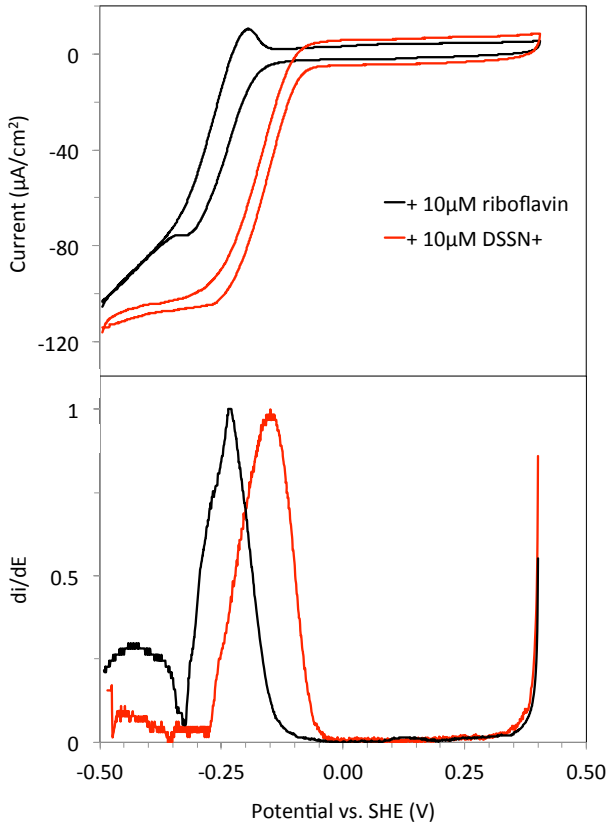

Figure 1.8. Turnover cyclic voltammograms (top) and corresponding first derivative plots (bottom) of *Shewanella* BEDs supplemented with 40mM fumarate to which either 10 μM riboflavin or 10 μM **DSSN+** was added at the beginning of device operation. Voltammograms were acquired near peak current of chronoamperometry operation poised at -300 mV vs. SHE. The scan rate was 2 mV/s.

1.4 Is DSSN+ Lysing Cells?

Instead of providing a possible conduit for electron flow into *Shewanella*, it is entirely possible that **DSSN+** is providing a means for intracellular components to escape. The enzyme responsible for fumarate reduction to succinate in this organism is a soluble flavocytochrome c_3 found in the periplasm.[44] It is entirely conceivable that **DSSN+** may disrupt the membrane and release the fumarate reductase into solution where it would be free to interact with the electrode and catalyze succinate production. To begin testing this

hypothesis, it was necessary to demonstrate whethere **DSSN+** could cause total lysis of *Shewanella* cells in solution. Shown in Figure 1.9 is a plot of OD_{600nm} over time of solutions of cells to which either 10 μM **DSSN+** or 500 μM of the detergent Triton X-100 was added. Triton X-100 rapidly lyses the cells as seen by a drastic decrease in OD_{600nm} within the first few minutes after addition. Contrastingly, **DSSN+** does not change the OD_{600nm} as it remains stable along with a control sample of just *Shewanella*, indicating that under these conditions the COE is not lysing the cells. Furthermore, Triton X-100 did not cause a significant current response in BEDs (Figure 1.10) demonstrating that simple lysis by a detergent could not cause the same response as **DSSN+**.

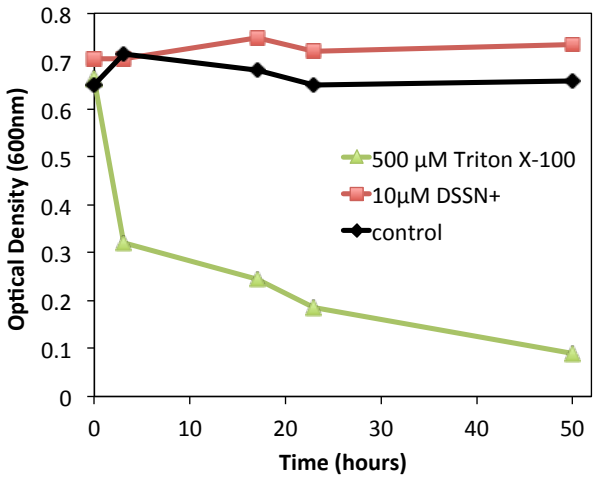

Figure 1.9. Change in OD_{600nm} of stationary phase *Shewanella* cells monitored at 30 °C in freshwater medium supplemented with 40 mM fumarate but without an electron donor, amino acids, or vitamins to mimic conditions in current consumption experiments. Cells were initially grown on lactate and fumarate. Culture tubes contained indicated concentrations of additives at the time of inoculation. Points are averages of 2 replicates. The path length of the culture tubes was 1.6 cm.

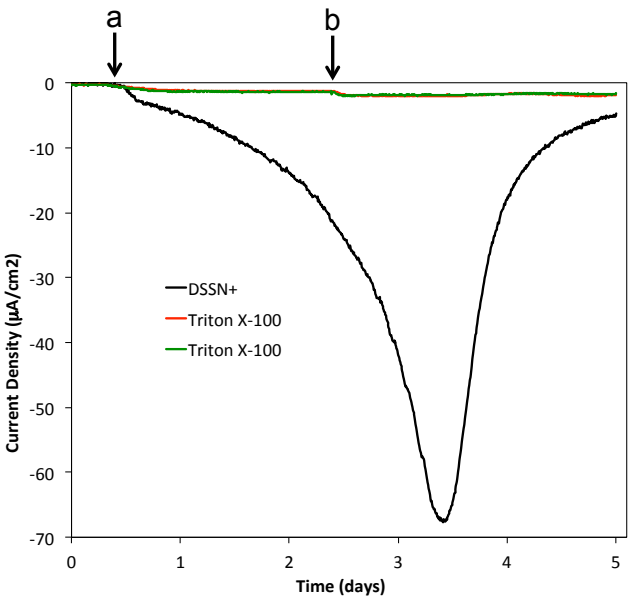

Figure 1.10. Current density vs. time of *Shewanella* BEDs run with 40mM fumarate electron acceptor at -300 mV vs. SHE. BEDs were inoculated at time 0. The red and green traces are duplicate devices treated the same. a) Addition of **DSSN+** (black) and Triton X-100 (red and green) to a final concentration of 5 µM. b) Addition of Triton X-100 to a final concentration of 500 µM (red and green).

1.5 The Role of Biofilm and Planktonic Cells

Previous experiments (Figure 1.3) demonstrated that planktonic cells were contributing to current consumption in *Shewanella* BEDs with **DSSN+**. In order to further probe the contributing components to the current response in our system, a *Shewanella* BED run with 10 µM **DSSN+** was stopped after 1.9 days of operation at a maximum current of -148 µA cm^{-2} (see Figure 1.11A inset, black) and separated into 3 "component devices" consisting of the following: (biofilm) the electrode and attached biofilm from the original device was placed into an BED with fresh medium and 40mM fumarate; (planktonic) the original BED solution was centrifuged, cells were rinsed and injected into a fresh BED with 40mM fumarate; and (supernatant) the cell-free supernatant from the centrifuged planktonic cells

was injected into an empty BED and 10 mM of additional fumarate was added. The results of this experiment are shown in Figure 1.11. Surprisingly, all 3 component devices consumed current. The biofilm showed the largest initial current response at -50 μA cm^{-2} but quickly dropped over the course of ~7 hours to assumed a steady current density between -10 μA cm^{-2} and -13 μA cm^{-2} that held for the remainder of operation (~1.5 days). The planktonic device reached a maximum current density of -23 μA cm^{-2} within an hour that gradually approached zero over the remainder of operation. Most interestingly, however, the supernatant device increased in current density from -15 μA cm^{-2} to -48 μA cm^{-2} over the course of ~2 hours and was the best performing device for the next 12 hours, following a similar trend in current density decline as the planktonic device. Compared to an un-separated control device also run with 10 μM **DSSN+**, the sum of the component devices followed a similar current density profile (Figure 1.11A, inset), indicating that the separation did not severely perturb the individual components and that an accurate analysis of current density contribution was obtained, *i.e.* the sum of the parts equaled the whole.

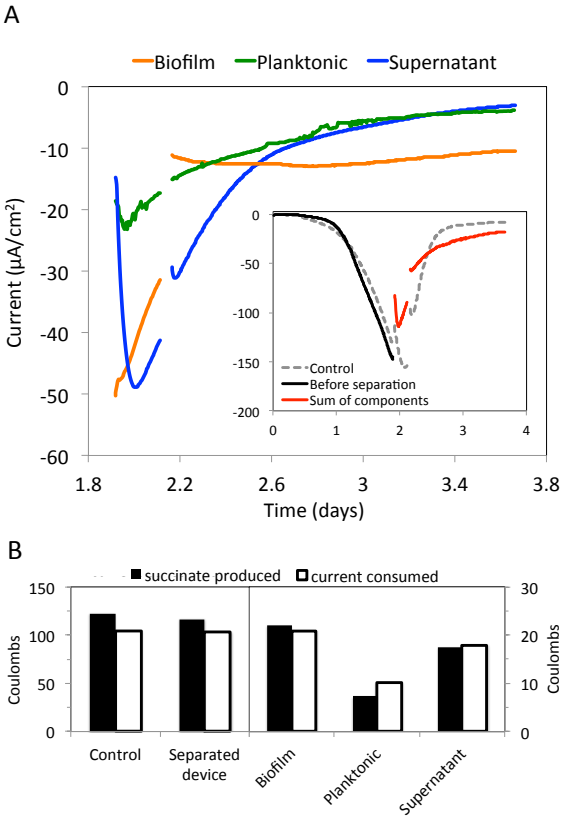

Figure 1.11. (A) Chronoamperometry of a *Shewanella* BED run with 10μM **DSSN+** that was separated into its three components: biofilm, planktonic cells and cell-free supernatant. Inset: Chronoamperometry of the device before separation (black trace), the mathematical sum of the individual components shown in the outset (red trace), and a control device containing 10μM **DSSN+** that was not separated (grey dashed trace). All devices were poised at -300 mV vs. SHE. Axis labels of the outset apply to the inset. Discontinuities in data are indicative of stoppages for analysis by cyclic voltammetry. (B) Total coulombs accumulated by the end of operation for all devices calculated from the current consumed (integration of chronoamperomentry) and the succinate produced as monitored by HPLC (assuming a 2 electron reduction of fumarate). Total coulombs of the "separated device" equals the sum of the individual components and the device before separation.

Figure 1.11B shows the total coulombs consumed during chronoamperometry compared with the total succinate produced (converted to coulombs assuming a 2 electron reduction from fumarate) by the individual devices as measured by HPLC at the end of operation. In general, the amount of current consumed matched well with the succinate produced in all

cases, which is indicative of the anticipated electrode-drive metabolic reduction of fumarate. Not anticipated, however was the succinate production, 90 μmol in total, by the cell-free supernatant, compared to 40 μmol and 110 μmol produced by the planktonic and biofilm cells, respectively. Succinate production in the supernatant indicates the presence of a catalyst capable of using electrons donated by the electrode for fumarate reduction, most likely the periplasmic fumarate reductase from *Shewanella*. Previous work with a related fumarate reductase, Ifc_3, isolated from *Shewanella frigidiemarina* and adsorbed onto graphite electrodes showed that this enzyme was capable of electrode driven fumarate reduction.[45] In fact the midpoint potential for the catalytic reduction observed in cyclic voltammograms in this study was -173 mV vs. SHE, close to the -150 mV vs. SHE midpoint potential observed in Figure 1.8 for the **DSSN+** device. The fact that fumarate reductase resides in the supernatant suggests outer membrane disruption and/or induced secretion of the enzyme by **DSSN+**.

1.6 DSSN+/Electrode Interaction

In order to determine if cell staining with **DSSN+** is sufficient for electron injection, *Shewanella* cultures were stained with 10μM **DSSN+** for 30 minutes at room temperature after over night growth, rinsed of any excess **DSSN+** and injected into two BEDs. This means that there was no **DSSN+** present in the device, only what had incorporated into the cells during staining outside of the device was present. Then only one device was supplemented with an addition 10μM **DSSN+** injected directly into the device solution. Surprisingly, Figure 1.12 shows that these two devices behaved very differently. The BED

that received no supplemental **DSSN+** (Figure 1.12, red trace) did not produce a current response over the duration of the experiment (~5.5 days). Confocal fluorescence microscopy of the working electrode of the un-supplemented device after operation (Figure 1.12 inset) confirms a sub-monolayer of cells containing **DSSN+** that appears indistinguishable from previous experiments where **DSSN+** was added to the BED and a current response was observed (Figure 1.4). The BED that received supplemental **DSSN+ (**Figure 1.12, blue trace), displayed a response similar to what was seen in previous experiments, steadily increasing in current over the course of ~1.5 days, reaching a maximum current density of ~56 μA cm^{-2} before slowly declining back to baseline over the next 3 days. This indicates the necessity for free **DSSN+** in the BED solution and suggests that it may also be interacting with a non-biological component of the BED to promote electron injection.

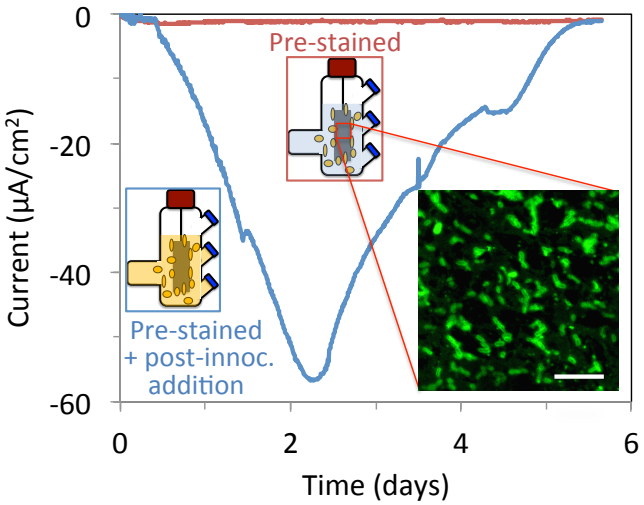

Figure 1.12. Chronoamperometry of two BEDs poised at -300 mV vs. SHE employing *Shewanella* that were pre-stained with 10μM **DSSN+** and rinsed prior to injection into the device. One device then received an injection of **DSSN+** to a final concentration of 10 μM immediately following injection of the cells (blue trace). Illustrations of the working electrode chambers depicting both conditions are included, with orange color representing components containing **DSSN+**. Inset: Confocal fluorescence micrograph of the electrode of the "Pre-stained" device at the end of operation. Fluorescence signal is attributed to cells stained with **DSSN+**. Scale bar is 10 μm.

It was hypothesized that the non-biological component interacting with **DSSN+** must be the graphite electrode and that **DSSN+** in solution is adsorbing onto the electrode in order to promote electron injection into *Shewanella*. A logical question then becomes is **DSSN+** adsorption onto graphite electrodes sufficient to cause electrode driven fumarate reduction in *Shewanella*? To answer this question, 2 graphite electrodes were "pre-stained" in a 10 μM solution of **DSSN+** for 30 minutes then dipped in fresh medium several times to rinse prior to exposure to *Shewanella* in a fresh BEDs containing no **DSSN+**. The results of this were compared to standard control devices run with no **DSSN+** and 10 μM **DSSN+** added directly to the BED as in the original experiments. The resulting chronoamperometry plots, shown in Figure 1.13, show a current response indicative of fumarate reduction for all devices except

the no **DSSN+** device. The duplicate pre-stained electrode devices quickly reached maximum current densities of ~2.5 and ~7 μA cm^{-2} after only 6 – 7 hours of operation. In contrast, the normal device with **DSSN+** continued to increase past 11 μA cm^{-2} and did not peak by the end of the experiment at 18 hours once the pre-stained devices had already declined to < 1 μA cm^{-2}. This indicates that while electrode adsorption by **DSSN+** is sufficient to cause a current response, this response is greatly diminished compared to when **DSSN+** is allowed to interact with both the cells and the electrode in the BED. So while *Shewanella* staining alone is not sufficient to induce a current response, electrode staining is, and the two conditions combined synergistically enhance current production.

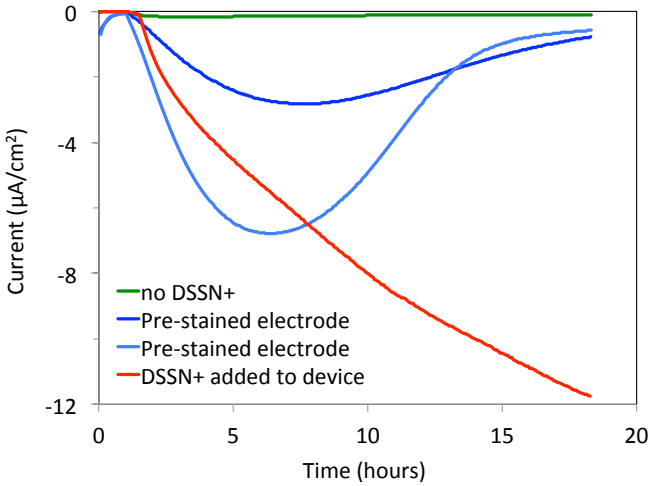

Figure 1.13. Chronoamperometry of *Shewanella* BEDs poised at -300 mV vs. SHE. Prior to injection of cells, the working graphite electrodes of the devices represented by the blue traces were soaked in a separate 10 μM **DSSN+** solution to coat the electrodes with **DSSN+**. No additional **DSSN+** was added to these devices. **DSSN+** was added to a concentration of 10 μM to the device represented by the red trace just after inoculation with *Shewanella* that occurred at time = 2 hours.

Finally, for the purpose of quantifying **DSSN+** adsorption to graphite electrodes, BEDs without *Shewanella* were constructed. 10 μM **DSSN+** in freshwater medium was added to BEDs under 4 conditions: (1) no graphite electrode, (2) a graphite electrode at open circuit, (3) a graphite electrode poised at -300 mV vs. SHE and (4) poised at +400 mV vs. SHE, a potential often used for electron extraction in microbial fuel cells. Aliquots from the 4 reactors were analyzed by UV-vis absorbance at 420 nm, 20 minutes after addition of **DSSN+**. The absorbance of the no electrode device was taken to be the maximum amount of **DSSN+** available for adsorption to the graphite electrode, controlling for any adsorption to other surfaces like the glass vessel, counter and reference electrodes. The results of the experiment are shown in Table 1.1. Aliquots from open circuit and +400 mV electrodes showed ~15 % less absorbance than the no electrode control meaning that about 15 % of the original 10 μM **DSSN+** solution had adsorbed to the graphite electrode. The -300 mV electrode showed more than twice the adsorption at ~35 %. This is perhaps unsurprising considering the 4 cationic charges per **DSSN+** molecule. Normalizing the number of charges adsorbed to the graphite electrode area gives on the order of 10^{15} to 10^{16} charges per cm^2. This calculation becomes relevant when considering reports of cationic biocidal surfaces containing quaternary ammonium groups. It has been found in the case of *E. coli* that a charge density threshold of 10^{14} – 10^{15} charges per cm^2 is sufficient to kill the bacteria through contact most likely through displacement of divalent cations in the outer membrane leading to membrane disruption.[46,47] Thus it is now reasonable to assume that **DSSN+** can adsorb onto graphite electrodes in sufficient amounts to cause damage to cells, which likely plays a role in the electrode driven fumarate reduction.

Table 1.1. DSSN+ adsorption to poised graphite electrodes

	DSSN+ adsorbed to graphite[a]		
Potential vs. SHE	% of total	nmol cm^{-2}	charges[b] cm^{-2}
open circuit	14.9 %	3.13	7.54×10^{15}
+400 mV	14.9 %	3.05	7.35×10^{15}
-300 mV	34.6 %	7.24	1.74×10^{16}

[a] Calculated from UV-vis absorbance measurements of surrounding solution (initially 10 μM) after 20 mins. [b] 4 positive charges per molecule.

1.7 Summary and Proposed Mechanism

In summary microbial electrosynthesis of succinate from fumarate was performed by addition of the COE **DSSN+** and *Shewanella* to BEDs poised at a reducing potential. Close correlation was observed between the number of electrons injected into the BEDs and those found in the reduced product succinate, indicating an efficient process. The Mtr respiratory pathway in *Shewanella*, which has been implicated in both outward[39] and inward[32] electron transfer in published studies is not involved in **DSSN+** mediated inward electron transfer, proven through experiments with Mtr deletion mutants. It was shown that the biofilm, planktonic cells and most telling, the surrounding cell-free solution consumed significant current in a *Shewanella* BED employing **DSSN+**. That the cell-free solution produced succinate using electrons supplied by the electrode indicated the presence of free fumarate reductase that had escaped from the periplasm of the cells. Furthermore, turnover cyclic voltammetry of a working *Shewanella* BED with **DSSN+** produced a curve consistent with catalytic reduction and a midpoint potential within 23 mV of a published value for a

fumarate reductase from *Shewanella*.[45] Cells that were stained with **DSSN+** then rinsed and injected into a BED did not elicit a current response, however, adding exogenous **DSSN+** to the BED solution did, suggesting that **DSSN+** was interacting with the graphite working electrode. This interaction was proven through an experiment indicating that **DSSN+** can adsorb to graphite electrodes in an amount that can create a highly cationic surface capable of causing damage to the cells.[46,47] In addition, BEDs run with electrodes that had been "pre-stained" in a solution of **DSSN+** consumed current, though the response was much smaller than those run with **DSSN+** added directly to the BED solution, indicating a synergistic effect between **DSSN+** adsorbed onto the electrode and incorporated into cells.

In conclusion, a proposed mechanism for the action of **DSSN+** on Shewanella electrosynthesis is presented in Figure 1.14. **DSSN+** is depicted adsorbed to the graphite electrode and also incorporated into the outer memebrane of *Shewanella* (note that it is entirely possible that **DSSN+** may exist in other areas of the cell. See Chapter 4). Cells coming into contact with the graphite electrode either as a temporary (planktonic) or semi-permanent (biofilm) interaction are disrupted to at least an extent to which the periplasmic fumarate reductase can interact directly with the electrode (Figure 1.14A). Once the otuer membrane is disrupted, fumarate reductase may completely exit the cell and exist in solution, free to catalyze electrode driven fumarate reduction to succinate (Figure 1.14B). That **DSSN+** interacts with both graphite electrodes and cells to facilitate bioelectronic communication gives this synthetic strategy the potential to increase the performance of existing bioelectronic systems, increase the number of applicable organisms, and act as an alternative to more complex strategies to induce favorable bioelectronics interactions.

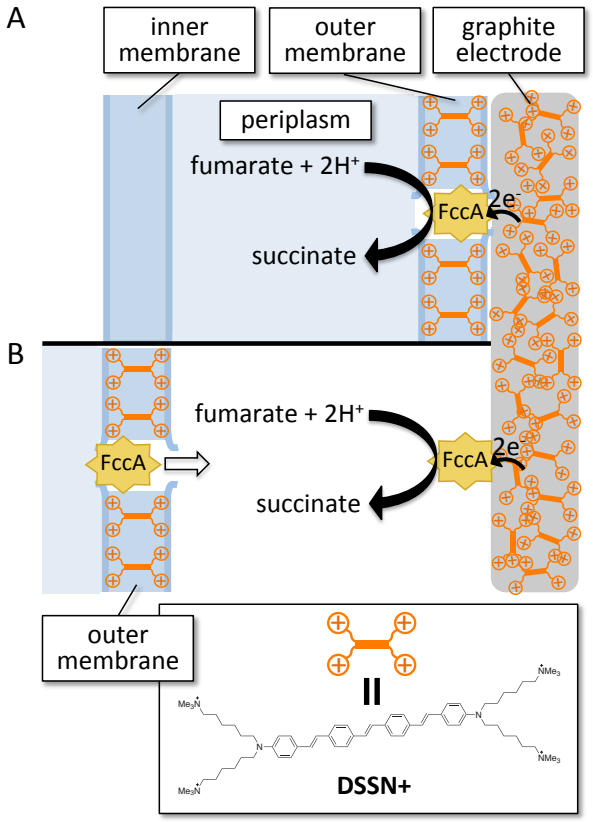

Figure 1.14. Proposed mechanism of electrode-driven succinate production facilitated by outer membrane disruption by **DSSN+**. (A) The outer membranes of cells in the electrode biofilm or planktonic cells coming into contact with the **DSSN+** -coated electrode can be disrupted allowing fumarate reductase (FccA) to interact with the electrode. (B) After membrane disruption by sufficient contact with the highly cationic electrode surface, FccA can be released from the cell where it is free to be reduced by the electrode.

1.8 Experimental

Chemicals and Reagents. All chemicals and reagents were purchased from Aldrich, Fisher, Acros, VWR, or Alpha Aesar and used as received. The conjugated oligoelectrolyte, **DSSN+**, was synthesized as previously described.[13]

Cell Cultures. *Shewanella oneidensis* MR-1 (ATCC 700550) and deletion mutants ΔMtrB and ΔMtrC (a generous gift from the lab of Dr. Derek Lovley) were cultured anaerobically using N_2-CO_2 (80:20) in the freshwater medium described below at 30ºC supplemented with sodium L-lactate (40 mM) electron donor and sodium fumarate (40 mM) electron acceptor. Casamino acids (0.1% w/v) were added as sources of essential amino acids. The freshwater medium employed consisted of the following: $HaHCO_3$, 2.5 g L^{-1}; NH_4Cl, 0.25 g L^{-1}; NaH_2PO_4, 0.06 g L^{-1}; KCl, 0.1 g L^{-1}; vitamin mix, 10 mL L^{-1}; mineral mix, 10 mL L^{-1}. The vitamin mix employed was composed of: biotin, 0.002 g L^{-1}; pantothenic acid, 0.005 g L^{-1}; B-12, 0.0001 g L^{-1}; p-aminobenzoic acid, 0.005 g L^{-1}; thioctic acid (alpha lipoic), 0.005 g L^{-1}; nicotinic acid, 0.005 g L^{-1}; thiamine, 0.005 g L^{-1}; riboflavin, 0.005 g L^{-1}; pyridoxine HCl, 0.01 g L^{-1}; folic acid, 0.002 g L^{-1}. The mineral mix employed was composed of: NTA trisodium salt, 1.5 g L^{-1}; $MgSO_4$, 3 g L^{-1}; $MnSO_4$, 0.5 g L^{-1}; NaCl, 1 g L^{-1}; $FeSO_4 \cdot 7\ H_2O$, 0.1 g L^{-1}; $CaCl_2 \cdot 2\ H_2O$, 0.1 g L^{-1}; $CoCl_2 \cdot 6\ H_2O$, 0.1 g L^{-1}; $ZnCl_2$, 0.13 g L^{-1}; $CuSO_4 \cdot 5\ H_2O$, 0.01 g L^{-1}; $AlK(SO_4)_2 \cdot 12\ H_2O$, 0.01 g L^{-1}; H_3BO_3, 0.01 g L^{-1}; $Na_2MoO_4 \cdot 2\ H_2O$, 0.025 g L^{-1}; $NiCl_2 \cdot 6\ H_2O$, 0.024 g L^{-1}; $Na_2WO_4 \cdot 2\ H_2O$, 0.025 g L^{-1}.

Upon reaching an OD_{600nm} of ~0.5, cells were concentrated via centrifuge at ~8000 x *g* for 10 minutes, re-suspended in freshwater medium and used to inoculate H-cell devices (~5 mL of concentrated cells injected). The medium used in the H-cells and in re-suspending the bacteria after growth were devoid of lactate, casamino acids and vitamins.

H-cell setup and monitoring. H-cells were prepared and constructed as previously described.[48] Working electrodes were 0.5" x 1" x 3" graphite blocks (Mersen USA) with the top 1" x 0.5" face covered in epoxy in order to insulate the lead connection, giving a total

working surface area of 9.5 in^2 or 61.3 cm^2. The working electrode chambers were equipped with Ag/AgCl reference electrodes (Edaq ET072) that were interfaced via embedding within one of the butyl rubber septa that seal each of the three utility ports on each H-cell chamber. Poised potential and current monitoring at the cathode-working electrodes was achieved using a Gamry potentiostat (Reference 600, Series G 300 or Series G 750 models) and multiplexer (model ECM8) setups. Gamry software (Framework Version 5.65, 2011) was used to measure and record the current response at 10 min intervals throughout each experiment. Both chambers were continuously bubbled with N_2-CO_2 (80:20) throughout the experiment.

High performance liquid chromatography (HPLC) analysis. HPLC analysis of organic acid metabolites was performed using an Aminex HPX-87H column (Bio-rad), a 0.004 M H_2SO_4 mobile phase (0.6 mL min^{-1}) and UV detection at 210 nm.

Calculations. Cumulative electrons drawn were determined via integration of current vs. time traces. The electrons appearing in succinate were calculated based on a 2-electron reduction process from values obtained by HPLC analysis of aliquots removed from H-cell cathode chambers on daily intervals.

Confocal Microscopy Analysis. Following device operation the cathodes were removed without touching the surface (by holding the protruding electrical connection). Confocal microscopy analysis of cathode biomass was performed by first dipping the cathodes in freshwater medium to remove any unattached biomass. The electrode surface was then imaged based upon excitation of **DSSN+** via 488 nm argon laser. No additional fluorescent stain was employed. The instrumentation employed was either a Leica TCS SP5

confocal microscope with HCX PL APO CS 20, HCX APO 63 and HCX PL APO CS 100X objectives or an Olympus FluoView 1000 spectral scanning microscope equipped with a 60 x 1.30 silicon oil immersion lens.

1.9 References

1. Lovley, D. R. Powering microbes with electricity: direct electron transfer from electrodes to microbes. *Environ. Microbiol. Rep.* **3,** 27–35 (2010).
2. Rosenbaum, M., Aulenta, F., Villano, M. & Angenent, L. T. Cathodes as electron donors for microbial metabolism: Which extracellular electron transfer mechanisms are involved? *Bioresour. Technol.* **102,** 324–333 (2011).
3. Rabaey, K. & Rozendal, R. A. Microbial electrosynthesis — revisiting the electrical route for microbial production. *Nat. Rev. Micro.* **8,** 706–716 (2010).
4. Gregory, K. B. & Lovley, D. R. Remediation and recovery of uranium from contaminated subsurface environments with electrodes. *Environ. Sci. Technol* **39,** 8943–8947 (2005).
5. Strycharz, S. M. *et al.* Reductive dechlorination of 2-chlorophenol by Anaeromyxobacter dehalogenanswith an electrode serving as the electron donor. *Environ. Microbiol. Rep.* **2,** 289–294 (2010).
6. Ayyasamy, P. M., Chun, S. & Lee, S. Desorption and dissolution of heavy metals from contaminated soil using Shewanella sp. (HN-41) amended with various carbon sources and synthetic soil organic matters. *J. Hazard. Mater.* **161,** 1095–1102 (2009).
7. Ganigué, R., Puig, S., Batlle-Vilanova, P., Balaguer, M. D. & Colprim, J. Microbial electrosynthesis of butyrate from carbon dioxide. *Chem. Commun.* **51,** 3235–3238

(2015).

8. Aulenta, F., Catapano, L., Snip, L., Villano, M. & Majone, M. Linking Bacterial Metabolism to Graphite Cathodes: Electrochemical Insights into the H2-Producing Capability of Desulfovibrio sp. *ChemSusChem* **5,** 1080–1085 (2012).

9. Tremblay, P.-L. & Zhang, T. Electrifying microbes for the production of chemicals. *Front. Microbiol.* **6,** (2015).

10. Guo, K., Prévoteau, A., Patil, S. A. & Rabaey, K. ScienceDirectEngineering electrodes for microbial electrocatalysis. *Curr. Opin. Biotech.* **33,** 149–156 (2015).

11. Garner, L. E., Thomas, A. W., Sumner, J. J., Harvey, S. P. & Bazan, G. C. Conjugated oligoelectrolytes increase current response and organic contaminant removal in wastewater microbial fuel cells. *Energy Environ. Sci.* **5,** 9449–9452 (2012).

12. Kirchhofer, N. D. *et al.* The conjugated oligoelectrolyte DSSN+ enables exceptional coulombic efficiency via direct electron transfer for anode-respiring Shewanella oneidensis MR-1-a mechanistic study. *Phys. Chem. Chem. Phys.* **16,** 20436–20443 (2014).

13. Garner, L. E. *et al.* Modification of the Optoelectronic Properties of Membranes via Insertion of Amphiphilic Phenylenevinylene Oligoelectrolytes. *J. Am. Chem. Soc.* **132,** 10042–10052 (2010).

14. Wu, X. *et al.* A Role for Microbial Palladium Nanoparticles in Extracellular Electron Transfer. *Angew. Chem. Int. Ed.* **50,** 427–430 (2010).

15. Hasan, K., Patil, S. A., Leech, D., Hägerhäll, C. & Gorton, L. Electrochemical

communication between microbial cells and electrodes via osmium redox systems. *Biochem. Soc. Trans.* **40,** 1330–1335 (2012).

16. Nevin, K. P. *et al.* Power output and columbic efficiencies from biofilms of Geobacter sulfurreducens comparable to mixed community microbial fuel cells. *Environ. Microbiol.* **10,** 2505–2514 (2008).
17. Logan, B. E. Exoelectrogenic bacteria that power microbial fuel cells. *Nat. Rev. Micro.* **7,** 375–381 (2009).
18. Schaetzle, O., Barrière, F. & Baronian, K. Bacteria and yeasts as catalysts in microbial fuel cells: electron transfer from micro-organisms to electrodes for green electricity. *Energy Environ. Sci.* **1,** 607–620 (2008).
19. Thrash, J. C. & Coates, J. D. Review: Direct and Indirect Electrical Stimulation of Microbial Metabolism. *Environ. Sci. Technol.* **42,** 3921–3931 (2008).
20. Gregory, K. B., Bond, D. R. & Lovley, D. R. Graphite electrodes as electron donors for anaerobic respiration. *Environ. Microbiol.* **6,** 596–604 (2004).
21. Park, D. H. & Zeikus, J. G. Utilization of electrically reduced neutral red by Actinobacillus succinogenes: physiological function of neutral red in membrane-driven fumarate reduction and energy conservation. *J. Bacteriol.* **181,** 2403–2410 (1999).
22. Kim, T. S. & Kim, B. H. Electron flow shift inClostridium acetobutylicum fermentation by electrochemically introduced reducing equivalent. *Biotechnol. Lett.* (1988).
23. Watanabe, K., Manefield, M., Lee, M. & Kouzuma, A. Electron shuttles in

biotechnology. *Curr. Opin. Biotech.* **20,** 633–641 (2009).

24. Wilkinson, S., Klar, J. & Applegarth, S. Optimizing Biofuel Cell Performance Using a Targeted Mixed Mediator Combination. *Electroanalysis* **18,** 2001–2007 (2006).

25. Park, D. H. & Zeikus, J. G. Electricity generation in microbial fuel cells using neutral red as an electronophore. *Appl. Environ. Microbiol.* **66,** 1292 (2000).

26. Bullen, R. A., Arnot, T. C., Lakeman, J. B. & Walsh, F. C. Biofuel cells and their development. *Biosens. Bioelectron.* **21,** 2015–2045 (2006).

27. Torres, C. I. *et al.* A kinetic perspective on extracellular electron transfer by anode-respiring bacteria. *FEMS Microbiol. Rev.* **34,** 3–17 (2010).

28. Jensen, H. M. *et al.* Engineering of a synthetic electron conduit in living cells. *Proc. Natl. Acad. Sci.* **107,** 19213–19218 (2010).

29. Yi, H. *et al.* Selection of a variant of Geobacter sulfurreducens with enhanced capacity for current production in microbial fuel cells. *Biosens. Bioelectron.* **24,** 3498–3503 (2009).

30. Strycharz, S. M. *et al.* Gene expression and deletion analysis of mechanisms for electron transfer from electrodes to Geobacter sulfurreducens. *Bioelectrochemistry* **80,** 142–150 (2011).

31. Hartshorne, R. S. *et al.* Characterization of an electron conduit between bacteria and the extracellular environment. *Proc. Natl. Acad. Sci. USA* **106,** 22169 (2009).

32. Ross, D. E., Flynn, J. M., Baron, D. B., Gralnick, J. A. & Bond, D. R. Towards Electrosynthesis in Shewanella: Energetics of Reversing the Mtr Pathway for Reductive Metabolism. *PLoS ONE* **6,** e16649 (2011).

33. Okamoto, A., Hashimoto, K. & Nealson, K. H. Flavin Redox Bifurcation as a Mechanism for Controlling the Direction of Electron Flow during Extracellular Electron Transfer. *Angew. Chem. Int. Ed.* **53,** 10988–10991 (2014).

34. Bond, D. R. & Lovley, D. R. Electricity production by Geobacter sulfurreducens attached to electrodes. *Appl. Environ. Microbiol.* **69,** 1548 (2003).

35. Lovley, D. R. *et al.* Geobacter metallireducens gen. nov. sp. nov., a microorganism capable of coupling the complete oxidation of organic compounds to the reduction of iron and other metals. *Arch. Microbiol.* **159,** 336–344 (1993).

36. Schuetz, B., Schicklberger, M., Kuermann, J., Spormann, A. M. & Gescher, J. Periplasmic Electron Transfer via the c-Type Cytochromes MtrA and FccA of Shewanella oneidensis MR-1. *Appl. Environ. Microbiol.* **75,** 7789–7796 (2009).

37. Uría, N., Muñoz Berbel, X., Sánchez, O., Muñoz, F. X. & Mas, J. Transient Storage of Electrical Charge in Biofilms of Shewanella oneidensisMR-1 Growing in a Microbial Fuel Cell. *Environ. Sci. Technol* **45,** 10250–10256 (2011).

38. Coursolle, D. & Gralnick, J. A. Modularity of the Mtr respiratory pathway of Shewanella oneidensis strain MR-1. *Mol. Microbiol.* **77,** 995–1008 (2010).

39. Coursolle, D., Baron, D. B., Bond, D. R. & Gralnick, J. A. The Mtr Respiratory Pathway Is Essential for Reducing Flavins and Electrodes in Shewanella oneidensis. *J. Bacteriol.* **192,** 467–474 (2009).

40. Myers, C. R. Fumarate reductase is a soluble enzyme in anaerobically grown Shewanella putrefaciens MR-1. *FEMS Microbiol. Lett.* **98,** 13–20 (1992).

41. Lanthier, M., Gregory, K. B. & Lovley, D. R. Growth with high planktonic biomass

in Shewanella oneidensisfuel cells. *FEMS Microbiol. Lett.* **278,** 29–35 (2008).

42. Kim, H. J. *et al.* A mediator-less microbial fuel cell using a metal reducing bacterium, Shewanella putrefaciens. *Enzyme Microb. Tech.* **30,** 145–152 (2002).

43. Brutinel, E. D. & Gralnick, J. A. Shuttling happens: soluble flavin mediators of extracellular electron transfer in Shewanella. *Appl. Microbiol. Biotechnol.* **93,** 41–48 (2011).

44. Reid, G. A., Miles, C. S., Moysey, R. K., Pankhurst, K. L. & Chapman, S. K. Catalysis in fumarate reductase. *Biochim. Biophys. Acta* **1459,** 310–315 (2000).

45. Butt, J. N., Thornton, J., Richardson, D. J. & Dobbin, P. S. Voltammetry of a Flavocytochrome c3: The Lowest Potential Heme Modulates Fumarate Reduction Rates. *Biophys. J.* **78,** 1001–1009 (2000).

46. Kugler, R. Evidence of a charge-density threshold for optimum efficiency of biocidal cationic surfaces. *Microbiology* **151,** 1341–1348 (2005).

47. Murata, H., Koepsel, R. R., Matyjaszewski, K. & Russell, A. J. Permanent, non-leaching antibacterial surfaces—2: How high density cationic surfaces kill bacterial cells. *Biomaterials* **28,** 4870–4879 (2007).

48. Nevin, K. P., Woodard, T. L., Franks, A. E., Summers, Z. M. & Lovley, D. R. Microbial electrosynthesis: feeding microbes electricity to convert carbon dioxide and water to multicarbon extracellular organic compounds. *mBio* **1,** e00103– 10 (2010).

2. Synthesis, Characterization and Biological Affinity of a Near IR Emitting Conjugated Oligoelectrolyte

2.1 Introduction

DSSN+ and several structural analogs have been used to increase the performance of various bioelectronics systems such as microbial fuel cells[1-3] and microbial electrosynthesis devices.[4] This increase in the flow of electron equivalents between microorganisms and electrodes is presumably due to favorable modification of the microbe–electrode interface. A clear membrane specificity for **DSSN+** can be seen in bioimaging examples of bacteria[2] and yeast.[5] Additionally, **DSSN+** and related COEs have been shown to increase ion conductance across mammalian membranes.[6]

Studies have appeared that show how different COEs (and CPEs) exhibit different toxicity toward microorganisms.[7] The ionic arrangement and density impacts the biocidal activity and specific lipid affinity.[8,9] To better understand the influence of molecular topology on the interactions of COEs with different cells, we present herein the synthesis, characterization and biological affinity of a novel COE, **ZCOE** (Figure 2.1), with a topological distribution of ionic functionalities and red-shifted optical properties that allow one to differentiate its preferred cellular localization relative to the more established **DSSN+**.

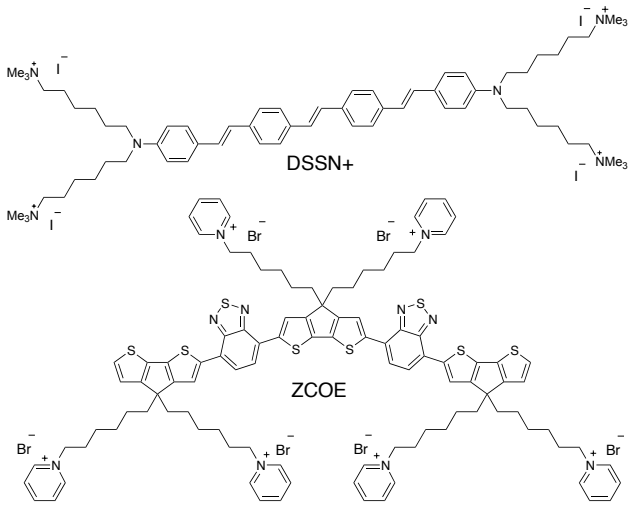

Figure 2.1. COE chemical structures used in this chapter.

2.2 Synthesis and Characterization of ZCOE

The synthesis of **ZCOE** was performed by Dr. Zac Henson and is shown in Figure 2.2. Details are provided in the Experimental section. Briefly, deprotonation at the bridgehead position of cyclopentadithiophene, followed by reaction with 1,6-dibromohexane affords compound **1**. Treatment of **1** with 1 or 2 equivalents of *n*-butyllithium, followed by treatment with Me_3SnCl yields either the mono- (**3**) or bis- (**2**) stannylated compounds. Stille coupling of **2** with 4,7-dibromobenzo[*c*][1,2,5]thiadiazole accesses the dibrominated species **4**, which can then undergo another Stille coupling reaction with **3** to access the neutral precursor **5**. Treatment of **5** with pyridine generates **ZCOE**.

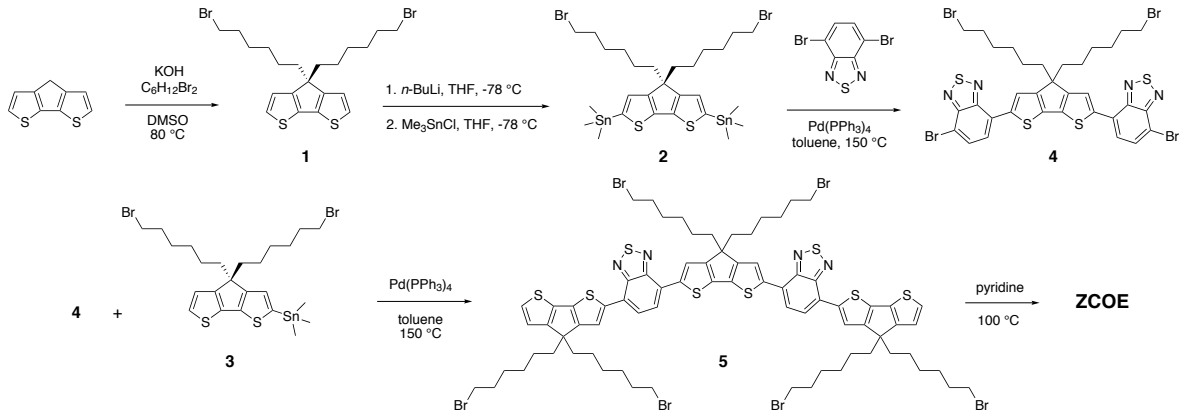

Figure 2.2. Synthetic preparation of ZCOE

The photophysical features of **ZCOE** were probed via UV-Vis absorption and photoluminescence spectroscopies in various solvents and the results are shown in Table 2.1 and Figure 2.3. The neutral precursor **5** was used for characterization in toluene and chloroform due to solubility considerations. Overall, one finds broad low energy absorption from ~500–800 nm and a sharp high energy band from ~350–450 nm with minimal solvatochromatic effects. The photoluminescence spectra of **ZCOE** exhibit a weak, broad, and featureless emission band stretching from ~650 nm–1000 nm. The emission maximum exhibits a 36 nm hypsochromic shift as solvent polarity decreases from chloroform (758 nm) to toluene (722 nm) and is accompanied by an increase in quantum yield (Φ) from ~3% to ~5%. Furthermore, no photoluminescence was detected from **ZCOE** dissolved in water. Low Φ values are typical for dyes that emit in this range,[10] as anticipated by the energy gap law.[11] It is worth pointing out that molecular design principles borrowed from organic optoelectronics give **ZCOE** its red-shifted optical attributes. More specifically, a modular approach of alternating electron-rich/donating cyclopentadithiophene and electron-

poor/accepting benzothiadiazole building blocks has previously resulted in broad, red-shifted absorption profiles due to charge transfer between donor and acceptor units.[12]

	Toluene[a]	Chloroform[a]	Methanol	Water
λ_{abs}	633 nm	637 nm	620 nm	630 nm
ε[b]	7.6	7.8	5.6	4.1
λ_{em}	722 nm	758 nm	N/A[c]	N/A[d]
Φ	4.7%	2.6%	0.4%	N/A[d]

[a] Compound **5** used due to solubility considerations. [b] L mol^{-1} cm^{-1} × 10^{-4}. [c] λ_{em} not determined due to high signal to noise. [d] No detectable emission in water.

Table 2.1. Absorption maximum (λ_{abs}), molar extinction coefficient (ε), emission maximum (λ_{em}) and quantum yield (Φ) of 5 and **ZCOE** in different solvents.

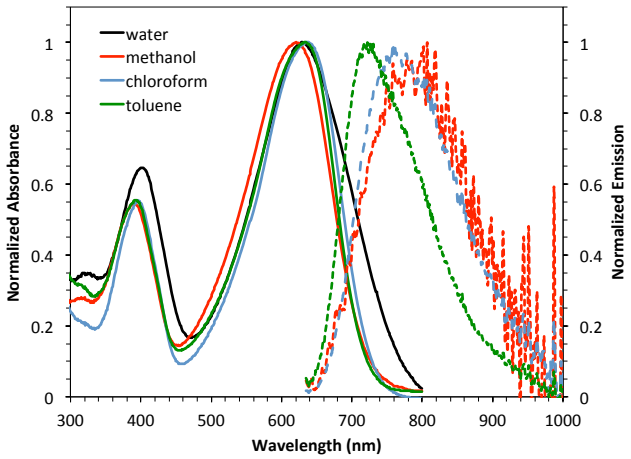

Figure 2.3. Normalized absorption spectra (solid lines) and emission spectra (dashed lines) of **ZCOE** in water and methanol and of the non-ionic neutral precursor **5** in chloroform and toluene. Note that there was no emission detected in water. Excitation was 633 nm.

2.2 Interaction with *E. coli* and Yeast

To visualize the interaction of **ZCOE** with a common bacterium and compare it to **DSSN+**, *E. coli* cells were incubated for 20 minutes with 5 μM **ZCOE** and **DSSN+** and

examined by confocal microscopy. Spectral separation of the two chromophores is achieved due to the far-red absorption (optimally excited by a 635 nm laser) and near-IR emission of **ZCOE** in contrast to the more blue-shifted optical attributes of **DSSN+**, which is excited by a 405 nm laser. An illustration of this is shown in Figure 2.4. Both COEs present cell-specific emission with no background fluorescence, as shown in Figure 2.5, due to their low quantum yields in polar media. Emission from **ZCOE** is mostly diffuse and featureless, plausibly due to an electrostatic association with the negatively charged bacterial surface,[13] which is in contrast to the "halo" pattern of **DSSN+** around the edges of the cells consistent with membrane intercalation.

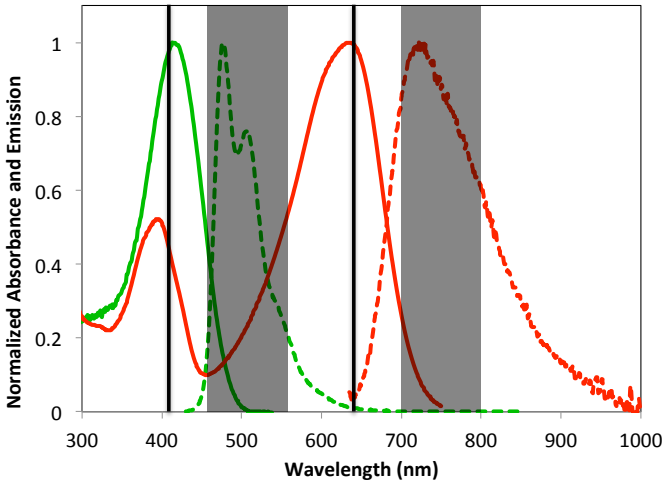

Figure 2.4. The absorbance (solid lines) and photoluminescence (dotted lines) spectra of **DSSN+** (green) and **ZCOE** (red). Black lines indicate laser excitation wavelengths used in confocal microscopy experiments (405 and 635 nm). Shaded areas indicate emission collection windows showing no overlap in terms of emission collected from each COE.

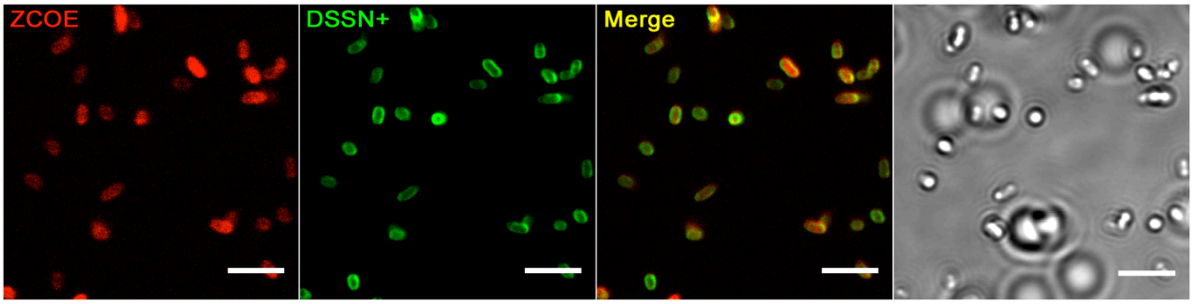

Figure 2.5. Single plane confocal micrograph and corresponding brightfield image of *E. coli* cells stained with 5 μM **ZCOE** and **DSSN+**. Scale bars are 5 μm.

Subsequent selectivity experiments by confocal microscopy involved yeast cells that were incubated for 20 minutes with 5 μM **ZCOE**. In contrast to the indiscriminate staining of *E. coli*, **ZCOE** displays bright intracellular fluorescence in only certain yeast cells (Figure 2.6, top). These same cells are also stained by propidium iodide, a membrane-impermeable dye that binds DNA, commonly used as an indicator of membrane permeability or "dead" stain.[14] Extensive colocalization of the two dyes is observed: 82% (37 of 45) of cells displaying **ZCOE** fluorescence also display PI fluorescence and 93% (37 of 40) of cells displaying PI fluorescence also display **ZCOE** fluorescence, based on analysis of 8 images (additional images shown in Figure 2.7). Therefore, it is reasonable to conclude that **ZCOE** can only enter yeast cells that have compromised membranes. One possible explanation is that its molecular topology, unlike that of **DSSN+**, cannot find suitable accommodation within and transfer through the lipid membrane due to the additional ionic groups on the center of the molecule. However, due to the negatively charged yeast cell surface[15] as in *E. coli*, one would expect some association of **ZCOE**. In fact, very weak fluorescence is observed near the circumference of cells when the brightness of the image in Figure 2.6 (top left) is adjusted above the saturation point (Figure 2.8).

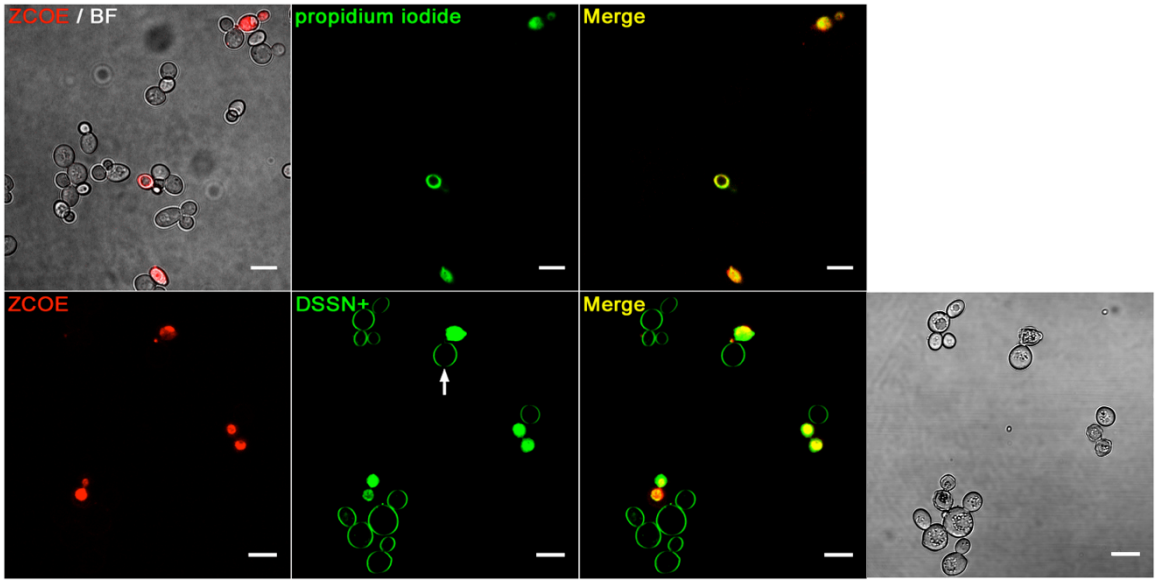

Figure 2.6. Two single plane confocal and brightfield (BF) micrographs of yeast cells both stained with 5 μM **ZCOE** and either propidium iodide (top) or **DSSN+** (bottom). Arrow indicates axial attenuated emission from **DSSN+** when illuminated by the polarized light.[5] Scale bars are 10 μm.

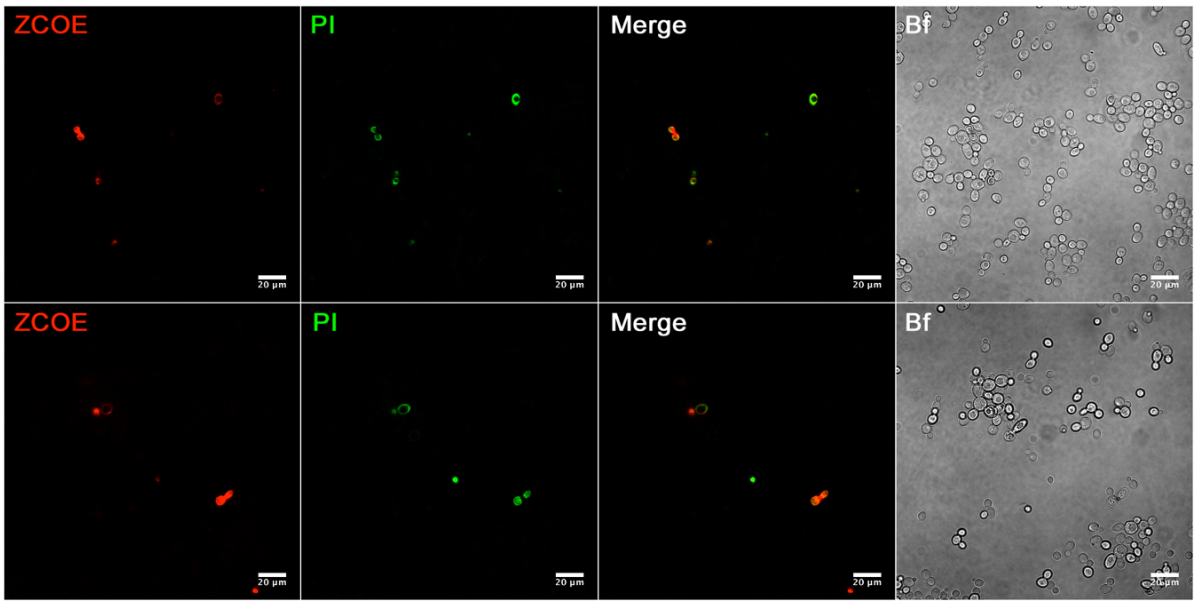

Figure 2.7. Single plane confocal fluorescence micrographs of yeast cells stained with 5 μM **ZCOE** and propidium iodide (PI). Top and bottom rows are from different areas of the same sample. The significant colocalization suggest that **ZCOE** mostly stains cells susceptible to propidium iodide staining and does not stain healthy cells. Bf = brightfield. Scale bars are 20 μm.

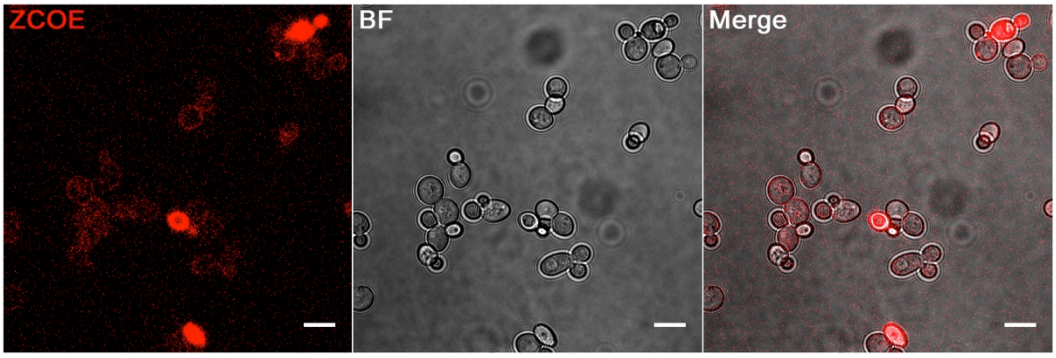

Figure 2.8. Single plane confocal and brightfield (BF) micrographs from Figure 2 (top) of main text showing yeast cells stained with 5 μM **ZCOE**. The brightness has been increased well above the saturation point in order to observe weak **ZCOE** emission associated with the circumference of healthy cells most likely due to an electrostatic interaction with the negatively charge yeast cell surface. Scale bars are 10 μm.

When yeast cells were stained with both COEs at 5 μM (Figure 2.6, bottom), cells displaying **ZCOE** fluorescence also exhibit intracellular **DSSN+** staining. This is in contrast to the remainder of cells stained with **DSSN+** that present a fluorescent "halo" around the circumfrence of the cells. Indication of lipid membrane intercalation by **DSSN+** in these cells is the symmetrically uneven membrane staining pattern, which is similar to what has been observed in liposomal systems with this COE.[5] Regions of attenuated emission run north/south (see arrow in Figure 2.6, bottom) as a result of the linearly structured chromophore being specifically oriented to span the width of the lipid bilayer. As a result of this alignment, efficient excitation and emission of the chromophore is governed by the direction of polarization of the incident photons, in this case from the polarized 405 nm laser. **ZCOE** is not expected to orient in a similar manner because ionic groups located on the center of the molecule make it unfavorable for **ZCOE** to intercalate and remain in the nonpolar region of the lipid bilayer.

2.3 Interaction with Mammalian Cells

As a final point of comparison, COS-1 (green monkey kidney cells) cells were pulse stained with 5 μM **ZCOE** and **DSSN+** for 20 minutes, rinsed and imaged with a laser scanning confocal microscope both immediately and after ~12 hours of incubation in fresh growth medium. The resulting images are shown in the top and bottom of Figure 2.9, respectively. Soon after staining, emission for both **ZCOE** and **DSSN+** exhibit similar localization to both intracellular puncta as well as the plasma membrane. After ~12 hours, however, **ZCOE** emission is entirely confined to intracellular groupings of small puncta while **DSSN+** emission both colocalizes with **ZCOE** and is retained within the plasma membranes. A replicate experiment is shown in Figure 2.10 utilizing a spinning disk confocal microscope. In these images, unlike Figure 2.9, orientation effects from a polarized excitation source are removed and the optical section is thicker allowing for detection of more fluorescence signal from **DSSN+** retained in the plasma membrane and further demonstrates its difference in localization compared to **ZCOE**.

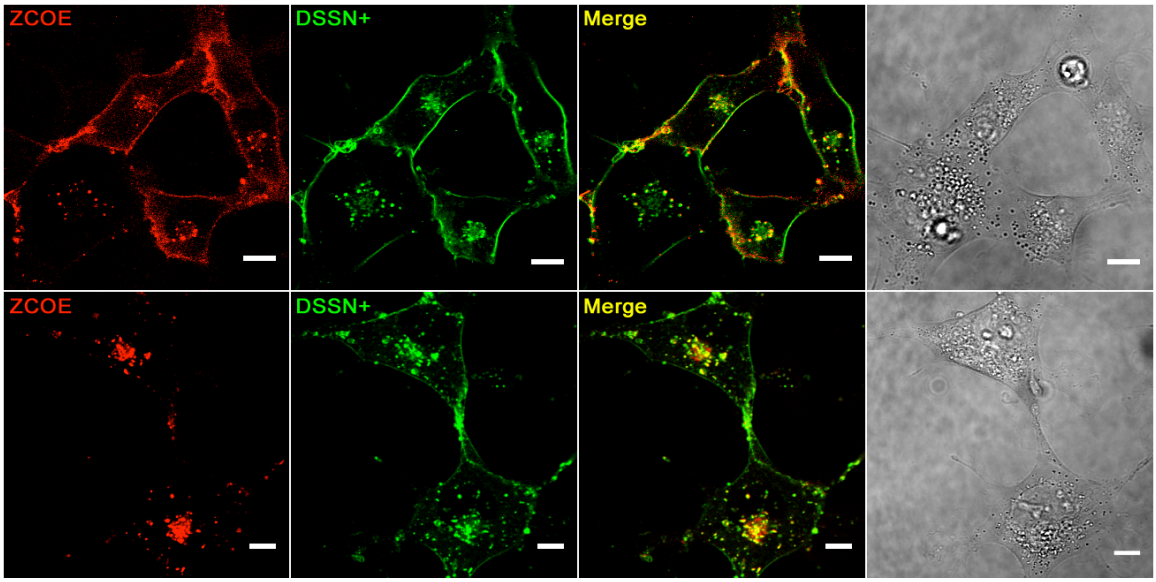

Figure 2.9. Single plane confocal micrographs and corresponding brightfield images of COS-1 cells pulse stained with 5 μM **ZCOE** and 5 μM **DSSN+** imaged soon after staining (top) and after ~12 hours (bottom). Scale bars are 10 μm.

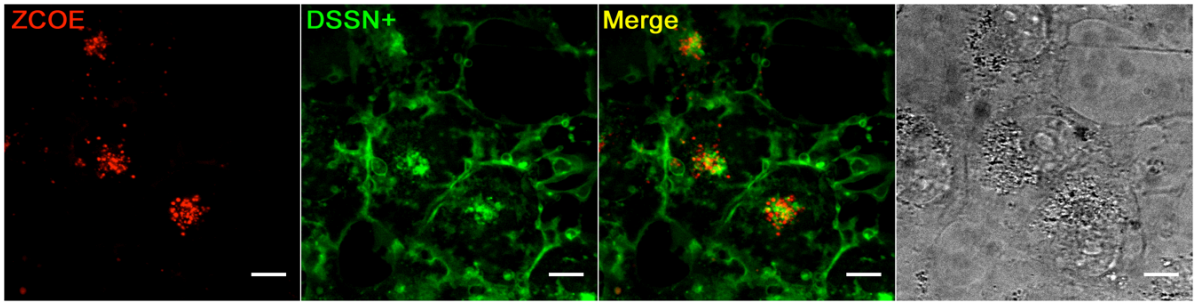

Figure 2.10. Single plane confocal fluorescence micrograph and brightfield image (right) of COS-1 cells pulse stained with 5 μM **ZCOE** and **DSSN+** imaged ~12 hours after staining. This image was obtained on a spinning disk confocal microscope and provides a thicker optical section and non-polarized excitation light compared to the laser scanning image in Figure 2.8, which removes orientation effects (see arrow in Figure 2.4) and provides better excitation of **DSSN+** in order to highlight its retention in the plasma membrane**.** Scale bars are 10 μm.

2.4 ZCOE Endocytosis in Mammalian Cells

Upon observing the small, round structures displaying **ZCOE** emission (Figues 2.9 and 2.10) that were similar to previous work with cationic conjugated polyelectroltytes,[16] it was hypothesized that **ZCOE** was being endocytosed.[17] To test this hypothesis, COS-1 cells

were stained for 20 minutes with 0.5 mg/mL fluorescently labeled 10k molecular weight dextran and 5 μM **ZCOE.** Dextran is membrane impermeable and commonly used to label endosomes of COS-1 cells.[18] The two compounds were administered sequentially, dextran first, separated by adequate rinsing in order to limit the possibility of the positively charged **ZCOE** electrostatically associating with the negatively charged dextran in solution and resulting in a false positive endocytosed aggregate. As seen in Figure 2.11, 12 hours after pulse staining, significant colocalization of **ZCOE** and dextran is observed in intracellular groupings of small (< 1 μm diameter**)** puncta. This suggests that **ZCOE** is in fact being internalized by COS-1 cells via endocytosis though it does not necessarily rule out other modes of entry.

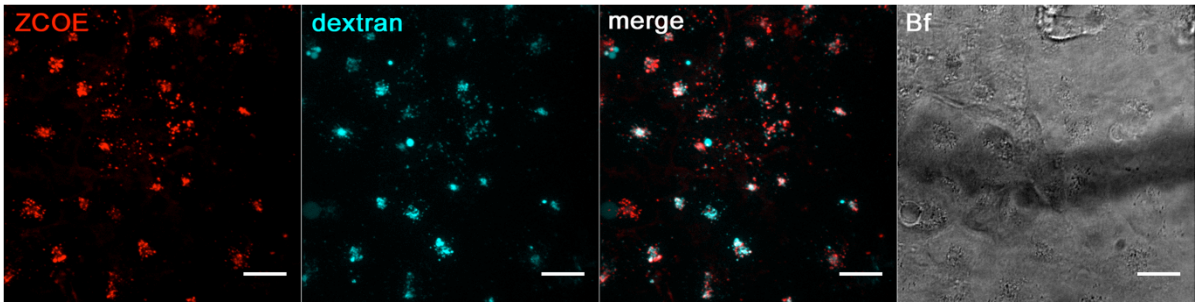

Figure 2.11. Single plane confocal micrograph and corresponding brightfield image of COS-1 cells sequentially pulse stained with 10k dextran-Oregon Green 488 then 5 μM **ZCOE** imaged 12 hours after staining. Scale bars are 20 μm.

To delve further into the endocytosis hypothesis, COS-1 cells were stained with 5 μM **ZCOE,** rinsed and incubated in growth medium for 12 hours then stained with LysoTracker Green (Figure 2.12) to mark acidic cellular compartments associated with endocytosis such as late endosomes and lysosomes.[19] Good colocalization is observed between the two dyes indicating that some **ZCOE** is trafficked to these acidic compartments.

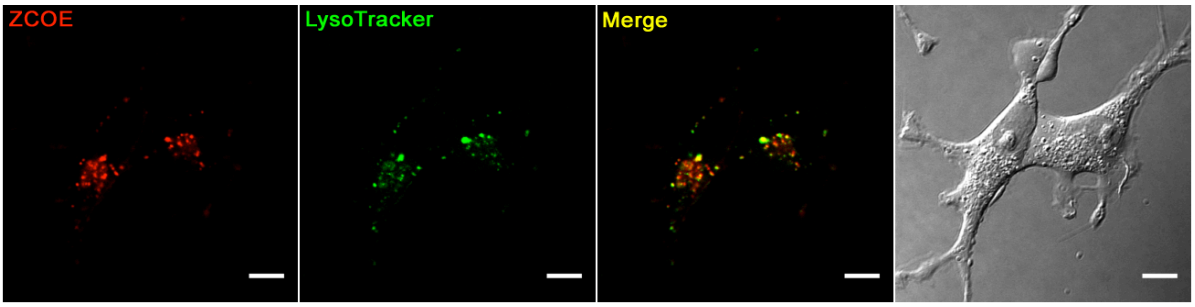

Figure 2.12. Single plane confocal micrograph and corresponding brightfield image of COS-1 cells initially pulse stained with 5 μM **ZCOE** and then 12 hours after with LysoTracker Green. Scale bars are 10 μm.

Further evidence indicating endocytosis is the localization of some **ZCOE** to late endosomes. COS-1 cells expressing either GFP-tagged Rab7[18] or Rab9[20] proteins were imaged 12 hours after pulse staining with **ZCOE** and the results are shown in Figure 2.13 and Figure 2.14, respectively. In the figures, arrows point to areas of significant colocalization of ZCOE and the GFP-tagged Rab proteins and in some cases emission from **ZCOE** is observed inside of a ring of GFP fluorescence, which is an indication of the COE's containment within these endocytotic vesicles.

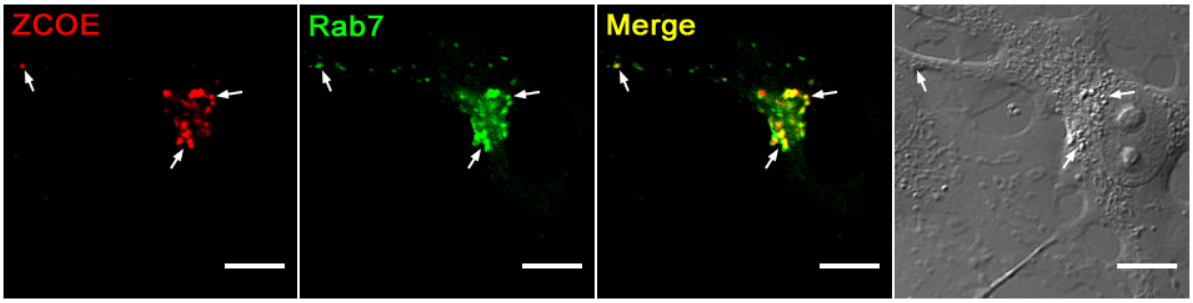

Figure 2.13. Single plane confocal micrograph and accompanying brightfield of a COS-1 cell expressing GFP-tagged Rab7 to identify late endosomes, and stained with 5 μM **ZCOE**. Image was taken ~12 hours after being pulse labeled with **ZCOE**. Arrows indicate example regions of colocalization. Scale bars are 10 μm.

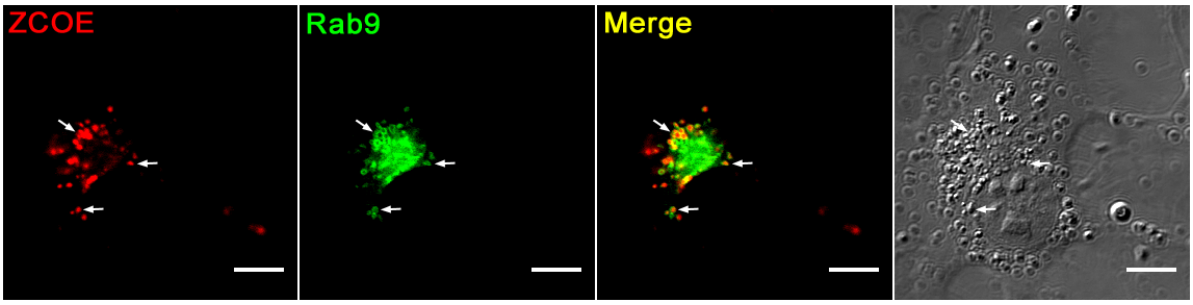

Figure 2.14. Single plane confocal micrograph and accompanying brightfield of a COS-1 cell expressing GFP-tagged Rab9 to identify late endosomes and stained with 5 μM **ZCOE**. Image was taken ~12 hours after being pulse labeled with **ZCOE**. Arrows indicate example regions of colocalization. Scale bars are 10 μm.

2.5 Conclusion

In conclusion we report the synthesis and photophysical characterization of a new COE containing molecular design elements incorporated to differentiate its interaction with biological systems from those of the more established **DSSN+**. Specifically, **DSSN+** contains four, long axis-terminating pendant ionic groups which mimic the distribution of hydrophilic and hydrophobic components of a lipid bilayer, whereas **ZCOE** contains six evenly distributed pendant ionic groups across its π-conjugated backbone making it more hydrophilic and less likely to persist in a hydrophobic lipid environment. Consistent with their differing ionic topologies, **DSSN+** generally accumulated in lipid membranes, whereas **ZCOE** exhibited less specific staining patterns likely governed by electrostatic interactions with cell surfaces. In *E. coli*, **ZCOE** displays cell-associated emission most likely as a result of interactions with the negatively charged surface of the bacteria. In yeast **ZCOE** similarly associates with the outside of cells, but accumulates inside certain cells that, based on dual staining with propidium iodide, have compromised membranes. In mammalian cells, emission from **ZCOE** initially appears similarly to **DSSN+**, most likely due to association

with the negatively charged mammalian cell surface,[16] but after 12 hours all **ZCOE** fluorescence is confined to intracellular puncta that show a significant degree of colocalization with LysoTracker and other late endosome markers, suggesting it has been subjected to an endocytotic pathway, which is not uncommon for polycationic molecules.[16,21] The results of these imaging experiments demonstrate the impact that the structural differences of COEs, especially the distribution of ionic groups, can have on their interaction with biological systems, and should help guide future synthetic design of COEs for biological applications.

2.6 Experimental

Reagents. Unless otherwise noted, all chemicals were purchased from Fisher or Sigma Aldrich and were used as received. 10,000 MW Dextran Oregon Green 488 was purchased from Invitrogen. Oxazine 1 was purchased from Exciton.

Synthesis of 4,4-bis(6-bromohexyl)-4*H*-cyclopenta[2,1-*b*:3,4-*b'*]dithiophene (1) has previously been reported.[22]

Synthesis of 4,4-bis(6-bromohexyl)-2,6-bis(trimethylstannyl)-4*H*-cyclopenta[2,1-*b*:3,4-*b'*]dithiophene (2): Compound 1 (0.380 g, 0.754 mmol) was dissolved in THF and cooled to -78 °C. *n*-BuLi (1.58 mmol) was added dropwise and stirred for 30 minutes. The solution was allowed to warm to room temperature and stirred for 1 hour before being cooled back to -78 °C. A THF solution of trimethyltin chloride (1.73 mmol) was then injected and the solution was stirred for 1 hour before being warmed to room temperature and stirred overnight. The mixture was quenched with water, extracted with hexanes and

dried over magnesium sulfate. Volatiles were removed to yield 0.560 g (89% yield) of a light brown oil, which was used without further purification. **^{1}H NMR (500 MHz, $CDCl_3$):** δ 6.92 (s, 2H), 3.33 (t, 4H), 1.81 (m, 4H), 1.74 (m, 4H), 1.30 (m, 4H), 1.16 (m, 4H), 0.98 (m, 4H), 0.38 (s, 18H).

Synthesis of 5-(trimethylstannyl)-4,4-bis(6-bromohexyl)-4H-cyclopenta[2,1-*b*;3,4-*b*']dithiophene (3): Compound 1 (0.300 g, 0.595 mmol) was dissolved in THF and cooled to -78 °C. *n*-BuLi (0.600 mmol) was added dropwise and stirred for 30 minutes. The solution was allowed to warm to room temperature and stirred for 1 hour before being cooled back to -78 °C. A THF solution of trimethyltin chloride (0.773 mmol) was then injected and the solution was stirred for 1 hour before being warmed to room temperature and stirred overnight. The mixture was quenched with water, extracted with hexanes and dried over magnesium sulfate. Volatiles were removed to yield 0.380 g (96% yield) of a light brown oil, which was used without further purification. **^{1}H NMR (500 MHz, CD_2Cl_2):** δ 7.15 (d, 1H), 6.99 (s, 1H), 6.95 (d, 1H), 3.34 (t, 4H), 1.84 (m, 4H), 1.73 (m, 4H), 1.29 (m, 4H), 1.16 (m, 4H), 0.96 (m, 4H), 0.39 (s, 9H).

Synthesis of 7,7'-(4,4-bis(6-bromohexyl)-4*H*-cyclopenta[1,2-*b*:5,4-*b*']dithiophene-2,6- diyl)bis(4-bromobenzo[1,2,5]thiadiazole) (4): Compound 2 (0.460 g, 0.554 mmol), 4,7-dibromobenzo[*c*][1,2,5]thiadiazole (0.978 g, 3.32 mmol), $Pd(PPh_3)_4$ (5 mol% cat.) and toluene were added to a 5 mL reaction vial. The vial was sealed and heated under microwave conditions for 2 minutes at 80 °C, 2 minutes at 110 °C, 2 minutes at 140°C and 45 minutes at 160 °C. The product was purified via column chromatography with a chloroform gradient. Volatiles were removed and the product was slurried in methanol,

filtered and collected. 0.340 g (65% yield) of a dark solid was collected. **^{1}H NMR (600 MHz, $CDCl_3$):** δ 8.12 (s, 2H), 7.89 (d, 2H), 7.78 (d, 2H), 3.35 (t, 4H), 2.07 (m, 4H), 1.78 (p, 4H), 1.37 (m, 4H), 1.28 (p, 4H), 1.15 (m, 4H).

Synthesis of 7,7'-(4,4-bis(6-bromohexyl)-4*H*-cyclopenta[1,2-*b*:5,4-*b*']dithiophene-2,6-diyl)bis(4-(4,4-bis(6-bromohexyl)-4*H*-cyclopenta[1,2-*b*:5,4-*b*']dithiophen-2-yl)benzo[*c*][1,2,5]thiadiazole) (5): Compound **3** (0.32 g, 0.344 mmol), Compound **4** (0.550 g, 0.825 mmol), Pd(PPh3)4 (5 mol% cat.) and toluene were added to a 5 mL reaction vial. The vial was sealed and heated under microwave conditions for 2 minutes at 80 °C, 2 minutes at 110 °C, 2 minutes at 140 °C and 45 minutes at 160 °C. The product was purified via column chromatography with a chloroform gradient. Volatiles were removed and the product was slurried in methanol, filtered and collected. 0.417 g (68% yield) of a dark solid was collected. **^{1}H NMR (600 MHz, CD_2Cl_2):** δ 8.17 (s, 2H), 8.14 (s, 2H), 7.98–7.91 (m, 4H), 7.33 (d, 2H), 7.07 (d, 2H), 3.38 (m, 12H), 2.14–2.08 (m, 4H), 2.02 (m, 8H), 1.83–1.73 (m, 12H), 1.43–1.00 (m, 36H).

Synthesis of 2,1,3-benzothiadiazole, 4,4'-[4,4-bis(6-pyridiniumhexyl)-4*H*-cyclopenta[2,1-*b*:3,4-*b*']dithiophene-2,6-diyl]bis[7-[4,4-bis(6-pyridiniumhexyl)-4*H*-cyclopenta[2,1-*b*:3,4-*b*']dithien-2-yl]hexabromide (ZCOE): Compound **5** (0.25 g, 0.141 mmol) was stirred in pyridine at room temperature for 5 days. After 2 days, methanol was added to aid dissolution of the ionic species. Volatiles were removed, and the resulting solid was slurried in hexanes and filtered to collect 0.298 g (94% yield) of a dark solid. **^{1}H NMR (600 MHz, Methanol-d4):** δ 8.94 (d, 12H), 8.48 (t, 4H), 8.43 (t, 2H), 8.23 (s, 2H), 8.07 (s,

2H), 8.00 (t, 8H), 7.96 (t, 4H), 7.79 – 7.69 (m, 4H), 7.31 (d, 2H), 7.06 (d, 2H), 4.65–4.49 (m, 12H), 2.21 (d, 4H), 2.14–2.01 (m, 8H), 1.96 (m, 12H), 1.48–1.23 (m, 28H), 1.06 (s, 8H).

Photophysical properties. UV-vis spectroscopy was performed using 1 cm path length quartz cuvettes and a Beckman Coulter DU 800 spectrophotometer. The photoluminescence quantum yield (PLQY) and emission spectra were measured using a custom-built fluorimeter. The samples were excited at 633 nm with a He-Ne laser (JDS Uniphase) attenuated to microwatt level. The emission was collected at 90 degrees by a system of lenses and focused on the entrance slit of a monochromator (Acton Research SpectraPro-500) after passing through a long wavelength-pass interference filter (Omega Filters) blocking the laser light. The dispersed spectrum was recorded by a charge-coupled device camera (Princeton Instruments PIXIS:400). Inhomogeneity of the instrument's spectral response was corrected by recording the spectrum of a black body-like light source (Ocean Optics) and calculating appropriate correction factors. PLQY was determined relative to 1 μM solution of Oxazine 725 (Exciton Inc., PLQY = 11%[23]) in ethanol following a standard reference-based method.[24] Optical absorption of samples at 633 nm was equalized to that of the reference sample.

Cell Culture and transfection. *Escherichia coli* K-12 (ATCC 10798) were grown aerobically in Luria Broth (10 g/L bacto tryptone, 5 g/L yeast extract, 10 g/L NaCl) overnight at 37°C. The yeast *Saccharomyces cerevisiae* (type II, Sigma Aldrich YSC2) were grown aerobically, overnight at 37°C in a selective medium containing the following per liter: 40 g dextrose, 10 g casamino acids, 3.4 g yeast nitrogen base, 10.6 g $(NH_4)_2SO_4$, 2.7 g Na_2HPO_4, 4.28 g NaH_2PO_4, 20 mg ampicillin, 20 mg kanamycin, and 10mL of penicillin–

streptomycin–neomycin solution (Sigma P4083). COS-1 cells (ATCC) were grown at 37°C under 5% CO_2 in Dulbecco's Modified Eagle Medium-RS (HyClone) containing 5% heat-inactivated fetal calf serum supplemented with 1X GlutaMax (Life Technologies) using standard techniques. The cells were cultured on 8-well chambered coverglass (Fisher 12565338) coated with poly-D-lysine (PDL, Sigma P7405). To prepare the coverglass, wells were washed twice with 70% ethanol then allowed to sit for 2 hours completely covered with a 0.1 mg/mL solution of PDL in sterile water, then rinsed 4 times with sterile water and allowed to air dry. To identify late endosomal compartments, in some experiments COS-1 cells were transfected with plasmids encoding GFP-tagged Rab7 or GFP-Rab9 using FuGENE 6 (Roche) according to the manufacturer's instructions. Cells were imaged 48 hours after transfection.

Cell Staining. Before staining, *E. coli* and yeast cells were rinsed twice from their growth medium with PBS buffer containing the following: 137 mM NaCl, 2.7 mM KCl, 10 mM Na_2HPO_4 and 1.8 mM KH_2PO_4 at pH 7.4. *E. coli* cells were centrifuged for 5 minutes at 7000 rcf and yeast cells for 3 minutes at 5000 rcf. 0.5 **m**L of OD_{600} ~1 cells were stained with 5 μM **DSSN+**, **ZCOE**, or propidium iodide and allowed to sit in the dark for 20 minutes at room temperature before rinsing twice. Samples to be imaged were then resuspended in 100 μL of PBS and 5 μL were dropped onto a clean glass slide and a cover slip placed on top. Cover slips were sealed with clear nail polish and all samples were imaged within 2 hours. COS-1 cultured on chambered coverglass were rinsed of their growth medium 3 times with sterile imaging buffer (IB) containing : 140 mM NaCl, 1.7 mM $CaCl_2$, 2.5 mM KCl, 1 mM $MgCl_2$, 20 mM HEPES at pH 7.4. Chambers were then

immersed in 0.5 mL of appropriate COE dye solutions at 5 μM in IB for 20 minutes at 37°C in the dark. Cells were rinsed 3 times to remove excess dye and placed back in IB for imaging within 2 hours. 12-hour samples were placed back in growth medium after initial imaging and incubated over night for imaging again the next day. For LysoTracker staining, these 12-hour samples were immersed in 0.5 mL of 50 nM LysoTracker Green in growth medium for 10 minutes, rinsed 3 times with IB and imaged soon after.

Confocal Microscopy. Unless indicated otherwise, all images were obtained via laser scanning confocal microscopy using an Olympus FluoView 1000 spectral scanning microscope. A 60 x 1.30 silicon oil immersion lens was used. Below is a table with excitation and emission settings that were used for each dye.

Chromophore	Excitation	Emission window
DSSN+	405 nm diode laser	460 nm – 560 nm
GFP / LysoTracker Green	488 nm argon laser	500 nm – 560 nm
Propidium Iodide	488 nm argon laser	570 nm – 670 nm
ZCOE	635 nm diode laser	700 nm – 800 nm

When indicated an Olympus DSU spinning disk confocal with environmental chamber (37°C, humidified 5% CO_2) and a 60 x 1.42 or 100 x 1.4 oil immersion lens was used to image COS-1 cells. A 89000 Sedat Quad filter set was used. Excitation and emission combinations for each dye are as follows:

Chromophore	Excitation	Emission
DSSN+	ET402/15x	ET525/36m
ZCOE	ET645/30x	ET705/72m

All images were processed using ImageJ.

Rasband, W.S., ImageJ, U. S. National Institutes of Health, Bethesda, Maryland, USA, http://imagej.nih.gov/ij/, 1997-2012.

2.7 References

1. Wang, V. B. *et al.* Improving charge collection in Escherichia coli-carbon electrode devices with conjugated oligoelectrolytes. *Phys. Chem. Chem. Phys.* **15,** 5867–5872 (2013).
2. Hou, H. *et al.* Conjugated oligoelectrolytes increase power generation in E. coli microbial fuel cells. *Adv. Mater.* **25,** 1593–1597 (2013).
3. Garner, L. E., Thomas, A. W., Sumner, J. J., Harvey, S. P. & Bazan, G. C. Conjugated oligoelectrolytes increase current response and organic contaminant removal in wastewater microbial fuel cells. *Energy Environ. Sci.* **5,** 9449–9452 (2012).
4. Thomas, A. W. *et al.* A lipid membrane intercalating conjugated oligoelectrolyte enables electrode driven succinate production in Shewanella. *Energy Environ. Sci.* **6,** 1761–1765 (2013).
5. Garner, L. E. *et al.* Modification of the Optoelectronic Properties of Membranes via Insertion of Amphiphilic Phenylenevinylene Oligoelectrolytes. *J. Am. Chem. Soc.* **132,** 10042–10052 (2010).
6. Du, J. *et al.* Increased ion conductance across mammalian membranes modified with conjugated oligoelectrolytes. *Chem. Commun.* **49,** 9624–9626 (2013).
7. Wang, Y., Schanze, K. S., Chi, E. Y. & Whitten, D. G. When Worlds Collide:

Interactions at the Interface between Biological Systems and Synthetic Cationic Conjugated Polyelectrolytes and Oligomers. *Langmuir* **29,** 10635–10647 (2013).

8. Wang, Y., Chi, E. Y., Schanze, K. S. & Whitten, D. G. Membrane activity of antimicrobial phenylene ethynylene based polymers and oligomers. *Soft Matter* **8,** 8547 (2012).
9. Wang, Y. *et al.* Direct Visualization of Bactericidal Action of Cationic Conjugated Polyelectrolytes and Oligomers. *Langmuir* **28,** 65–70 (2012).
10. Ellinger, S. *et al.* Donor–Acceptor–Donor-based π-Conjugated Oligomers for Nonlinear Optics and Near-IR Emission. *Chem. Mater.* **23,** 3805–3817 (2011).
11. Turro, N. J. *Modern Molecular Photochemistry*. (University Science Books, 1991).
12. Horie, M. *et al.* Cyclopentadithiophene-benzothiadiazole oligomers and polymers; synthesis, characterisation, field-effect transistor and photovoltaic characteristics. *J. Mater. Chem.* **22,** 381–389 (2012).
13. Hillberg, A. L. & Tabrizian, M. Biorecognition through Layer-by-Layer Polyelectrolyte Assembly: In-Situ Hybridization on Living Cells. *Biomacromolecules* **7,** 2742–2750 (2006).
14. Deere, D. *et al.* Flow cytometry and cell sorting for yeast viability assessment and cell selection. *Yeast* **14,** 147–160 (1998).
15. De Nobel, J. G. & Barnett, J. A. Passage of molecules through yeast cell walls: a brief essay-review. *Yeast* **7,** 313–323 (1991).
16. McRae, R. L., Phillips, R. L., Kim, I.-B., Bunz, U. H. F. & Fahrni, C. J. Molecular Recognition Based on Low-Affinity Polyvalent Interactions: Selective Binding of a

Carboxylated Polymer to Fibronectin Fibrils of Live Fibroblast Cells. *J. Am. Chem. Soc.* **130,** 7851–7853 (2008).

17. Zhu, C., Liu, L., Yang, Q., Lv, F. & Wang, S. Water-Soluble Conjugated Polymers for Imaging, Diagnosis, and Therapy. *Chem. Rev.* **112,** 4687–4735 (2012).

18. Misaki, R., Nakagawa, T., Fukuda, M., Taniguchi, N. & Taguchi, T. Spatial segregation of degradation- and recycling-trafficking pathways in COS-1 cells. *Biochem. Bioph. Res. Co.* **360,** 580–585 (2007).

19. Lai, S. K. *et al.* Privileged delivery of polymer nanoparticles to the perinuclear region of live cells via a non-clathrin, non-degradative pathway. *Biomaterials* **28,** 2876–2884 (2007).

20. Gong, Q., Huntsman, C. & Ma, D. Membrane Trafficking Review Series: Clathrin-independent internalization and recycling. *J. Cell Mol. Med.* **12,** 126–144 (2007).

21. Joliot, A. & Prochiantz, A. Transduction peptides: from technology to physiology. *Nat. Cell Biol.* **6,** 189–196 (2004).

22. Henson, Z. B., Zhang, Y., Nguyen, T.-Q., Seo, J. H. & Bazan, G. C. Synthesis and properties of two cationic narrow band gap conjugated polyelectrolytes. *J. Am. Chem. Soc.* **135,** 4163–4166 (2013).

23. Sens, R. & Drexhage, K. H. Fluorescence quantum yield of oxazine and carbazine laser dyes. *J. Lumin.* **24-25,** 709–712 (1981).

24. Lakowicz, J. R. *Principles of Fluorescence Spectroscopy*. (Springer Science & Business Media, 2007).

3. Pendant Ionic Groups of Conjugated Oligoelectrolytes Govern Their Ability to Intercalate into Microbial Membranes

3.1 Introduction

Lipid bilayers are found ubiquitously in nature, constituting the semipermeable barrier separating biological cells from their surroundings and forming a dynamic scaffold for the intricate organization of proteins in complex metabolic reactions. Modifying this pervasive interface through synthetic constructs is a challenging task with enormous potential for therapeutics, industrial applications and basic science.[1] With this intention, many complex molecular and supramolecular structures have been synthesized as synthetic ion channels[2-4] or transmembrane electron transporters[5-8] with structural motifs facilitating the passage of charged species through the hydrophobic bilayer core.

Conjugated oligoelectrolytes (COEs) are water-soluble molecules with π-conjugated backbones bearing pendant ionic groups. Certain conjugated oligoelectrolytes (COEs) have attracted attention for their ability to spontaneously intercalate into lipid bilayers and, in turn, modify the membrane transport properties.[9] This modification has been shown to boost the performance of a variety of microbial bioelectronic devices.[10-12] This technology relies on overcoming the electronically insulating character of lipid membranes in order to link intracellular metabolism to extracellular electronics; a feat that few bacteria are naturally able to do.[13] Although the mechanism by which COEs improve bioelectronic interactions may be situation dependent,[14-16] their ability to favorably modify the microbe-electrode

interface through spontaneous intercalation into lipid membranes is presumed paramount to their function.

A number of COE structural modifications have been studied and proven consequential to their biological interactions. Molecular length affected both mammalian membrane patch stability in ion conduction experiments[15] and microbial toxicity,[17] where a bolaamphiphilic, phenylenevinylene COE, **DSSN+** (Scheme 1), is thought to more closely match the width of lipid bilayers and consequently provided more membrane stability and lower toxicity when compared to shorter and longer analogues. Furthermore, molecular topology, particularly the spatial distribution of the solubilizing ionic groups, impacts COE-membrane interactions and thus potential applications.[18,19]

In this chapter we take advantage of synthetic flexibility to access three COEs through simple one- or two-step procedures from a common starting material in order to understand of the effect of different pendant ionic groups on membrane and bioelectronic interactions. Specifically, the trimethylammonium groups of **DSSN+** were substituted with either aromatic cationic pyridinium groups or anionic carboxylate groups to provide **DSSNpyr** and **DSSNcarb** (see Figure 3.1 for chemical compositions). As described in more detail below, we find remarkable selective interactions that are tuned to the choice of charge within the COE structure.

3.2 Synthesis of COE Ionic Group Analogs

Figure 3.1 provides a summary of the synthetic route for the preparation of the new COEs. Complete details can be found in the Experimental section. The synthesis of **DSSN+** has been reported previously.[9] Starting from the tetraiodo-substituted precursor of **DSSN+**

(compound **1**), **DSSNpyr** is obtained via quaternization with pyridine. In a two-step process, **1** is treated with potassium cyanide to obtain a tetracyano-substituted intermediated (compound **2**) which is then hydrolyzed under basic conditions to yield the tetracarboxylated derivative **DSSNcarb**.

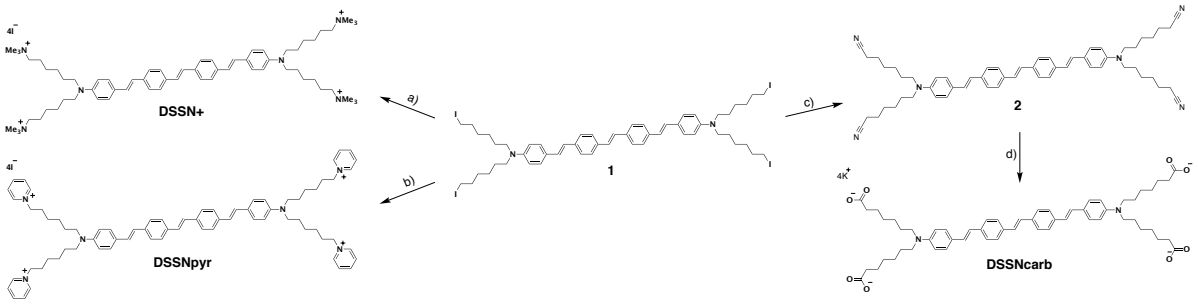

Figure 3.1. Synthesis of the COEs used in this study. Reagents and conditions: a) NMe3, THF, MeOH; b) pyridine (neat); c) KCN, 18-crown-6, MeCN; d) KOH, H2O, MeOH, 150 °C (microwave).

3.3 Incorporation into Model Membranes and *E. coli*

Liposomes composed of *E. coli* lipid extract were used as model membranes to compare the intercalating abilities of **DSSN+**, **DSSNpyr**, and **DSSNcarb**. In this experiment, COEs were added extraneously via concentrated aqueous solution to pre-formed liposomes in buffer. Aliquots were subsequently imaged via laser scanning confocal microscopy by direct excitation of the COE conjugated core. As seen in Figure 3.2, all COEs display circular emission profiles with negligible background emission, consistent with liposome incorporation and an environmentally sensitive fluorescence quantum efficiency.[9] Large liposomes (1–2 μm diameter) revealed uneven emission profiles characteristic of ordered orientation within the lipid bilayer. Specifically, the emission profiles become less intense along the vertical axis and more intense along the horizontal axis due to the varying

interaction between the transition dipole of the COE chromophore and the inherently polarized excitation laser.[9,20] The anisotropy in all three cases confirms their ability to predominantly span the lipid bilayer with the long axis of the molecule parallel with the lipid tails. Finally, emission from all COEs was observed in multiple layers of multilamellar liposomes (see Figure 3.3), suggesting that they are able to traverse a lipid bilayer. In the end, changing the ionic pendant groups of these COEs has no observable effect on liposome incorporation under the experimental conditions described here.

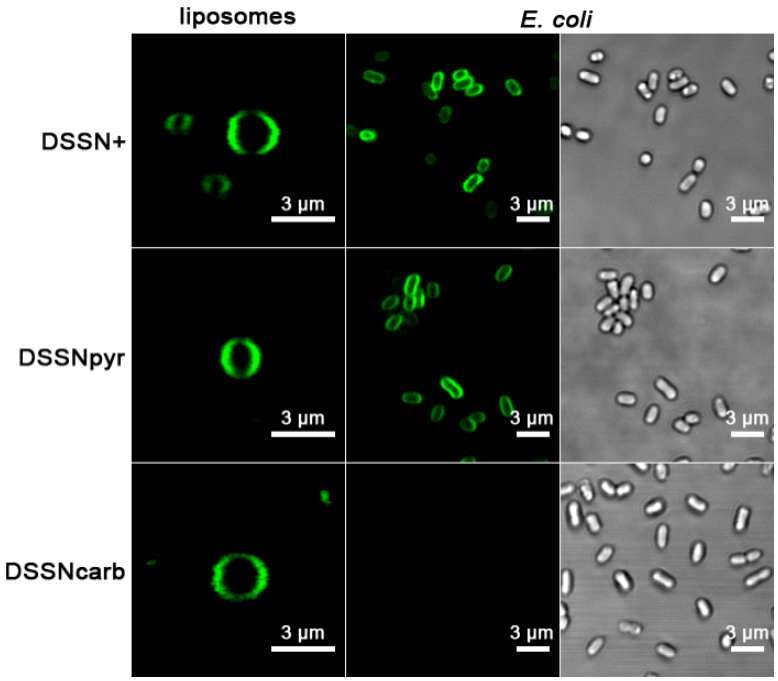

Figure 3.2. Confocal micrographs of *E. coli* lipid extract liposomes (left column) stained with 1 mol% COE based on lipid concentration and live *E. coli* cells (middle column) stained with 10 µM COE. Corresponding brightfield images of *E. coli* are shown (right column). Laser excitation was at 405 nm with emission collected 480 – 580 nm.

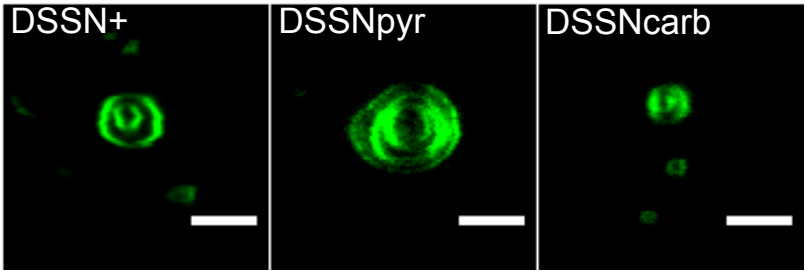

Figure 3.3. Confocal micrographs of *E. coli* lipid extract multilamellar liposomes stained with 1 mol% COE based on lipid concentration. These images are taken from the same samples as Figure 1 in the main text but are intended to highlight the COE ability to penetrate inner layers of multilamellar liposomes. Jaggedness in some images results from liposome movement during laser scanning image collection. Laser excitation was at 405 nm with emission collected 480 – 580 nm. Scale bars are 3 μm.

Turning from model membranes to *in vivo* interactions, *E. coli* cells were stained and the results are shown in Figure 3.2. The cationic COEs (**DSSN+** and **DSSNpyr**) successfully intercalated into the cell membranes, as evidenced by their emission profiles associated with the edges of the cells. In contrast, **DSSNcarb** gave no detectable emission, indicating that the anionic COE remained in solution. Considering that **DSSNcarb** can intercalate into liposomes of *E. coli* lipids but cannot intercalate into the membranes of *E. coli* cells, a previously unconsidered interaction must be governing the ability of COEs to intercalate into cell membranes. This interaction is most reasonably assumed to be with the anionic lipopolysaccharide (LPS) layer surrounding the outer membrane of *E. coli* and most gram-negative bacteria;[21] a feature that gives these cells a negative surface charge and has been exploited for electrostatic interactions with oligo- and polyelectrolytes.[22-27] Under these circumstances, electrostatic attraction and repulsion of LPS with cationic and anionic COEs, respectively, provides the means for gating membrane intercalation.

Lastly, in order to test if 10 μM COEs hinder the growth of *E. coli*, a growth experiment was conducted by monitoring the optical density of cell cultures at 600 nm (OD_{600nm}). The

results in Figure 3.4 demonstrate that under these conditions **DSSNcarb** has no effect on cell growth while the positively charged COEs (**DSSN+** and **DSSNpyr**) show slightly reduced growth. These results support the results in Figure 3.2 in that **DSSNcarb** again shows no interaction with *E. coli* whereas the positively charged COEs associate with and affect the bacteria.

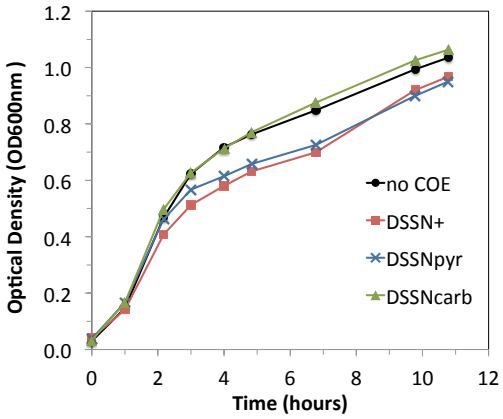

Figure 3.4. Growth of *E. coli* in LB medium supplemented with 10 μM COE compared to a no-COE control. 35 μL of an overnight culture was used to inoculate 3.5 mL of LB in tubes at 37 ºC shaking at 200 rpm. Results shown are an average of 4 cultures.

3.4 Effects on Microbial Fuel Cells

As discussed in the introduction, **DSSN+** has been shown to improve the performance of microbial fuel cells (MFCs) when added in concentrations ≥ 10 μM.[28] **DSSNpyr** and **DSSNcarb** were therefore compared with **DSSN+** and a control with no-COE using two-chamber U-tube MFCs[29,30] employing *E. coli* as the biocatalyst and Luria broth as the organic fuel. In these devices, microbes oxidize organic matter in the anaerobic anode chamber releasing CO_2, protons and electrons, the later of which can be collected at the anode electrode. Completing the circuit is the cathode reaction that combines protons,

electrons and O_2 to form water in a chamber that is separated by a proton exchange membrane and open to air.[31]

COEs were added to the MFC anaerobic anode chambers to a final concentration of 10 μM prior to inoculation with an overnight culture of *E. coli* to an OD_{600nm} of 0.1. The potential across a 10 kΩ resistor was monitored for 46 hours. Graphite felt served as the electrode material. Figure 3.5a shows the voltage generated over time for the MFCs, reported as an average of triplicate devices for each condition. The first noteworthy observation is that devices run with **DSSNcarb** performed nearly identically to no-COE controls, with both reaching a maximum sustained average potentials of approximately 4.5 mV after ~33 hours. **DSSN+** and **DSSNpyr** devices exhibited greater than 6-fold improvement over the control as shown by the corresponding maxima of 36 mV and 28 mV, respectively.

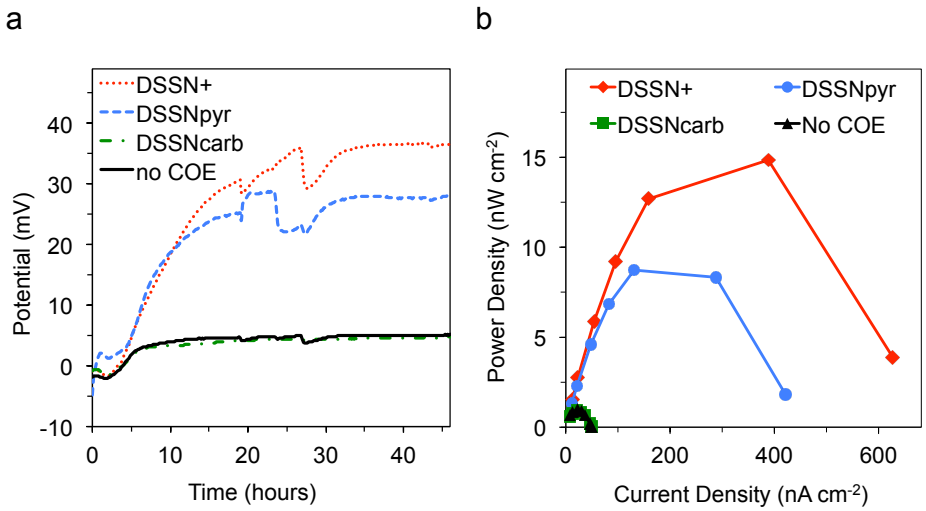

Figure 3.5. (a) Average potential generation over 46 hours of triplicate *E. coli* MFCs run with 0 or 10 μM of the three COEs. Sharp spikes in data result from the dislodging of CO_2 bubbles formed in the anode chamber by *E. coli*. (b) Average power generation of each set of triplicate devices obtained after 46 hours of operation.

At the end of MFC operation shown in Figure 3.5a, power density curves were obtained for each device by varying the resistance between the anode and cathode and measuring the voltage once it stabilized (~20 minutes). The results of this experiment are shown in Figure 3.5b. One observes that devices run with **DSSN+** and **DSSNpyr** gave greater than 9-fold improvement with maximum power densities of ~15 nW cm^{-2} and ~9 nW cm^{-2}, respectively. The control devices and **DSSNcarb** led to maximum power densities of less than 1 nW cm^{-2}. These experiments, together with those in Figure 3.5a, show that while the synthetic change from trimethylammonium to pyridinium slightly decreased MFC performance, the change to a negatively charged carboxylate completely eliminated any performance enhancement under these experimental conditions.

As a final examination after MFC operation, carbon felt anode electrodes from the devices were compared by confocal microscopy and representative images are shown in Figure 3.6. In the case of **DSSN+** and **DSSNpyr**, no additional dyes were added; therefore, any resulting emission is from COEs present at the start of operation. **DSSN+** and **DSSNpyr** electrodes displayed emission patterns consistent with COEs incorporated into *E. coli* cells: the patterns comprised mostly of short rod-shaped objects ~2 μm by ~0.5 μm, comparable to the *E. coli* in Figure 3.2. The **DSSNcarb** and no-COE electrodes gave no emission under identical settings (images not shown). In order to determine if cells were attached to these electrodes they were stained with 5 μM DAPI, a nucleic acid stain; representative images are shown in the bottom row of Figure 3.6. Both **DSSNcarb** and no-COE electrodes exhibit cell attachment to the graphite felt fibers via DAPI staining, indicating that **DSSNcarb** was not inhibiting cell attachment. Comparing all four MFC conditions, electrode coverage by *E.*

coli is similar. Additionally, DAPI staining of **DSSN+** and **DSSNpyr** device electrodes (Figure 3.7) showed that all cells displaying DAPI emission also displayed COE emission, suggesting that all cells on the electrode have COEs incorporated. These results suggest a direct correlation between COE membrane intercalation and increased voltage and power generation in MFCs under these experimental conditions.

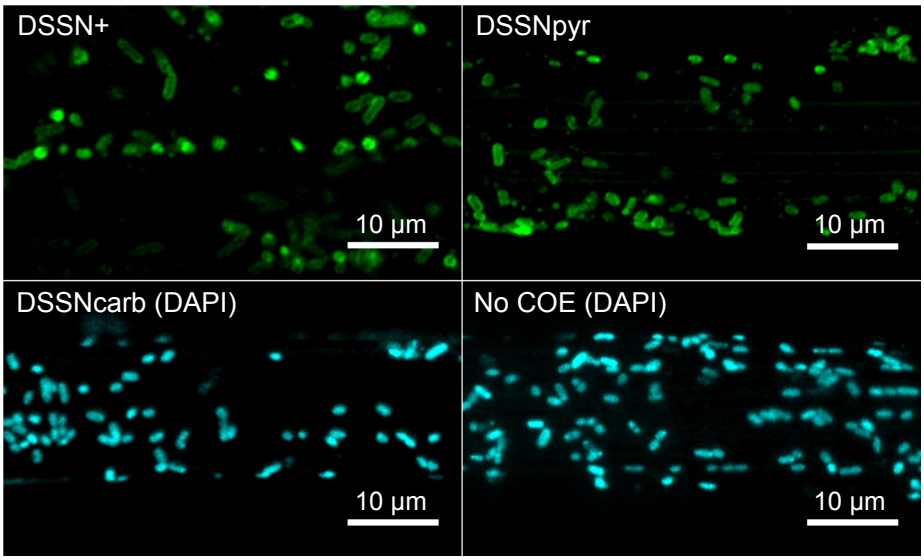

Figure 3.6. Representative confocal micrographs of graphite felt fibers from the MFC anodes after operation. No emission was detected for **DSSNcarb** or no-COE electrode fibers (images not shown) prior to staining with 5 µM DAPI. Laser excitation was at 405 nm with emission collected 500 – 600 nm and 420 – 520 nm for COEs and DAPI, respectively.

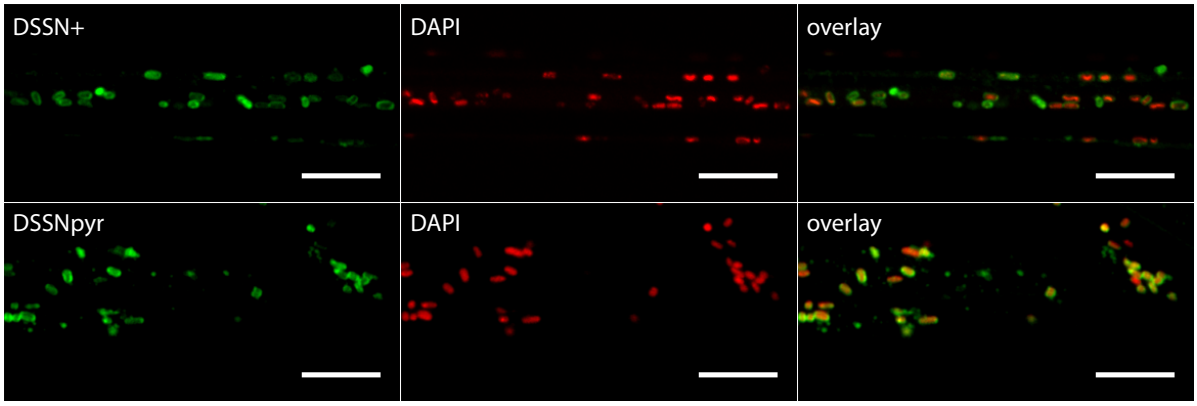

Figure 3.7. Confocal micrographs of graphite felt electrode fibers after MFC operation with COEs then subsequently stained with nucleic acid stain DAPI. Excitation for DAPI was 405 nm with emission collected 415 – 450 nm as to not collect COE emission, which starts after 450 nm.[9] Excitation for COEs was 488 nm in order to avoid exciting DAPI, with emission collected 500 – 600 nm. Scale bars are 10 μm.

3.5 Conclusion

In conclusion, two novel COEs were synthesized based on the membrane intercalating **DSSN+** by changing its pendant ionic groups from trimethylammonium to either pyridinium (**DSSNpyr**) or carboxylate (**DSSNcarb**). Based on confocal microscopy, **DSSN+**, **DSSNpyr** and **DSSNcarb** can be classified as membrane intercalating due to their ability to spontaneously intercalate into liposomes composed of *E. coli* lipid extract. We have determined, however, that this attribute does not necessarily impart the ability to incorporate into the membranes of live *E. coli*, as **DSSNcarb** was unable to do so. Additional cell surface components must participate in preventing this anionic COE from penetrating into the membrane, and we propose that the anionic LPS content in *E. coli* may be playing an important role in this charge selectivity.[21] We surmise that hydrophobic interactions between the molecular core of COEs and lipid tails play a role in the ability of COEs to persist within a membrane as evidenced by the inability of a cationic COE with a more hydrophilic core to

intercalate and remain in biological membranes,[18] but that electrostatic interactions first govern intercalation. Furthermore, both cationic COEs were able to incorporate into *E. coli* membranes and improved the performance of *E. coli* MFCs, while **DSSNcarb** did not. This suggests that there is a direct correlation between a COE's ability to intercalate into membranes and its ability to improve MFC performance. Information gained from this study will expand a growing collection of synthetic design rules for biologically relevant COEs that are finding utility in bioelectrochemical devices as well as biological detection[32-35] and imaging applications.[36,37]

3.6 Experimental

Chemicals and Reagents. Unless otherwise noted, all chemicals and materials were purchased from Fisher or Sigma Aldrich and were used as received. *E. coli* lipid extract was purchased from Avanti Polar Lipids.

Synthesis of compound **1** and **DSSN+** has previously been reported.[9]

Synthesis of 2. A 250 mL round bottom flask was charged with **1** (1 eq., 1 g, 0.8 mmol), potassium cyanide (20 eq., 1.04 g, 15.9 mmol), 18-crown-6 (1 eq., 0.21 g, 0.8 mmol), and 200 mL of acetonitrile and equipped with a reflux condenser. The resulting solution was stirred under reflux for 24 hours. The solution was then allowed to cool and the solvent was removed by rotary evaporation. The residue was dissolved in CH_2Cl_2 and washed with water (2X) and brine. The combined organic phases were dried over $MgSO_4$ and the solvent removed to yield crude **2**. NMR analysis indicated the crude consisted almost entirely of a mixture of 18-crown-6 and the target compound. Further purification was achieved via silica gel chromatography. 0.380 g (60% yield) of an orange solid was collected. ^{1}H NMR (500

MHz, CD_2Cl_2): δ 7.50 (d, *J* = 8.5 Hz, 4H), 7.47 (d, *J* = 8.5 Hz, 4H), 7.38 (d, d, *J* = 8.8 Hz, 4H), 7.12 (s, 2H), 7.06 (d, *J* = 16.2 Hz, 2H), 6.89 (d, *J* = 16.2 Hz, 2H), 6.63 (d, *J* = 8.8 Hz, 4H), 3.31 (t, 8H), 2.35 (t, 8H), 1.65 (m, 16H), 1.50 (m, 8H), 1.38 (m, 8H). FD-MS: 850 (M^+), 823 ($(M\text{-}CN)^+$), 425 (M^{2+}). Elemental analysis (CHN) calculated: C, 81.84; H, 8.29; N, 9.87. Found: C, 81.10; H, 8.26; N, 8.67.

Synthesis of DSSNcarb. A 25 mL microwave reaction tube was charged with **2** (1 eq., 0.1 g, 0.116 mmol), 8 M aq. potassium hydroxide (100 eq., 1.5 mL, 11.7 mmol), water (3.5 mL) and methanol (15 mL), sealed, and placed into the reaction chamber of a Biotage Initiator microwave reactor. Under rigorous stirring at (900 RPM) the temperature of the reaction solution was ramped from ~ 30 °C (temperature upon sealing) to 100 °C over the course of 2 min and then further increased to 150 °C and stirred at this temperature for 2 hours. The reaction solution, now homogenous following the microwave and still warm was allowed to cool. The solvent was removed and the crude product dissolved in methanol. The target compound was then precipitated and washed with diethyl ether. 41 mg (30% yield) of an orange solid was collected. ^{1}H NMR (500 MHz, CD_3OD): δ 7.51 (d, *J* = 8.3 Hz, 4H), 7.47 (d, *J* = 8.3 Hz, 4H), 7.37 (d, *J* = 8.65 Hz, 4H), 7.14 (s, 2H), 7.07 (d, *J* = 16.2 Hz, 2H), 6.90 (d, *J* = 16.2 Hz, 2H), 6.65 (d, *J* = 8.65 Hz, 4H), 3.31 (m, 8H), 2.17 (t, 8H), 1.62 (m, 16H), 1.39 (m, 16H). ^{13}C NMR (800 MHz, CD_3OD): δ 182.98, 149.26, 139.21, 137.20, 130.04, 128.80, 128.68, 127.73, 127.16, 125.99, 124.01, 112.93, 66.90, 39.28, 30.84, 28.42, 28.14, 27.90, 15.44. IR (cm^{-1}): 1655, 1560 (peaks indicative of carboxylate functional groups, other IR absorbance peaks omitted).

Synthesis of DSSNpyr. Compound **1** (0.25 g, 0.141 mmol) was stirred in ~100 mL of pyridine at room temperature for 4 days. After 2 days, ~100 mL methanol was added to aid dissolution. Volatiles were removed and the resulting solid was slurried in hexanes and filtered to collect 0.291 g (93% yield) of an orange solid. ^{1}H NMR (500 MHz, DMSO-d_6) δ 9.11 (d, J = 5.6 Hz, 8H), 8.63 (t, J = 7.8 Hz, 4H), 8.19 (t, J = 7.5 Hz 8H), 7.58 (d, J = 8.3Hz, 4H), 7.53 (d, J = 8.3Hz, 4H), 7.40 (d, J = 8.6 Hz, 4H), 7.25 (s, 2H), 7.15 (d, J = 16.2 Hz, 2H), 6.94 (d, J = 16.2 Hz, 2H), 6.63 (d, J = 8.4 Hz, 4H), 4.62 (t, J = 7.4 Hz, 8H), 3.28 (m, 8H), 1.94 (m, 8H), 1.52 (m, 8H), 1.33 (m, 16H). ESI/TOF-MS: 265 $(M\text{-}4I)^{4+}$, 396 $((M\text{-}3I)^{3+}$), 658 $(M\text{-}2I)^{2+}$. Elemental analysis (CHN) calculated: C, 56.57; H, 5.77; N, 5.35. Found: C, 57.6; H, 6.67; N, 4.71.

Confocal microscopy. All images were obtained via laser scanning confocal microscopy using an Olympus FluoView 1000 spectral scanning microscope equipped with a 60 x 1.30 silicon oil immersion lens. All images were processed using ImageJ.

Cell culture. *Escherichia coli* K-12 (ATCC 10798) was grown aerobically in Luria Broth (10 g L^{-1} bacto tryptone, 5 g L^{-1} yeast extract, 10 g L^{-1} NaCl) overnight at 37°C and used for both imaging and inoculum of microbial fuel cells (MFCs).

Cell staining. Before staining, *E. coli* was rinsed twice from the growth medium with phosphate buffered saline (PBS) containing the following: 137 mM NaCl, 2.7 mM KCl, 10 mM Na_2HPO_4 and 1.8 mM KH_2PO_4 at pH 7.4. *E. coli* cells were centrifuged for 4 minutes at 6000 rcf. 0.5 mL of OD_{600nm} 1 cells were stained with 10 μM COE and allowed to sit in the dark for 20 minutes at room temperature before rinsing twice. Samples to be imaged were then resuspended in 100 μL of PBS and 5 μL were dropped onto a clean glass slide and a

cover slip placed on top. Cover slips were sealed with clear nail polish and all samples were imaged within 2 hours.

MFC construction and operation. U-tube MFCs were constructed as previously described.[9,11] In short, devices were assembled from two L-shaped glass tubes separated by a Nafion® N117 membrane and sealed using an O-ring and a 28/15 stainless steel pinch clamp. Nafion® membranes were treated at 80 ºC in 3% hydrogen peroxide solution, followed by ultrapure water, then 0.5 M sulfuric acid solution, and ultrapure water again for 1 hour each. Anode and cathode electrodes were constructed out of carbon felt (2 cm x 5 cm), strung with titanium wire and placed in their respective chambers. Assembled devices were filled with ultrapure water and sterilized by autoclaving. After sterilization, the water was removed and the anode and cathode chambers were filled with sterile LB medium. Concentrated aqueous COE (DSSN+, DSSNcarb-, or DSSNpyr+) solutions were added to the anode chambers to a final concentration of 10 μM. Both chambers were then inoculated with overnight *E. coli* culture to a starting OD_{600} of 0.1. The final volume in all chambers was 20 mL. Anode chambers were sealed with a sterile silicon stopper and cathode chambers were loosely capped by a sterile glass scintillation vial, with the cathode only partially submerged to promote "air–wicking". The assembled devices were then connected to an external resistor of 10 kΩ, a multiplexer and a digital multimeter (PXI-2575, PXI-4065, National Instruments, Austin, TX) controlled by a LabView program for automatic data acquision. Power densities were characterized by switching through a series of external resistors (1, 10, 51, 100, 200, 500 and 1000 kΩ) after 46 hours of operation. Densities were

estimated by normalizing by the area of the felt electrodes (10 cm^2) as previously calculated.[28] Each condition was run in triplicate.

MFC electrode imaging. An approximately 1 cm x 1 cm square was cut from the carbon felt anode electrodes and dipped twice in PBS to dislodge loosely attached cells. For DAPI staining, the square was submerged in a solution of 5 μM DAPI in PBS for ~30 minutes. One edge of the square was then touched to a paper towel to wick away most of the moisture. A large drop of silicone immersion oil was placed directly onto the square and this was placed face down onto a piece of cover glass. A piece of tape was used to secure the square to the glass before imaging.

Liposome preparation. 25 mg *E. coli* lipid extract was dissolved in 5 mL chloroform in a 25 mL round bottom flask. The solvent was removed via rotary evaporation to yield a film coating the bottom of the flask. The flask was placed under vacuum overnight. The lipid film was dissolved in 5 mL PBS by rotating the flask in a 30 °C water bath for 1 hour. This solution was then sonicated to near clarity while in an ice bath. The resulting liposome solution was used in aliquots for confocal characterization. COEs were added extraneously from concentrated stock solutions in PBS to ~1 mol% of lipid, roughly estimated assuming an average lipid molecular weight of 800 g mol^{-1}.

3.7 References

1. Matile, S. & Fyles, T. Transport Across Membranes. *Acc. Chem. Res.* **46,** 2741–2742 (2013).
2. Matile, S., Vargas Jentzsch, A., Montenegro, J. & Fin, A. Recent synthetic transport systems. *Chem. Soc. Rev.* **40,** 2453 (2011).

3. Fyles, T. M. Synthetic ion channels in bilayer membranes. *Chem. Soc. Rev.* **36,** 335–347 (2007).

4. Sakai, N. & Matile, S. Synthetic Ion Channels. *Langmuir* **29,** 9031–9040 (2013).

5. Fuhrhop, J. H., Krull, M., Schulz, A. & MOBIUS, D. Bolaform Amphiphiles with a Rigid Hydrophobic Bixin Core in Surface Monolayers and Lipid-Membranes. *Langmuir* **6,** 497–505 (1990).

6. Arrhenius, T. S., Blanchard-Desce, M., Dvolaitzky, M., Lehn, J. M. & Malthete, J. Molecular devices: Caroviologens as an approach to molecular wires $# x02014; synthesis and incorporation into vesicle membranes. *Proc. Natl. Acad. Sci. USA* **83,** 5355 (1986).

7. Nango, M. *et al.* Manganese porphyrin-mediated electron transfer across a liposomal membrane and on an electrode modified with a lipid bilayer membrane. *Langmuir* **14,** 407–416 (1998).

8. Kugimiya, S.-I., Lazrak, T., Blanchard-Desce, M. & Lehn, J.-M. Electron conduction across vesicular bilayer membranes induced by a caroviologen molecular wire. *J. Chem. Soc. Chem. Commun.* 1179–1182 (1991).

9. Garner, L. E. *et al.* Modification of the Optoelectronic Properties of Membranes via Insertion of Amphiphilic Phenylenevinylene Oligoelectrolytes. *J. Am. Chem. Soc.* **132,** 10042–10052 (2010).

10. Hou, H. *et al.* Conjugated oligoelectrolytes increase power generation in E. coli microbial fuel cells. *Adv. Mater.* **25,** 1593–1597 (2013).

11. Garner, L. E., Thomas, A. W., Sumner, J. J., Harvey, S. P. & Bazan, G. C.

Conjugated oligoelectrolytes increase current response and organic contaminant removal in wastewater microbial fuel cells. *Energy Environ. Sci.* **5,** 9449–9452 (2012).

12. Thomas, A. W. *et al.* A lipid membrane intercalating conjugated oligoelectrolyte enables electrode driven succinate production in Shewanella. *Energy Environ. Sci.* **6,** 1761–1765 (2013).
13. Logan, B. E. Exoelectrogenic bacteria that power microbial fuel cells. *Nat. Rev. Micro.* **7,** 375–381 (2009).
14. Kirchhofer, N. D. *et al.* The conjugated oligoelectrolyte DSSN+ enables exceptional coulombic efficiency via direct electron transfer for anode-respiring Shewanella oneidensis MR-1-a mechanistic study. *Phys. Chem. Chem. Phys.* **16,** 20436–20443 (2014).
15. Du, J. *et al.* Increased ion conductance across mammalian membranes modified with conjugated oligoelectrolytes. *Chem. Commun.* **49,** 9624–9626 (2013).
16. Sivakumar, K. *et al.* Membrane permeabilization underlies the enhancement of extracellular bioactivity in Shewanella oneidensis by a membrane-spanning conjugated oligoelectrolyte. *Appl. Microbiol. Biotechnol*. **98,** 9021–9031 (2014).
17. Hinks, J. *et al.* Modeling Cell Membrane Perturbation by Molecules Designed for Transmembrane Electron Transfer. *Langmuir* **30,** 2429–2440 (2014).
18. Thomas, A. W., Henson, Z. B., Du, J., Vandenberg, C. A. & Bazan, G. C. Synthesis, characterization, and biological affinity of a near-infrared-emitting conjugated oligoelectrolyte. *J. Am. Chem. Soc.* **136,** 3736–3739 (2014).

19. Wang, Y. *et al.* Dark Antimicrobial Mechanisms of Cationic Phenylene Ethynylene Polymers and Oligomers against Escherichia coli. *Polymers* **3,** 1199–1214 (2011).

20. Quesada, E., Acuña, A. U. & Amat-Guerri, F. New Transmembrane Polyene Bolaamphiphiles as Fluorescent Probes in Lipid Bilayers. *Angew. Chem. Int. Ed.* **40,** 2095–2097 (2001).

21. Wilson, W. W., Wade, M. M., Holman, S. C. & Champlin, F. R. Status of methods for assessing bacterial cell surface charge properties based on zeta potential measurements. *J. Microbiol. Meth.* **43,** 153–164 (2001).

22. Hillberg, A. L. & Tabrizian, M. Biorecognition through Layer-by-Layer Polyelectrolyte Assembly: In-Situ Hybridization on Living Cells. *Biomacromolecules* **7,** 2742–2750 (2006).

23. Wang, Y. *et al.* Understanding the Dark and Light-Enhanced Bactericidal Action of Cationic Conjugated Polyelectrolytes and Oligomers. *Langmuir* **29,** 781–792 (2013).

24. Kahraman, M., Zamaleeva, A. I., Fakhrullin, R. F. & Culha, M. Layer-by-layer coating of bacteria with noble metal nanoparticles for surface-enhanced Raman scattering. *Anal. Bioanal. Chem.* **395,** 2559–2567 (2009).

25. Fakhrullin, R. F. & Lvov, Y. M. "Face-Lifting" and "Make-Up" for Microorganisms: Layer-by-Layer Polyelectrolyte Nanocoating. *ACS Nano* **6,** 4557–4564 (2012).

26. Priya, A. J., Vijayalakshmi, S. P. & Raichur, A. M. Enhanced Survival of Probiotic Lactobacillus acidophilus by Encapsulation with Nanostructured Polyelectrolyte Layers through Layer-by-Layer Approach. *J. Agric. Food Chem.* **59,** 11838–11845 (2011).

27. Eby, D. M. *et al.* Bacterial Sunscreen: Layer-by-Layer Deposition of UV-Absorbing Polymers on Whole-Cell Biosensors. *Langmuir* **28,** 10521–10527 (2012).

28. Wang, V. B. *et al.* Improving charge collection in Escherichia coli-carbon electrode devices with conjugated oligoelectrolytes. *Phys. Chem. Chem. Phys.* **15,** 5867–5872 (2013).

29. Milliken, C. E. & May, H. D. Sustained generation of electricity by the spore-forming, Gram-positive, Desulfitobacterium hafniense strain DCB2. *Appl. Microbiol. Biotechnol.* **73,** 1180–1189 (2006).

30. Sund, C. J., Mcmasters, S., Crittenden, S. R., Harrell, L. E. & Sumner, J. J. Effect of electron mediators on current generation and fermentation in a microbial fuel cell. *Appl. Microbiol. Biotechnol.* **76,** 561–568 (2007).

31. Logan, B. E. *Microbial Fuel Cells*. (John Wiley & Sons, 2008).

32. Herland, A. *et al.* Electroactive Luminescent Self-Assembled Bio-organic Nanowires: Integration of Semiconducting Oligoelectrolytes within Amyloidogenic Proteins. *Adv. Mater.* **17,** 1466–1471 (2005).

33. Duarte, A., Chworos, A., Flagan, S. F., Hanrahan, G. & Bazan, G. C. Identification of Bacteria by Conjugated Oligoelectrolyte/Single-Stranded DNA Electrostatic Complexes. *J. Am. Chem. Soc.* **132,** 12562–12564 (2010).

34. Cai, L. *et al.* Butterfly-Shaped Conjugated Oligoelectrolyte/Graphene Oxide Integrated Assay for Light-Up Visual Detection of Heparin. *Anal. Chem.* **83,** 7849–7855 (2011).

35. Klingstedt, T. *et al.* Synthesis of a library of oligothiophenes and their utilization as

fluorescent ligands for spectral assignment of protein aggregates. *Org. Biomol. Chem.* **9,** 8356–8370 (2011).

36. Klingstedt, T. *et al.* Luminescent Conjugated Oligothiophenes for Sensitive Fluorescent Assignment of Protein Inclusion Bodies. *Chembiochem* **14,** 607–616 (2013).

37. Pu, K.-Y., Li, K., Zhang, X. & Liu, B. Conjugated Oligoelectrolyte Harnessed Polyhedral Oligomeric Silsesquioxane as Light-Up Hybrid Nanodot for Two-Photon Fluorescence Imaging of Cellular Nucleus. *Adv. Mater.* **22,** 4186–4189 (2010).

4. Tuning the Cell Surface Charge of *E. Coli* with Conjugated Oligoelectrolytes

4.1 Introduction

While the lipid membrane intercalation of COEs is well-documented, other biological interactions of COEs and their consequences have not yet been studied. Previously we showed that an anionic COE analogous to **DSSN+** was prevented from incorporating into *E. coli* membranes most likely due to electrostatic repulsion from the innate negative surface charge of the cells.[1] These negative charges occur mostly as ionized carboxyl and phosphate groups that are part of lipopolysaccharide (LPS) macromolecules composing the outer leaflet of most gram-negative bacteria.[2,3] Thus, an electrostatic attraction between cationic COEs and these anionic sugars forming the outermost extensions of *E. coli* are reasonable and should allow modulation of the overall surface charge of the cells.[4-6]

Furthermore, in studies concerning the effects of COEs on biological systems, COE concentrations are chosen in the low micromolar regime with no consideration given to the number of cells; the amount of COE that associates with each cell and that which is left in solution remains to be quantified. With this purpose, we compare 8 COEs varying in length and core substitutions for their association with E. coli and affect on cell zeta potential, finding a remarkable length dependence on these properties.

The chemical structures of the COEs used in this study are shown in Figure 4.1; their syntheses have been described in the literaterature. [7-9] Their basic structure can be described

by 3 – 5 phenylenevinylene repeat units (RUs) flanked on both ends by either an amine (COE1 series) or two meta-positioned alkoxy (COE2 series) linkages carrying trimethylammonium iodide terminated hexyl chains. Tetrafluorine substitution of the center phenyl ring of the 3-RU molecules offers variance of the central hydrophobic core to determine its role, if any, in cell association and cell surface charge.

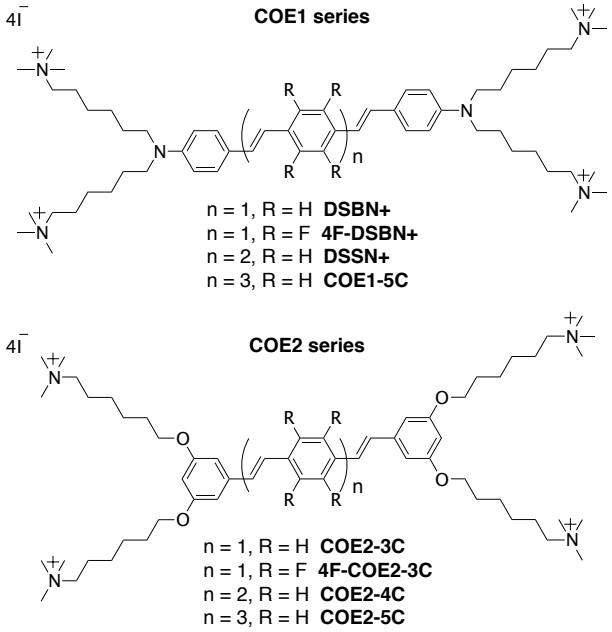

Figure 4.1. The chemical structures of COEs used in this chapter.

4.2 COE Series Comparison by Confocal Microscopy of Stained *E. coli*

In order to first visualize how each COE interacts with *E. coli*, we exploited the photoluminescent π-conjugated core of the molecules for fluorescence microscopy. Cells were stained with 10 μM solutions of COE for 1 hour and imaged with a laser scanning confocal microscope, the results of which are shown in Figure 4.2. As anticipated based on

the bolamphiphilic structure shared by the molecules, all COEs display an emission pattern around the edges of cells consistent with membrane intercalation. In this regard, the substitution of alkoxy pendant linkages for amine or the addition of 4 fluorine atoms to the center phenyl ring of the 3-RU COEs provides no discernable difference in terms of observable cell localization in *E. coli*.

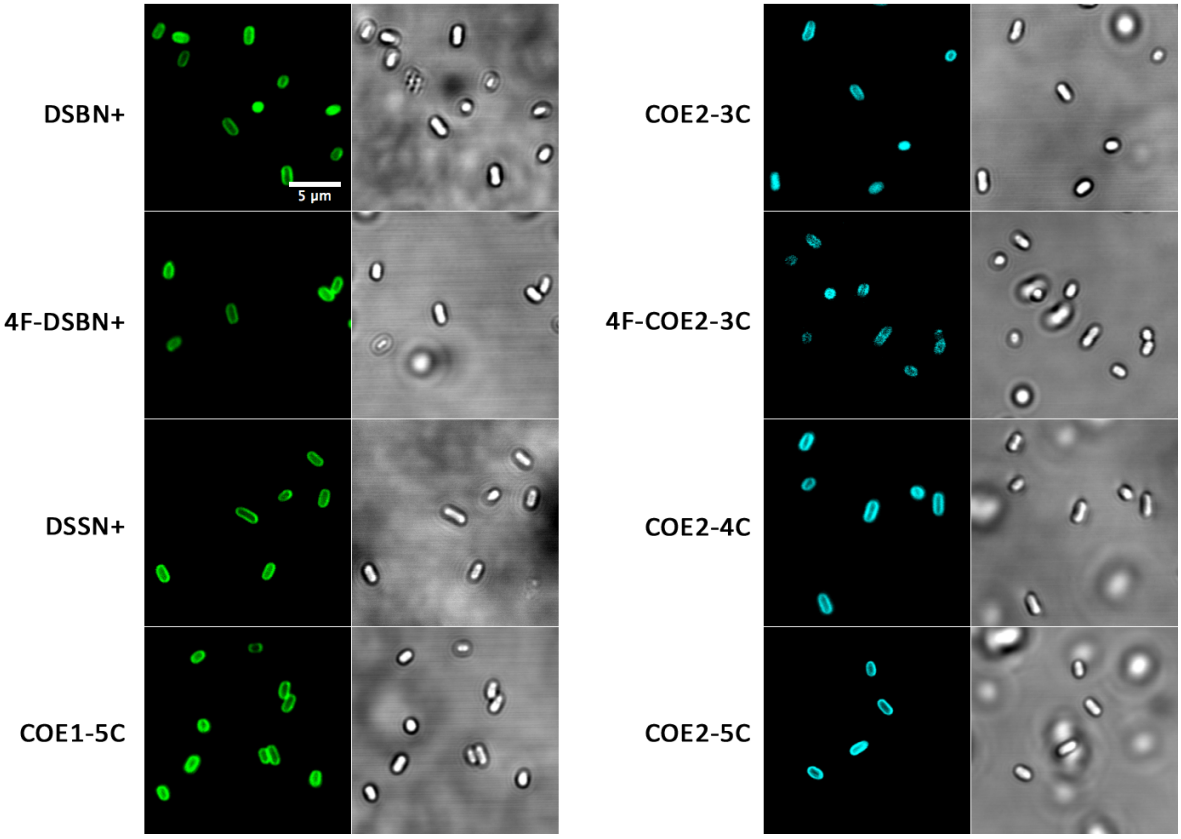

Figure 4.2. Laser scanning confocal micrographs and corresponding brightfield images of *E. coli* stained with 10 µM COE in PBS for 1 hour. Left panel is COE1 series (green), right panel is COE2 series (blue). Excitation wavelength was 405 nm for all images. 5 µm scale bar is the same for all images.

4.3 Quantifying Cell Association

Taking advantage of the strong visible light absorbing properties provided by the conjugated core of the molecules[7], the amount of each COE that associates with *E. coli* in

solution was quantified. Specifically, cells (OD_{600nm} = 0.9) were stained in 7 different concentrations of COE ranging from 1 – 40 μM for 1 hour in 50 mM phosphate buffered saline (PBS). A staining time of 1 hour was found sufficient to establish equilibrium (Figure 4.3). The cells were then centrifuged and the supernatant analysed by UV-vis absorption to determine the amount of COE left in solution (*i.e.,* not associated with the pelleted cells). This method is illustrated in Figure 4.4 for 10 μM and 20 μM **DSSN+**. Comparing the control spectra of the solutions containing just **DSSN+** in PBS (solid lines) to the spectra of the supernatants resulting from cell staining, one observes that at 10 μM, no discernable **DSSN+** is left in solution, meaning that all COE has associated with the cells. In contrast, at 20 μM a significant absorption is observed indicating that some **DSSN+** remains in the solution and did not associate with the *E. coli.*

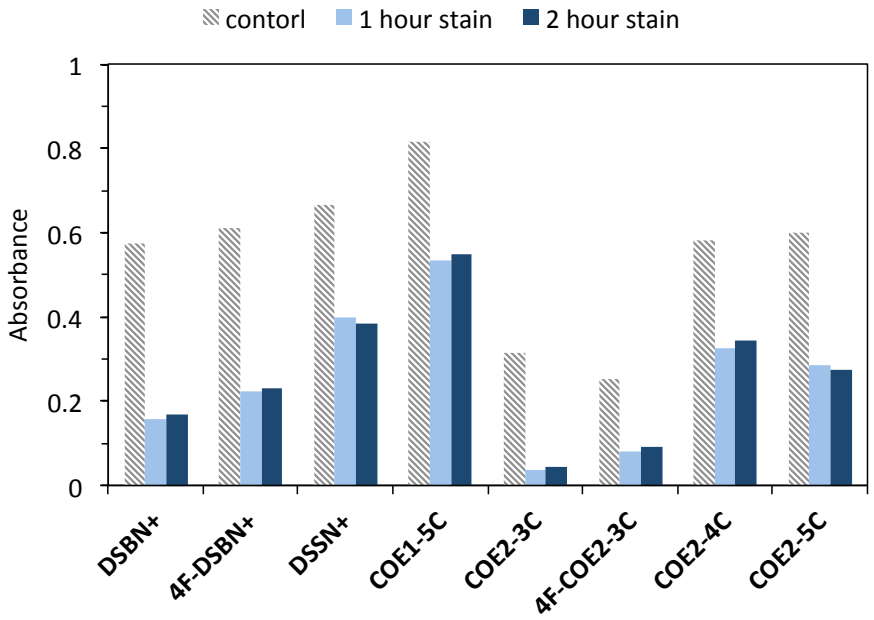

Figure 4.3. In order to demonstrate that the system had reached equilibrium after 1 hour, the supernatant of *E. coli* stained with 40 μM COE for 1 hour (light blue) and 2 hours (dark blue) were analysed by UV-vs absorption at 420 nm (COE1 series) and 380 nm (COE2

series). Note that a lower absorbance in the supernatant indicates less COE left in solution and more associated with cells. Shown in grey are 40 μM COE solutions in PBS (*i.e.* the amount of COE in solution with no cells present).

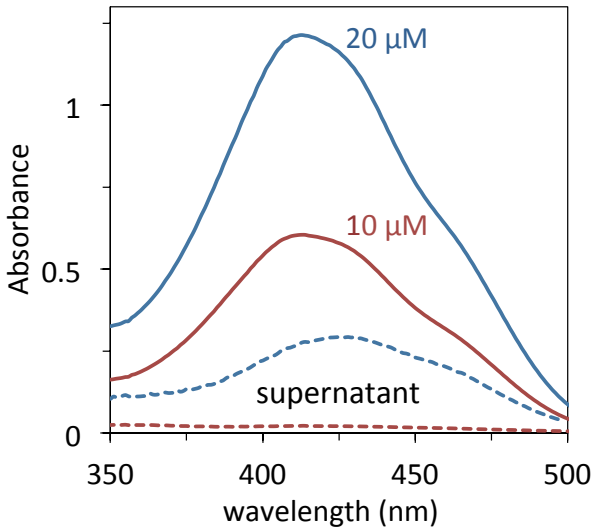

Figure 4.4. UV-vis absorption of 25 μM (blue, solid) and 10 μM (red, solid) **DSSN+** in PBS. After staining *E. coli* (OD_{600nm} = 0.9) for 1 hour with these concentrations of **DSSN+**, the cells are centrifuged and the **DSSN+** remaining in the supernatant (dashed lines) is measured in order to determine how much COE associates with cells.

4.4 COE Series Comparison by Cell Association

In subsequent experiments, the amount of COE associated with cells using this method was quantified by subtracting the absorbance of the supernatant of stained and centrifuged *E. coli* at a wavelength of 420 nm (COE1 series) or 380 nm (COE2 series) from control samples that did not contain cells. Figure 4.5 shows the trends in COE/cell association for the unfluorinated COEs at different staining concentrations normalized to 1 OD_{600nm} of cells. Interestingly, at concentrations between 1 – 15 μM for all 6 COEs, 100% association is observed resulting in a linear increase in COE association with increasing staining concentration, reaching ~15 nmol/OD_{600nm} at 15 μM staining concentration. Looking at the

COE1 series in Figure 4.5A, at concentrations > 15 μM the 4- and 5-RU COEs, **DSSN+** and **COE1-5C**, quickly reach a maximum association of ~ 16 nmol/OD_{600nm}. In contrast, the 3 RU COE, **DSBN+**, does not reach a plateau and attains a maximum association of 32 nmol/OD_{600nm} at 40 μM staining concentration. It should be noted that for COEs with toxicity data published (**DSBN+** and **DSSN+**) minimum inhibitory concentrations (normalized to cell count) required to reduce growth of *E. coli* are 2 orders of magnitude higher than the concentrations used in this study.[10,11] Furthermore, **DSBN+** is at least 10-times more toxic than **DSSN+**, which may be explained in part by the higher cell association compared to the saturation seen with **DSSN+**.

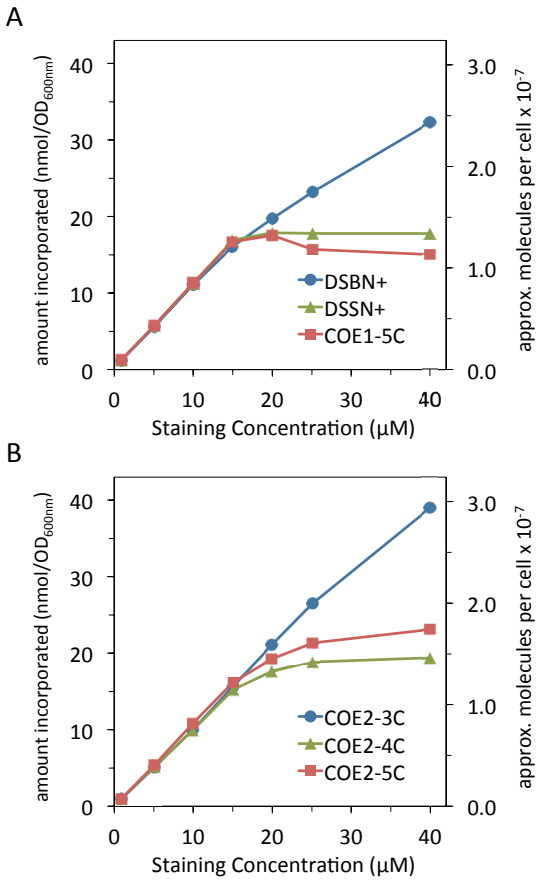

Figure 4.5. COE incorporated into *E. coli* cells as a function of staining concentration for (A) COE1 series and (B) COE2 series molecules. The amount of COE incorporated was calculated by subtracting the absorbance at 420 nm (COE1) or 380 nm (COE2) of the supernatant after centrifugation from that of the control staining solution with no cells. Approximate number of cells are assuming 1 OD_{600nm} = 10^9 cells mL^{-1}.

A similar trend is observed for the COE2 series in Figure 4.5B with maximum associations of 39, 19, 21 nmol for the 3-, 4- and 5- RU COEs, respectively. When comparing the two series of COEs, the COE2 series shows slightly greater maximum association suggesting that the structural modification afforded by the alkoxy pendant linkages provide a modest advantage in this respect. Regardless of series type, there is a clear dependence of COE association with *E. coli* on molecular length: the amount able to

associate with cells for the 4- and 5- RU COEs plateaus within the concentration range tested, while the 3-RU COEs do not.

Estimated on the secondary y-axes in Figure 4.5 are the number of COE molecules associated per cell at each staining concentration, with 1 OD_{600nm} corresponding to a concentration of 10^9 cells per mL[12]. With this estimation it can be seen that maximum COE associations observed in these experiments are greater than 10^7 molecules per cell for 4- and 5-RU COEs and greater than 2 x 10^7 for both 3-RU COEs. When comparing these numbers to an estimate of the number of lipids per *E. coli* cell[13] of ~2.2 x 10^7 one can see that the 4- and 5-RU COEs would approach a 1:1 lipid:COE ratio in cells and the 3-RU COEs surpass this threshold at the 40uM staining concentration. As discussed in the introduction, much evidence has been presented that COEs intercalate into microbial membranes, and up until this point, this has been the only interaction considered. With ratios at or above 1:1 lipid:COE per cell it is obvious that all the associated COE is not intercalating into lipid bilayers. A plausible hypothesis is that some COE is associating with the outside of the *E. coli*, which, with its net negative charge[14], is a likely candidate for electrostatic interaction with positively charged molecules[6,15,16].

4.5 Zeta Potential of Stained *E. coli*

In order to determine the effect of COE association on cell surface charge, stained *E. coli* from the previous experiment were washed and resuspended in PBS for zeta potential measurements,[14] the results of which are shown in Figure 4.6. Unstained cells were found to have an average zeta potential of about -22 mV under these conditions, indicating a net negative charge as expected from the exposed carboxylate and phosphoryl groups in the cell

wall of *E. coli*.[15] The cells stained with COE1 series follow a trend of increasing zeta potential to more positive values as the staining concentration increases. Maximum zeta potential values of -11, -2, and 2 mV are reached for the 3-, 4-, and 5-RU COEs, respectively, trending more positive with increasing molecular length. In addition, zeta potential values reflect the association trends observed in Figure 4.5A, in that the 4- and 5-RU COEs reach a plateau at a staining concentration of 20 μM, around the same concentration that cell association for these COEs plateaus. Despite having the highest maximum cell association of the COE1 series, the 3-RU COE causes the least change in zeta potential, but the trend reflects the association in that it does not appear to plateau in the concentration range tested.

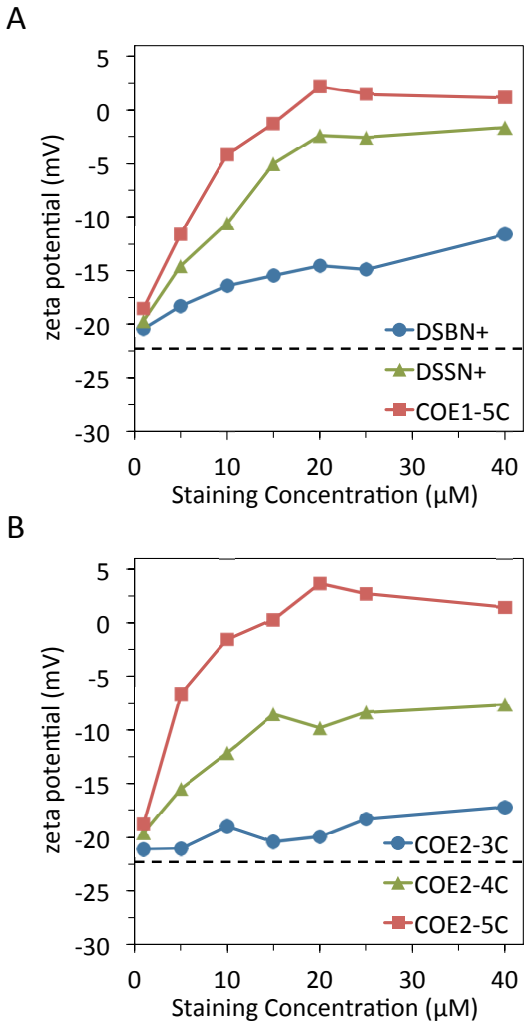

Figure 4.6. Zeta potential measurements of *E. coli* cells as a function of COE staining concentration for (A) COE1 series and (B) COE2 series. Data points are an average of 3 measurements. Dashed line represents the zeta potential of unstained *E. coli*.

The affect on *E. coli* zeta potential of the COE2 series is shown in Figure 4.6B. The COE2 series displays an evenly distributed length dependence with maximum zeta potential values for *E. coli* stained by each of the COEs separated by 10 mV, with maxima of -17, -7, and 3 mV observed for **COE2-3C**, **COE2-4C** and **COE2-5C**, respectively. Cells stained by the 3- and 4-RU COE2 molecules display noticeably less positive zeta potential values than their COE1 counterparts but ultimately a similar trend follows in that cells stained by longer

COEs result in more positive zeta potential values. Ultimately the change from amine to alkoxy linked pendant groups has only a minor influence on the COE zeta potential effects as a whole.

Rather than observing charge reversal towards high positive values as is seen in cases with cells being coated with positively charged polyelectrolytes[4,5,15], the trend towards charge neutralization with COEs in this experiment suggests that not many of the positive charges are extending beyond the LPS. COEs are much smaller in size than polyelectrolytes and easily intercalate into lipid membranes and perhaps also 'interdigitate' with the oligomeric sugars that form the core of LPS rather than coating the outside cells. In fact, this non-lipid portion of LPS in *E. coli* K12 is estimated to be ~2.1 nm[17,18]. This length is slightly larger than the 3-RU phenylenevinylene core and slightly smaller than the 4-RU conjugated core, which are estimated to be 1.8 nm and 2.4 nm respectively. With the 5-RU core estimated to be around 3 nm, one can begin to rationalize the length scales with the zeta potential results. More specifically, the 4- and 5-RU COEs have a greater chance of spanning the full length or even extending past the outermost LPS units than do the 3-RU COEs, possibly explaining the molecular length dependence of the zeta potential results.

4.6 Does Fluorine Substitution Matter?

Lastly, cell association and zeta potential experiments were carried out with the fluorine-substituted 3-RU COEs (4FCOEs), the results of which are plotted with the unsubstituted counterparts for comparison and are shown in Figure 4.7. Cell association for the 4FCOEs (Figure 4.7A) is largely indistinguishable from their unsubstituted counterparts until staining concentrations of ~25-40 μM at which point the 4FCOEs associate slightly less. At the

highest staining concentration tested (40 μM), there were approximately 2.1 x 10^7 and 2.3 x 10^7 molecules associated per cell for 4F-DSBN+ and 4F-COE2-3C, respectively. These values are 14% and 23% less than for DSBN+ and COE2-3C, respectively. A possible explanation for this deviation at higher staining concentrations is the polar-hydrophobic nature of fluorinated compounds,[19] making these molecules less likely to aggregate in the lipid membrane due to interactions between the cationic pendant groups and the fluorinated core.[10] Being less likely to aggregate or pack closely would result in less overall cell association. It is worth noting, however, that aggregation of COEs in a lipid membrane has yet to be experimentally proven.

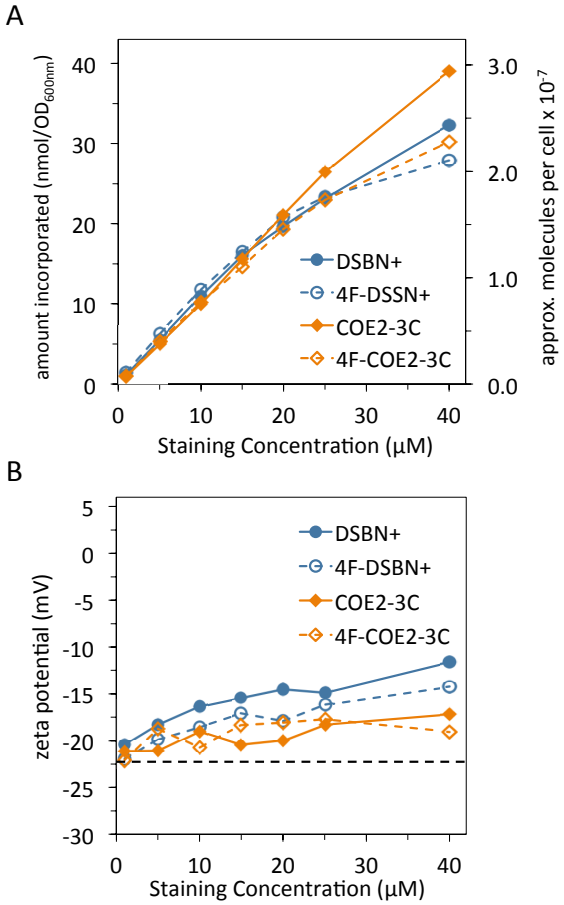

Figure 4.7. Comparing 3-ring COEs with (solid lines, closed symbols) and without (dashed lines, open symbols) fluorine substitution. (A) COE associated with *E. coli* as a function of staining concentration. Approximate number of cells assuming 1 OD_{600nm} = 10^9 cells mL^{-1}. (B) Zeta potential measurements of stained *E. coli* as a function of COE staining concentration. Black dashed line represents the zeta potential of unstained *E. coli*.

The zeta potential of *E. coli* stained with the 4FCOEs (Figure 4.7B) follows the same trend as the non-fluorinated COEs, in that a gradual increase in zeta potential is observed as staining concentration increases. Cells stained with 4F-DSBN+ reach a more positive maximum (-14 mV) than those stained with 4F-COE2-3C (-18 mV), with both maxima being slightly less positive than the corresponding unfluorinated COEs at -12 mV and -17 mV, respectively. Ultimately, fluorine substitution of the center ring of 3-RU COEs has minimal influence on cell association and zeta potential of stained *E. coli*.

4.7 Association and Surface Charge Effects on *Shewanella*

In order to determine if the association of COEs with *E. coli* and their effect on cell surface charge could be applied to other bacteria, similar experiments were performed with *Shewanella*. Unlike the previous experiments on *E. coli* only **DSBN+**, **DSSN+**, and **COE1-5C** were compared at 3 different concentrations and the results are shown in Figure 4.8. From the cell association experiments in Figure 4.8A, one observes similar levels of association to those of *E. coli* in Figure 4.5A. However, moving to the zeta potential measurements in Figure 4.8B, one observes a no significant effect on the surface charge of *Shewanella*. So despite having similar amounts of highly cationic COEs associated, they seem to not affect the surface charge of *Shewanella* cells. How can this be? First it should be noted that the inherent surface charge of *Shewanella* (-6.9 mV) is much closer to neutral than that of *E. coli* (-22 mV) indicating less exposed ionic groups at its outermost surface. This is most likely due to a hydrophobic capsular layer found in the *Shewanella* strain used in this study. In fact, it was found that this layer extends 20 to 30 nm from the cell surface.[20] So it is entirely possible that COEs are associating with *Shewanella* in a similar manner as with *E. coli* (based on association experiments) but that the zeta potential measurements are unable to detect this due to shielding by the capsule.

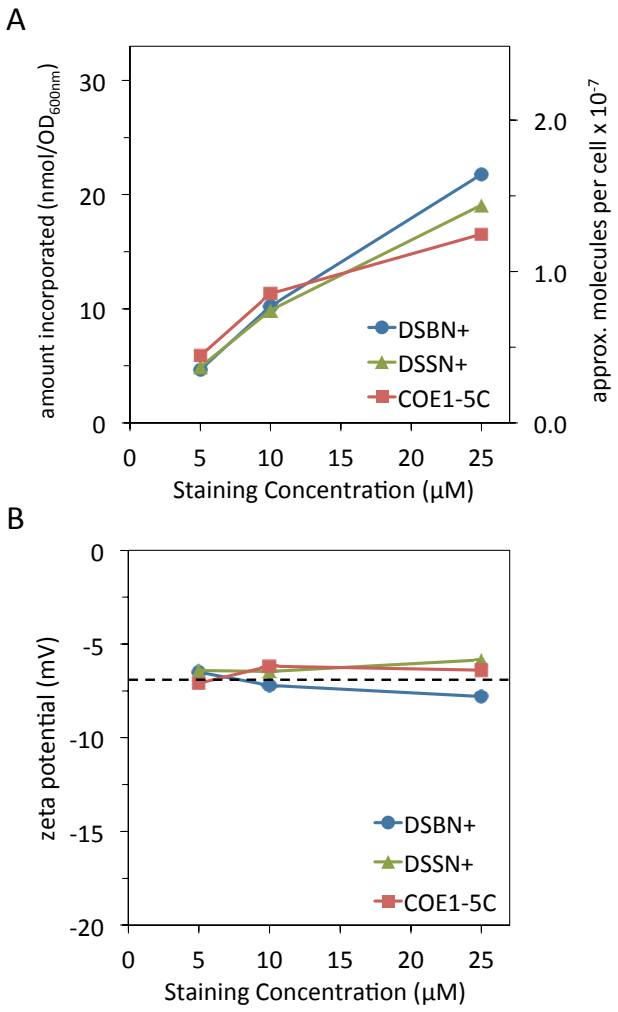

Figure 4.8. (A) COE associated with *Shewanella* as a function of staining concentration. Approximate number of cells assuming 1 OD_{600nm} = 10^9 cells mL^{-1}. (B) Zeta potential measurements of stained *Shewanella* as a function of COE staining concentration. Black dashed line represents the zeta potential of unstained *Shewanella* (-6.9 mV).

4.7 A Note on Salt Concentration

It has been suggested that electrostatic interactions play a dominant role in the interaction of COEs with bacteria (Chapter 3).[1] As such, one would expect salt concentration to play a role in the amount of COE that associates with cells in a given solution.[21] Specifically, more ions in solution would more effectively screen interactions between the

cationic COEs and negatively charged bacteria, and should result in a lower association. Until now the experiments presented in this chapter have been conducted in 50 mM PBS. In order to confirm the suspected implications of higher salt concentrations, both *E. coli* and *Shewanella* were stained with 25 μM **DSSN+** in 150 mM PBS and compared to the previous experiments in 50 mM, the results of which are shown in Figure 4.9A. As expected, much lower cell association is observed in the higher salt concentration (~5 nmol per OD_{600nm}) versus the lower salt concentration (> 17 nmol) for both *E. coli* and *Shewanella*. In addition, these cells were subjected to zeta potential measurements and the results are shown in Figure 4.9B. The *E. coli* stained with 25 μM **DSSN+** in 150 mM PBS had a zeta potential of -16 mV, which is much closer to unstained *E. coli* (-22 mV) than the cells stained in 50 mM PBS (-2.5 mV). This is in line with less COE association causing less change in zeta potential. Furthermore, the zeta potential of *E. coli* stained with 25 μM **DSSN+** in high salt is in good agreement with the zeta potential of cells stained with 5 μM in low salt (-15 mV, Figure 4.6A) since both of these conditions resulted in COE association of ~5 nmol per OD_{600nm}. For *Shewanella*, zeta potential measurements in Figure 4.9B show no difference between those stained in 50 mM or 150 mM PBS: both are very close to the zeta potential of unstained *Shewanella* (-6.9 mV). So despite differences in the amount of COE associated with the cells in the two salt concentrations, the zeta potential remains unchanged, which is in agreement with the results seen in Figure 4.8.

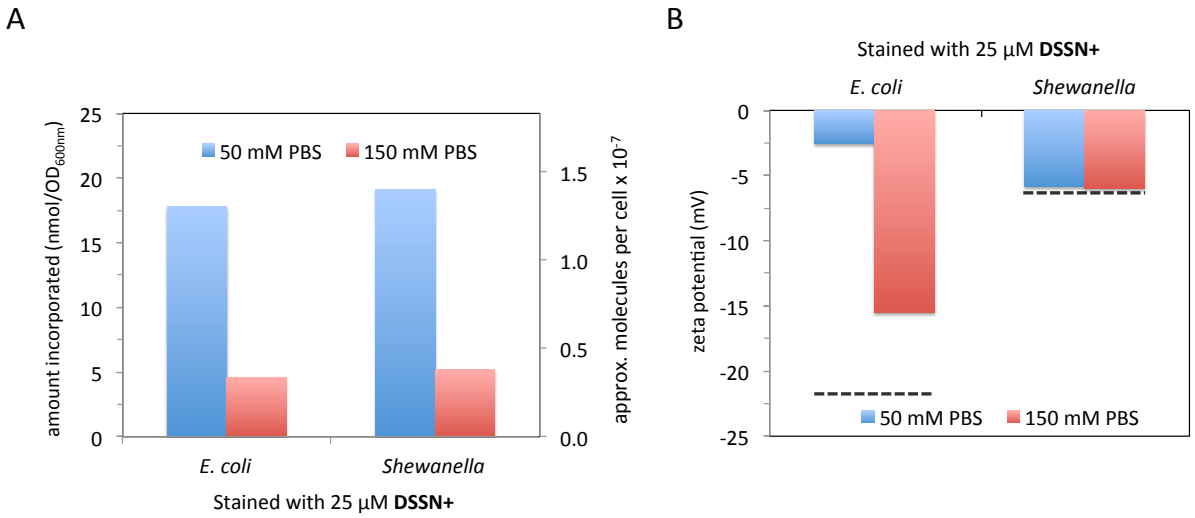

Figure 4.9. (A) The amount of COE associated with *E. coli* and *Shewanella* stained with 25 µM **DSSN+** in either 50 mM PBS or 150 mM PBS. Approximate number of cells assuming 1 OD_{600nm} = 10^9 cells mL^{-1}. (B) Zeta potential measurements of *E. coli* and *Shewanella* stained with 25 µM **DSSN+** in either 50 mM PBS or 150 mM PBS. Note that the measurements were done in 50 mM PBS. Black dashed lines represent the zeta potential of unstained cells.

While not an exhaustive set of experiments, this demonstrates without a doubt that salt concentrations can have a huge affect on the amount of COE associating with cells. This observation has implications for analyzing and comparing past results and for future work with COEs since the media used in experiments can have very different salt concentrations.

4.8 Conclusion

In conclusion, 8 COEs varying in length and substitutions to the aromatic core have been compared in terms of their association with *E. coli* and their effect on whole cell zeta potential. Confocal microscopy showed patterns consistent with lipid membrane association for all COEs. At low staining concentrations (< 20 µM) nearly 100% of COE in solution associates with cells, leaving none remaining in the supernatant of centrifuged samples. At higher concentrations, 3-RU COEs continue to associate while 4- and 5-RU COEs plateau,

reaching a maximum association that cannot be overcome by adding more COE to the staining solution. Cells stained with COEs generally showed more positive zeta potential values with increasing staining concentration, indicating a neutralization of anionic charges of the LPS by the cationic charges of the COEs. Additionally, more positive zeta potential values were observed for longer COEs suggesting that they are able to extend beyond the negatively charged oligomeric sugars of the *E. coli* LPS. This is supported by similar experiments with *Shewanella* showing that despite similar levels of association by COEs, the zeta potential of these cells is unchanged. This is most likely due to hydrophobic capsular polysaccharides in *Shewanella oneidensis* MR-1 that extend well beyond the outer membrane.[20] The other structural variations presented here, namely amine vs. alkoxy pendant linkages and fluorination of the aromatic core, proved less important than molecular length, as they had minimal effects on cell association and zeta potential when compared to analogues with the same number of repeat units. While fairly inconsequential in this regard, these changes alter the photophysical properties of the molecules and thus increase the number of COEs available for applications in bioimaging[22-26] and optoelectronics.[27,28] Most importantly, that the zeta potential of certain bacteria can be tuned by COE length and concentration has implications for technologies like microbial electronics, wastewater treatment, and others that rely on bacterial aggregation, adhesion and biofilm formation.[21,29-34]

4.6 Experimental

Cell culture. *Escherichia coli* K-12 (ATCC 10798) and *Shewanella oneidensis* MR-1 were grown aerobically in Luria Broth (10 g L^{-1} bacto tryptone, 5 g L^{-1} yeast extract, 10 g L^{-1} NaCl) overnight.

Cell staining for microscopy. Before staining, cells were rinsed twice from the growth medium with 50 mM phosphate buffered saline (PBS) containing the following: 45.7 mM NaCl, 0.9 mM KCl, 3.3 mM Na_2HPO_4 and 0.6 mM KH_2PO_4 at pH 7.4. 0.5 mL of OD_{600} = 0.9 cells were stained with 10 μM COE for 1 hour in the dark at room temperature before rinsing twice. Samples were then resuspended in 100 μL of PBS and 5 μL were dropped onto a clean glass slide and a cover slip placed on top. Cover slips were sealed with clear nail polish and all samples were imaged within 2 hours.

Confocal microscopy. All images were obtained via laser scanning confocal microscopy using an Olympus FluoView 1000S spectral scanning microscope equipped with a 60 x 1.30 silicon oil immersion lens. A 405 nm laser was used as the excitation source. For the COE1 series, emission was collected from 480 nm – 580 nm. For the COE2 series, emission was collected from 410 nm – 510 nm. All images were processed using ImageJ.

Cell association experiments. Cells at OD_{600} = 0.9 were stained in clear 96-well plates (BD Biosciences, San Jose, CA) at 20 °C for 1 hour in the dark with shaking. Total volume of each sample was 200 μL. After centrifugation of the plate (3500 rpm, 4 minutes), 100 μL of supernatant was transferred to a clean well for UV-Vis absorption with a Tecan M220 Infinite Pro plate reader (Tecan, Männedorf, Switzerland). Absorbance was measured at 420

nm for COE1 series and 380 nm for COE2 series molecules. Control samples with no cells were treated the same and their absorbance values represented the total COE from which the supernatant values were subtracted to give the amount associated with cells.

Zeta potential measurements. Stained, twice-rinsed cells were resuspended in PBS to their original OD_{600nm} = 0.9. 10 μL of each sample was diluted into 1 mL PBS for zeta potential measurements on a Malvern Zetasizer Nano ZS (Malvern Instruments, Malvern, U.K.) at 20 °C. Data points given are an average of 3 measurements each.

4.7 References

1. Thomas, A. W., Catania, C., Garner, L. E. & Bazan, G. C. Pendant ionic groups of conjugated oligoelectrolytes govern their ability to intercalate into microbial membranes. *Chem. Commun.* **51,** 9294–9297 (2015).
2. Kotra, L. P., Golemi, D., Amro, N. A., Liu, G.-Y. & Mobashery, S. Dynamics of the Lipopolysaccharide Assembly on the Surface of Escherichiacoli. *J. Am. Chem. Soc.* **121,** 8707–8711 (1999).
3. Nikaido, H. Molecular Basis of Bacterial Outer Membrane Permeability Revisited. *Microbiol. Mol. Biol. Rev.* **67,** 593–656 (2003).
4. Franz, B., Balkundi, S. S., Dahl, C., Lvov, Y. M. & Prange, A. Layer-by-Layer Nano-Encapsulation of Microbes: Controlled Cell Surface Modification and Investigation of Substrate Uptake in Bacteria. *Macromol. Biosci.* **10,** 164–172 (2010).
5. Balkundi, S. S., Veerabadran, N. G., Eby, D. M., Johnson, G. R. & Lvov, Y. M. Encapsulation of Bacterial Spores in Nanoorganized Polyelectrolyte Shells. *Langmuir* **25,** 14011–14016 (2009).

6. Eby, D. M. *et al.* Bacterial Sunscreen: Layer-by-Layer Deposition of UV-Absorbing Polymers on Whole-Cell Biosensors. *Langmuir* **28,** 10521–10527 (2012).

7. Garner, L. E. *et al.* Modification of the Optoelectronic Properties of Membranes via Insertion of Amphiphilic Phenylenevinylene Oligoelectrolytes. *J. Am. Chem. Soc.* **132,** 10042–10052 (2010).

8. Hou, H. *et al.* Conjugated oligoelectrolytes increase power generation in E. coli microbial fuel cells. *Adv. Mater.* **25,** 1593–1597 (2013).

9. Woo, H. Y. *et al.* Solvent Effects on the Two-Photon Absorption of Distyrylbenzene Chromophores. *J. Am. Chem. Soc.* **127,** 14721–14729 (2005).

10. Hinks, J. *et al.* Modeling Cell Membrane Perturbation by Molecules Designed for Transmembrane Electron Transfer. *Langmuir* **30,** 2429–2440 (2014).

11. Hinks, J. *et al.* Oligopolyphenylenevinylene-Conjugated Oligoelectrolyte Membrane Insertion Molecules Selectively Disrupt Cell Envelopes of Gram-Positive Bacteria. *Appl. Environ. Microbiol.* **81,** 1949–1958 (2015).

12. Sondi, I. & Salopek-Sondi, B. Silver nanoparticles as antimicrobial agent: a case study on E. coli as a model for Gram-negative bacteria. *J. Colloid Interf. Sci.* **275,** 177–182 (2004).

13. Neidhardt, F. C. & Curtiss, R. Escherichia Coli and Salmonella: Cellular and Molecular Biology. (1996).

14. Wilson, W. W., Wade, M. M., Holman, S. C. & Champlin, F. R. Status of methods for assessing bacterial cell surface charge properties based on zeta potential measurements. *J. Microbiol. Meth.* **43,** 153–164 (2001).

15. Hillberg, A. L. & Tabrizian, M. Biorecognition through Layer-by-Layer Polyelectrolyte Assembly: In-Situ Hybridization on Living Cells. *Biomacromol.* **7,** 2742–2750 (2006).

16. Kahraman, M., Zamaleeva, A. I., Fakhrullin, R. F. & Culha, M. Layer-by-layer coating of bacteria with noble metal nanoparticles for surface-enhanced Raman scattering. *Anal. Bioanal. Chem.* **395,** 2559–2567 (2009).

17. Lee, A. G. Lipid–protein interactions in biological membranes: a structural perspective. *Biochim. Biophys. Acta* **1612,** 1–40 (2003).

18. Kastowsky, M., Gutberlet, T. & Bradaczek, H. Molecular modelling of the three-dimensional structure and conformational flexibility of bacterial lipopolysaccharide. *J. Bacteriol.* **174,** 4798–4806 (1992).

19. Biffinger, J. C., Kim, H. W. & DiMagno, S. G. The Polar Hydrophobicity of Fluorinated Compounds. *Chembiochem* **5,** 622–627 (2004).

20. Korenevsky, A. A., Vinogradov, E., Gorby, Y. & Beveridge, T. J. Characterization of the Lipopolysaccharides and Capsules of Shewanella spp. *Appl. Environ. Microbiol.* **68,** 4653–4657 (2002).

21. Poortinga, A. T., Bos, R., Norde, W. & Busscher, H. J. Electric double layer interactions in bacterial adhesion to surfaces. *Surf. Sci. Rep.* **47,** 1–32 (2002).

22. Thomas, A. W., Henson, Z. B., Du, J., Vandenberg, C. A. & Bazan, G. C. Synthesis, characterization, and biological affinity of a near-infrared-emitting conjugated oligoelectrolyte. *J. Am. Chem. Soc.* **136,** 3736–3739 (2014).

23. Gwozdzinska, P. *et al.* Phenylenevinylene conjugated oligoelectrolytes as fluorescent

dyes for mammalian cell imaging. *Chem. Commun.* **50,** 14859–14861 (2014).

24. Pu, K.-Y., Li, K., Zhang, X. & Liu, B. Conjugated Oligoelectrolyte Harnessed Polyhedral Oligomeric Silsesquioxane as Light-Up Hybrid Nanodot for Two-Photon Fluorescence Imaging of Cellular Nucleus. *Adv. Mater.* **22,** 4186–4189 (2010).
25. Ding, D., Pu, K.-Y., Li, K. & Bin Liu. Conjugated oligoelectrolyte- polyhedral oligomeric silsesquioxane loaded pH-responsive nanoparticles for targeted fluorescence imaging of cancer cell nucleus. *Chem. Commun.* **47,** 9837–9839 (2011).
26. Song, W. *et al.* Star-shaped conjugated oligoelectrolyte for bioimaging in living cells. *Chin. Sci. Bull.* **58,** 2570–2575 (2013).
27. Lee, Y. *et al.* Enhanced Photocurrent Generation by Förster Resonance Energy Transfer between Phospholipid-Assembled Conjugated Oligoelectrolytes and Nile Red. *J. Phys. Chem. C* **117,** 3298–3307 (2013).
28. Kirchhofer, N. D., Rasmussen, M., Dahlquist, F., Minteer, S. & Bazan, G. C. The Photobioelectrochemical Activity of Thylakoid Bioanodes is Increased via Photocurrent Generation and Improved Contacts by Membrane-Intercalating Conjugated Oligoelectrolytes. *Energy Environ. Sci.* (2015). doi:10.1039/C5EE01707F
29. Nakao, R., Ramstedt, M., Wai, S. N. & Uhlin, B. E. Enhanced Biofilm Formation by Escherichia coli LPS Mutants Defective in Hep Biosynthesis. *PLoS ONE* **7,** e51241 (2012).
30. Palmer, J., Flint, S. & Brooks, J. Bacterial cell attachment, the beginning of a biofilm. *J. Ind. Microbiol. Biotechnol.* **34,** 577–588 (2007).
31. Liu, Y. *et al.* The influence of cell and substratum surface hydrophobicities on

microbial attachment. *J. Biotechnol.* **110,** 251–256 (2004).

32. Dunne, W. M. Bacterial Adhesion: Seen Any Good Biofilms Lately? *Clin. Microbiol. Rev.* **15,** 155–166 (2002).

33. Zita, A. & Hermansson, M. Effects of bacterial cell surface structures and hydrophobicity on attachment to activated sludge flocs. *Appl. Environ. Microbiol.* **63,** 1168–1170 (1997).

34. Ahimou, F., Denis, F. A., Touhami, A. & Dufrêne, Y. F. Probing Microbial Cell Surface Charges by Atomic Force Microscopy. *Langmuir* **18,** 9937–9941 (2002).